Article

Current Biology

Input density tunes Kenyon cell sensory responses in the *Drosophila* mushroom body

Graphical abstract

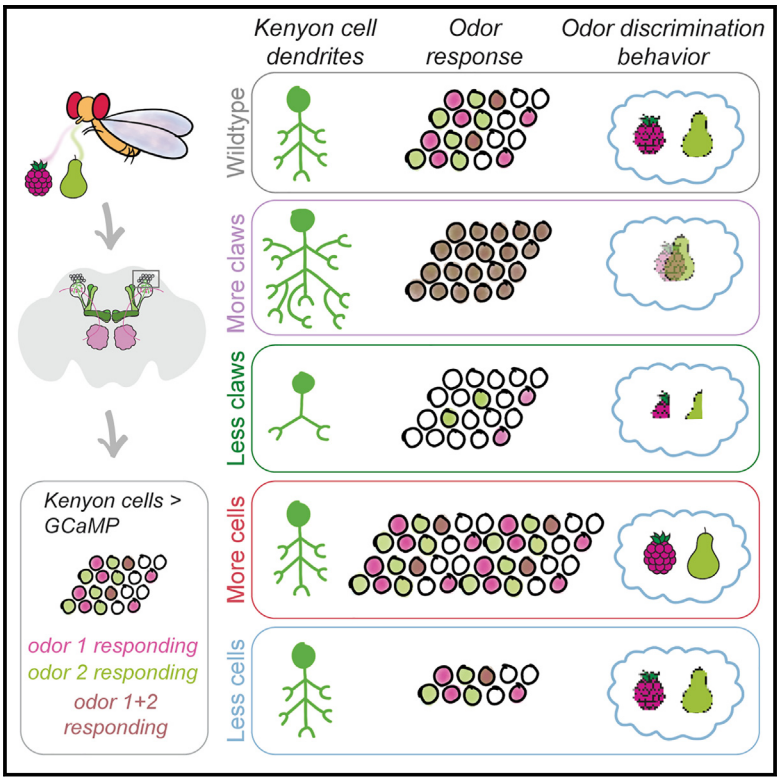

Highlights

- Odor representation in Kenyon cells is robust to changes in Kenyon cell number
- Altering Kenyon cell input density tunes the sparsity of their odor responses
- Mushroom body output neurons functionally accommodate changes to Kenyon cells
- Odor discrimination behavior correlates with changes in Kenyon cell odor responses

Authors

Maria Ahmed, Adithya E. Rajagopalan, Yijie Pan, ..., Dawen Cai, Glenn C. Turner, E. Josephine Clowney

Correspondence

jclowney@umich.edu

In brief

Ahmed et al. perturb mushroom body hard-wiring to test the Marr-Albus theory of pattern separation. By altering the number of Kenyon cells or their input density, they find that input density determines the sparsity of odor responses. Discrimination behavior is enhanced by increasing Kenyon cell number and degraded by making odor responses promiscuous.

Ahmed et al., 2023, Current Biology *33*, 1–19
July 10, 2023
https://doi.org/10.1016/j.cub.2023.05.064

CellPress

Please cite this article in press as: Ahmed et al., Input density tunes Kenyon cell sensory responses in the *Drosophila* mushroom body, Current Biology (2023), https://doi.org/10.1016/j.cub.2023.05.064

Current Biology

CellPress

Article

Input density tunes Kenyon cell sensory responses in the *Drosophila* mushroom body

Maria Ahmed,[1] Adithya E. Rajagopalan,[2,3] Yijie Pan,[1] Ye Li,[4] Donnell L. Williams,[1] Erik A. Pedersen,[1] Manav Thakral,[1] Angelica Previero,[1] Kari C. Close,[2] Christina P. Christoforou,[2] Dawen Cai,[4,5,6] Glenn C. Turner,[2] and E. Josephine Clowney[1,6,7,8,*]

[1]Department of Molecular, Cellular and Developmental Biology, University of Michigan, Ann Arbor, MI 48109, USA
[2]Howard Hughes Medical Institute, Janelia Research Campus, Ashburn, VA 20147, USA
[3]The Solomon H. Snyder Department of Neuroscience, Johns Hopkins University School of Medicine, Baltimore, MD 21205, USA
[4]Department of Cell and Developmental Biology, University of Michigan, Ann Arbor, MI 48104, USA
[5]Biophysics LS&A, University of Michigan, Ann Arbor, MI 48109, USA
[6]Michigan Neuroscience Institute Affiliate, University of Michigan, Ann Arbor, MI 48109, USA
[7]Twitter: @JosieClowney
[8]Lead contact
*Correspondence: jclowney@umich.edu
https://doi.org/10.1016/j.cub.2023.05.064

SUMMARY

The ability to discriminate sensory stimuli with overlapping features is thought to arise in brain structures called expansion layers, where neurons carrying information about sensory features make combinatorial connections onto a much larger set of cells. For 50 years, expansion coding has been a prime topic of theoretical neuroscience, which seeks to explain how quantitative parameters of the expansion circuit influence sensory sensitivity, discrimination, and generalization. Here, we investigate the developmental events that produce the quantitative parameters of the arthropod expansion layer, called the mushroom body. Using *Drosophila melanogaster* as a model, we employ genetic and chemical tools to engineer changes to circuit development. These allow us to produce living animals with hypothesis-driven variations on natural expansion layer wiring parameters. We then test the functional and behavioral consequences. By altering the number of expansion layer neurons (Kenyon cells) and their dendritic complexity, we find that input density, but not cell number, tunes neuronal odor selectivity. Simple odor discrimination behavior is maintained when the Kenyon cell number is reduced and augmented by Kenyon cell number expansion. Animals with increased input density to each Kenyon cell show increased overlap in Kenyon cell odor responses and become worse at odor discrimination tasks.

INTRODUCTION

In diverse bilaterians, chemosensory information is processed through parallel circuits that support innate versus learned responses.[1–6] Innate responses rely on the developmental specification of distinct cell types that wire in stereotyped patterns to connect sensory inputs to evolutionarily selected behavioral responses.[7–15] In contrast, regions devoted to learning appear more like *in silico* computers, with the same circuit motif repeated umpteen times.[16–20] Such repetitive organization allows learning circuits to function like switchboards, with the potential to connect any sensory representation to any behavioral output. The quantitative wiring parameters that set up an organism's potential to recognize stimuli and compute their meanings are dictated by the developmental identities of the neurons that comprise learning circuits.

An "expansion layer" is a representation structure where neurons receiving information about different sensory channels connect combinatorially onto a much larger set of postsynaptic cells.[16–18] These include the chordate pallium, cerebellum, and hippocampus; arthropod mushroom body; and cephalopod parallel lobe system. Marr and Albus hypothesized in the 1970s that cerebellum-like structures perform pattern separation. The ratio between sensory channels and expansion layer neurons and the number of sensory inputs that individual expansion layer neurons receive are theorized to be key parameters balancing perception, discrimination, and generalization.[10,16–18,21–28] However, the perceptual and behavioral effects of altering hard-wired circuit parameters have not been experimentally tested.

To do so, we initiate here a project of developmental circuit hacking. Using our knowledge of mushroom body structure and development in *Drosophila melanogaster*, we change quantitative relationships between presynaptic olfactory projection neurons (PNs) and postsynaptic Kenyon cells (KCs) *in vivo*.[29,30] We then test perceptual and behavioral capabilities of these hacked-circuit animals.

In the mushroom body calyx, individual KCs receive a median of 5–6 discrete inputs from among 52 types of olfactory PNs. PN-KC connections consist of multisynaptic "microglomerular" structures formed by presynaptic "boutons" from PNs and dendritic "claws" from KCs.[31–35] Individual KCs receive diverse odor

Please cite this article in press as: Ahmed et al., Input density tunes Kenyon cell sensory responses in the *Drosophila* mushroom body, Current Biology (2023), https://doi.org/10.1016/j.cub.2023.05.064

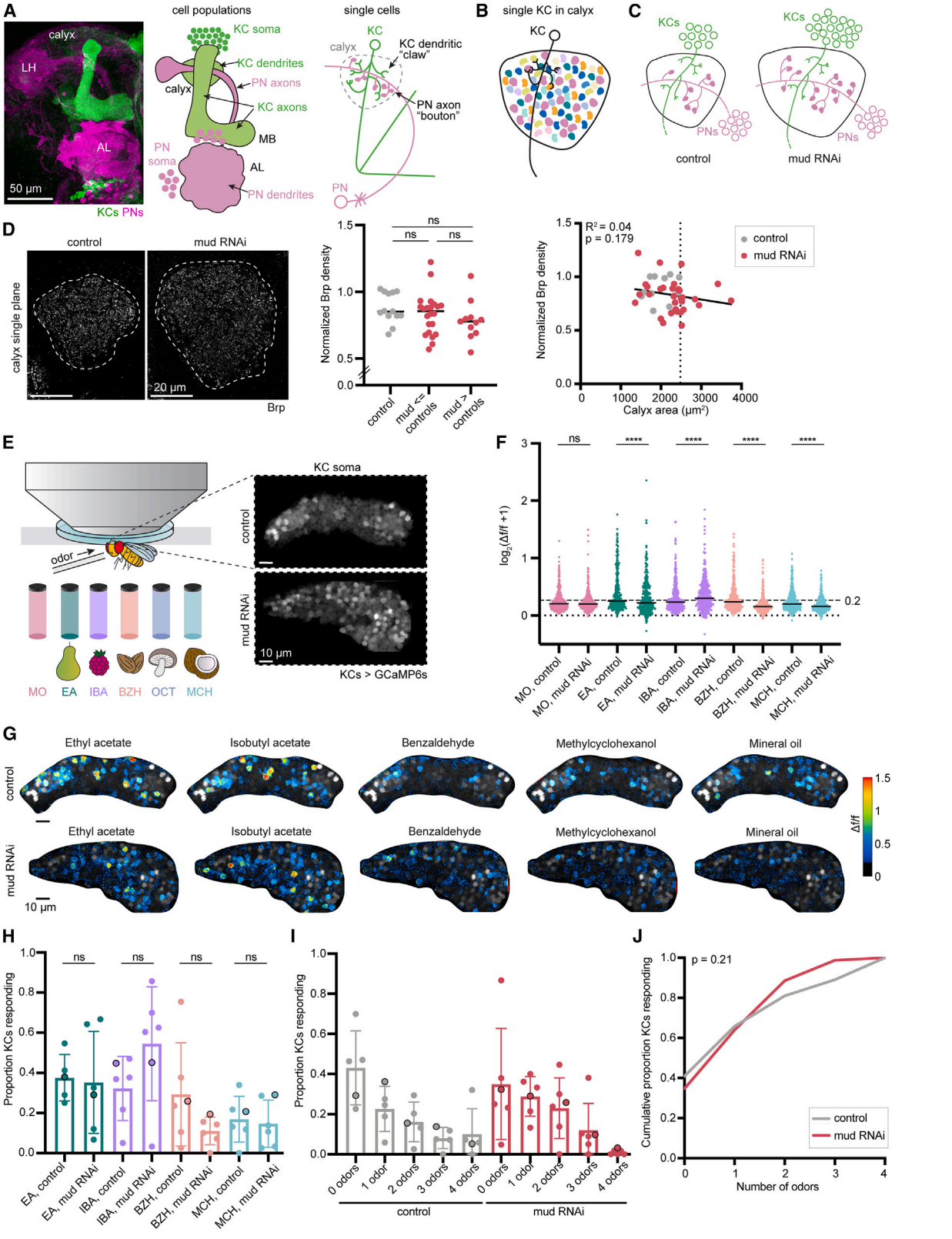

(legend on next page)

Please cite this article in press as: Ahmed et al., Input density tunes Kenyon cell sensory responses in the *Drosophila* mushroom body, Current Biology (2023), https://doi.org/10.1016/j.cub.2023.05.064

inputs that approximate a random sampling of available PN boutons. As KCs fire only when multiple inputs are active, they act as coincidence detectors with the potential to expand the animal's perception from single channels to combinations.[34,36–41] KCs send outputs to broadly ramifying mushroom body output neurons (MBONs) in the mushroom body lobes, where dopamine-mediated plasticity allows animals to learn durable associations between odors and coincident events.[42–47]

Previously, we developed methods to vary KC genesis. We found presynaptic olfactory PNs adjusted their output repertoire to the KC population.[29] This rule means that the number of KCs versus their number of inputs can be "programmed" as independent variables during development. Here, we develop methods to increase and decrease the KC claw number. We then test the effects of altering the KC number versus the input number on sensory representations and associative learning behavior. We find that changing KC number only modestly affects population-level odor responses. In contrast, KC odor responses change bidirectionally as we change KC dendritic claw number, such that KCs become less odor selective as their input number grows. Remarkably, animals with reduced KC population size can learn simple olfactory associations, animals with augmented sets of KCs show improved associative learning, and animals with an increased overlap in neuronal representations of odors become worse at fine discrimination. These results illuminate surprising functional and developmental principles and provide a novel method for testing the "purpose" of observed learning circuit architectures.

RESULTS

Sparse odor coding is preserved despite perturbations to Kenyon cell numbers

The ~2,000 mushroom body KCs receive combinatorial inputs from ~160 uniglomerular olfactory PNs that route 52 channels of olfactory information from the antennal lobe (Figures 1A and 1B).[48–52] Previously, we varied KC number from 500 to 4,000 and found that individual KCs retained their typical claw numbers (~6/cell), whereas PNs scaled their bouton numbers accordingly.[29] In mushroom bodies with fewer KCs, we observed that odor responses remained selective and sparse. To ask how supernumerary KCs respond to odors, we expanded KC neuroblasts using the *mud* knockdown method we described previously.[29] In this condition, KCs retain claw numbers similar to wild type, whereas PNs scale up their bouton production. To test if these claws retain full complements of input synapses, we immunostained for an active zone marker, Bruchpilot (Brp; Figures 1C and 1D).[53,54] As *mud*-driven KC expansion is stochastic, we grouped *mud* RNAi animals into "mud ≤ controls" and "mud > controls" based on their calyx size, which correlates with KC number.[29] Normalized Brp density was consistent across calyces of different sizes, suggesting that the number of input synapses per KC claw, and therefore per KC, is maintained in the increased-KC calyces (Figure 1D).

We expressed GCaMP6s in all KCs and imaged somatic responses to multiple odors in adult flies, as well as a mineral oil-only control to capture motion and solvent responses (Figure 1E). After motion correction and selection of *mud*-enlarged hemispheres, 6 hemispheres of each condition were stable enough to follow individual cells over time.[55] We plotted the response magnitude for all cells pooled; median odor responses were similar between control and increased-KC calyces, although the shapes of the distributions differed statistically (Figures 1F, 1G, and S1A). We next quantified the proportion of KCs per calyx responding to each odor, using a 20% increase in fluorescence as a cutoff for "responsiveness." The proportions were strikingly similar in the two conditions (Figure 1H), as we previously observed in reduced-KC calyces.[29] The variability in responses to each odor across different animals is expected due to the stochastic nature of the innervation of KCs by PNs.[34] Next, we asked how many odors each cell responded to. In each condition, ~50% of the cells responded to 0 or 1 odor, and ~10%–15% of the cells responded to all 4 odors (Figures 1I, 1J, and S1B). Among expanded calyces, calyx size did not predict response sparseness (Figure S1C). These results demonstrate that populations of supernumerary KCs still respond sparsely to odors and that individual cells remain odor selective.

Knocking down *Tao* in Kenyon cells increases dendritic claws per cell

We hypothesize that calyces with altered KC numbers retain sparse odor responses due to maintenance of dendritic claw numbers. We therefore searched for ways to directly alter the claw number. Tao is a kinase in the Mst/Ste20 family that interacts

Figure 1. Sparse odor coding is preserved when Kenyon cell numbers are increased

(A) PNs receive input from olfactory sensory neurons in the antennal lobe (AL) and project to the mushroom body calyx and the lateral horn (LH). In the calyx, KC dendritic claws grab PN presynaptic "boutons."

(B) An individual KC receives ~5–6 inputs from PNs innervating diverse AL glomeruli (different colors).

(C) Model of the effect of increasing KCs on calyx development, from Elkahlah et al.[29]

(D) Left: confocal slice of Brp in control and OK107>*mud* RNAi calyces. Circle: maximum cross-sectional area. Middle: Brp density, normalized to protocerebral bridge. Significance: unpaired t tests. Black horizontal bars: medians. Right: relation of normalized Brp density to maximum calyx area. Dotted line: cutoff to define Kenyon cell-increased brains (mud > controls). Each data point represents a single hemisphere.

(E) *In vivo* functional imaging preparation. Vials contain solvent (mineral oil; MO), ethyl acetate (EA), isobutyl acetate (IBA), benzaldehyde (BZH), octanol (OCT), and methylcyclohexanol (MCH). Responses were imaged from KC soma by GCaMP6s.

(F) Peak odor responses of pooled cells across hemispheres. Dashed line: 0.2 Δf/f threshold. Black horizontal bars: medians. Significance: Mann-Whitney test. n = 349–405 cells (control), 341 cells (*mud* RNAi) for each stimulus. Here and throughout, *p < 0.05; **p < 0.01; ***p < 0.001; ****p < 0.0001; ns, non-significant.

(G) Representative images of KC somatic odor responses in control and increased-KC hemisphere. Grayscale backdrop indicates the cells. See also Figure S1A.

(H and I) Proportion of cells in each hemisphere responding to each stimulus (Δf/f > 0.2) (H), and proportion responding to 0, 1 or multiple odors (I). Significance: unpaired t test. Bar plots in (H) and (I) show mean ± SD. Circled points highlight the hemispheres shown in (G).

(J) Mean cumulative proportion of cells responding from 0 to 4 odors, pooled from all control (gray; n = 349), or increased-KC *mud* RNAi (red; n = 341) cells. Significance: Kruskal-Wallis test; K-S distance = 0.139. Distributions for each hemisphere shown in Figure S1B.

See also Figure S1 Tables S1 and S2.

Please cite this article in press as: Ahmed et al., Input density tunes Kenyon cell sensory responses in the *Drosophila* mushroom body, Current Biology (2023), https://doi.org/10.1016/j.cub.2023.05.064

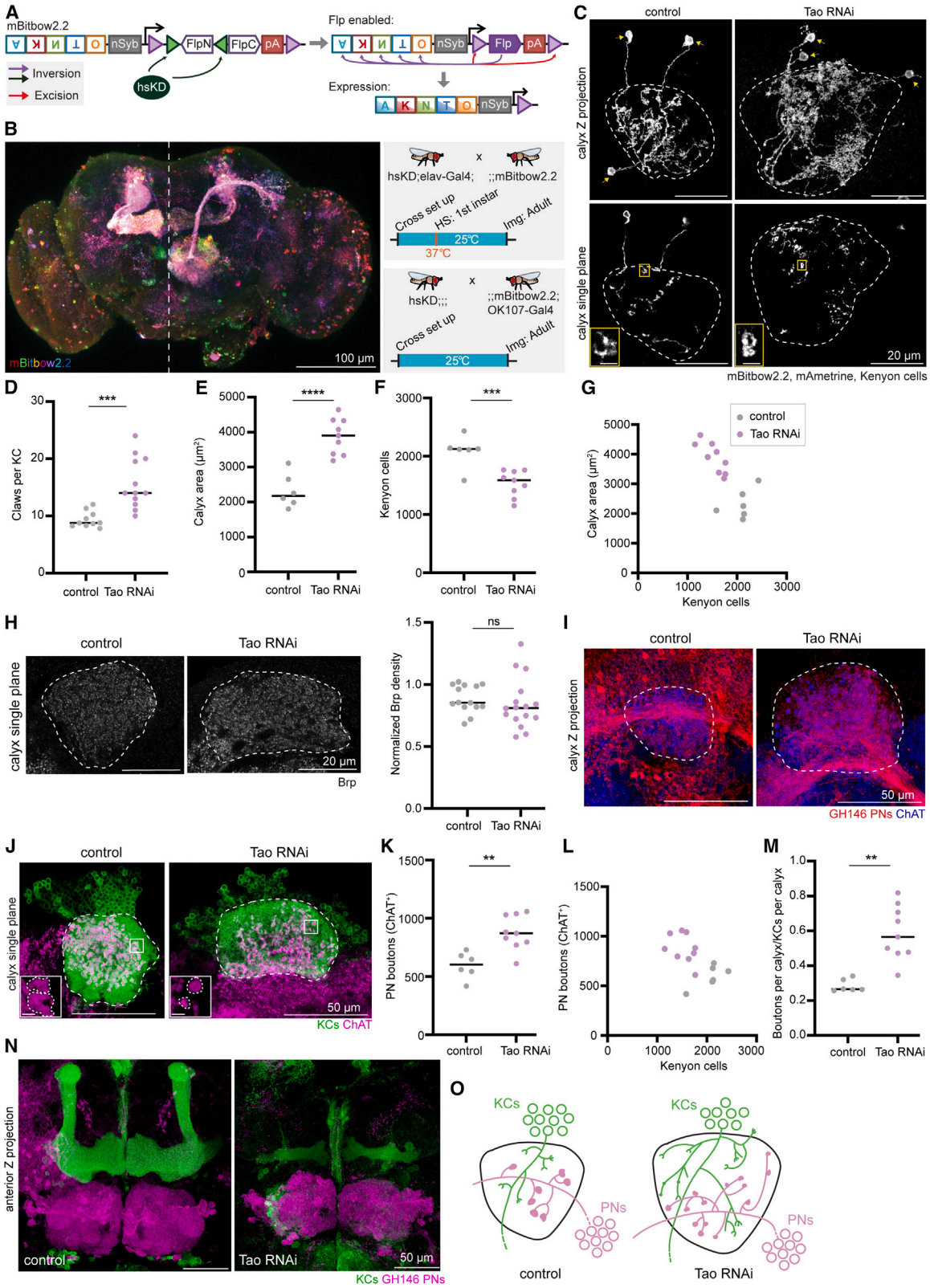

(legend on next page)

Please cite this article in press as: Ahmed et al., Input density tunes Kenyon cell sensory responses in the *Drosophila* mushroom body, Current Biology (2023), https://doi.org/10.1016/j.cub.2023.05.064

with par-1 to regulate microtubule dynamics and dendritic branching.[56–60] We found that knockdown of *Tao* in KCs expanded calyx size. To test if calyx expansion was due to expansion of dendritic arbors, we developed an ultra-sparse, double recombinase version of the Bitbow approach[61,62] that allows us to label ~1/1,000 Gal4-positive cells (Figures 2A, 2B, and S2). We observed a 50% increase in claw number in *Tao* knockdown KCs (Figures 2C–2E). The dendrites also spread out as if "searching" for more connections, occasionally going outside the calyx, and sometimes included highly branched processes that failed to form curved claws (Figures 2C and S2B). KC number decreased by 25% upon *Tao* knockdown; hence, the expansion of dendritic arbors is likely the dominant factor underlying calyx expansion (Figures 2E–2G). Consistent with previous publications, we also observed some KC axons that were missing or misdirected to the calyx.[59] Incursion of axons into the calyx could further inflate calyx area.

Despite the expansion of the calyx size, Brp density did not change (Figure 2H), suggesting that excess claws are each innervated by wild-type numbers of presynaptic sites. We then counted the number of ChAT-positive boutons (STAR Methods; Elkahlah et al.[29]). PN boutons increased with claws (Figures 2I and 2K–2M). Boutons appeared smaller in their cross-sectional area in the *Tao* RNAi animals, suggesting that KC claws might be shaping PN bouton structures (Figure 2J). Additionally, we observed a ventral shift of the PN axon tract in the calyx (Figure 2I). Gross antennal lobe morphology was unaffected (Figure 2N). We expect these anatomic effects would increase the odor inputs to each cell (Figure 2O).

Odor selectivity is reduced in Kenyon cells with increased dendritic claw numbers

We monitored odor responses in *Tao* knockdown KCs using GCaMP6s. Remarkably, twice as many KCs responded to each odor and mineral oil in the increased-dendrite condition (Figures 3A–3D and S3A). In some cases, we even observed all KCs responding to all stimuli (Figure 3A; red outlined points in Figures 3D and 3E). We measured Pearson correlation value between each stimulus and found that pairwise correlations in responses to each stimulus were higher in *Tao* knockdown animals (Figure 3B). We observed a sharp increase in cells that responded to all odors, from <20% in controls to a mean of 40% in increased-dendrite animals (Figures 3E, 3F, and S3B). This marks a striking change in sensory coding: odors no longer activate sparse populations of KCs and individual cells are no longer odor selective. The promiscuity produced by this hard-wired change to KC input number is similar to the effect of acute inhibition of the GABAergic interneuron APL, which scales population-level odor responses to overall sensory drive.[41]

Overexpressing dendritically targeted Dscam1 in Kenyon cells decreases Kenyon cell dendritic claws and odor responses

We next asked if we could reduce the claw number per cell. Dscam1-TM1 isoforms preferentially traffic to dendrites, and ectopic expression of single TM1 isoforms (e.g., Dscam$^{3.36.25.1}$) in KCs was previously shown to disrupt calyx morphology without altering the morphology of KC axons in the mushroom body lobes.[63] To ask if the changes in calyx morphology result from altered KC dendritic arbors, we overexpressed Dscam$^{3.36.25.1}$ in KCs and used mBitbow2.2 to visualize dendritic claws of individual cells (Figure 4A). The median number of claws per cell decreased to 1 (Figure 4B). Although KC number did not change, the calyx became markedly smaller, ChAT-positive boutons declined by half, and the PN axon tract shifted dorsally (Figures 4C–4J). KC axons and antennal lobes retained normal gross morphology, as previously reported (Figure 4K).[63] Overall, these anatomic effects were reciprocal to those in the *Tao* knockdown condition (Figures 2O and 4L).

Compared with controls, about half as many Dscam$^{3.36.25.1}$ KCs responded to each odor (Figures 5A–5C and S4A). 60% of cells responded to no odors, versus 20% in controls (Figures 5D, 5E, and S4B). Altogether, we see a striking change in odor coding in the decreased-dendrite animals: KCs become less

Figure 2. Knocking down *Tao* in Kenyon cells increases dendritic claws per cell and projection neuron bouton production

(A) mBitbow2.2 design. Transgene contains membrane-labeling mBitbow1.0[61] and a KD-controlled, self-excising flippase ("KDonFlp") under control of n-Synaptobrevin (nSyb) promoter. Inducible fluorescent proteins shown are mAmetrine (A), tdKatushka2 (K), mNeonGreen (N), mTFP1 (T), and mKO2 (O). Detailed schematic: Figure S2A; further description provided in the STAR Methods.

(B) Left: representative adult brain Z-projection demonstrating stochastic, dense mBitbow2.2 labeling in neurons, produced by heat shock; dashed line: midline. Right: genetic and temperature schemes for dense neuronal labeling (top) or sparse KC labeling (bottom).

(C) Without heat shock, mBitbow2.2-labels sparse KCs in control and KC>*Tao* RNAi: maximum Z-projection (top), single confocal slice (bottom). Dashed lines: calyx. Arrows: 3 KC soma labeled by mBitbow2.2 mAmetrine. Insets (yellow box): zoom in on a claw (scale bars, 2 μm).
See Figure S2B.

(D–G) Number of dendritic claws per Kenyon cell (D), maximum calyx cross-sectional area (E), number of KCs (F), and relationship between KC number and maximum calyx cross-sectional area (G) in control (gray) and KC>*Tao* RNAi hemispheres (purple). Throughout this figure, each data point represents a single hemisphere, black bars represent medians, and significance is by unpaired t test.

(H) Left: confocal slice showing Brp signal and maximum cross-sectional area (circled) of control and KC>*Tao* RNAi calyces. Right: quantification of Brp density, normalized to protocerebral bridge.

(I) Maximum intensity projection of GH146-labeled PN boutons in the calyx (red) in control and KC>*Tao* RNAi hemispheres. ChAT immunostaining (blue) indicates calyx extent.

(J) Representative confocal slices of control and KC>*Tao* RNAi calyces. OK107 labels KCs (green) and ChAT labels PN boutons (magenta). Dashed lines: calyx. Insets: bouton morphology (scale bars, 2 μm).

(K–M) PN bouton number (K and L) and ratio of ChAT$^+$ boutons per calyx versus KCs per calyx (M).

(N) Maximum intensity projections taken from anterior side of control and KC>*Tao* RNAi brains. KCs (green) show mushroom body lobes, which are diminished in KC>*Tao* RNAi brains. GH146$^+$ PNs (magenta) show antennal lobe and PN cell bodies.

(O) Summary of calyx anatomy.

See also Table S2.

Please cite this article in press as: Ahmed et al., Input density tunes Kenyon cell sensory responses in the *Drosophila* mushroom body, Current Biology (2023), https://doi.org/10.1016/j.cub.2023.05.064

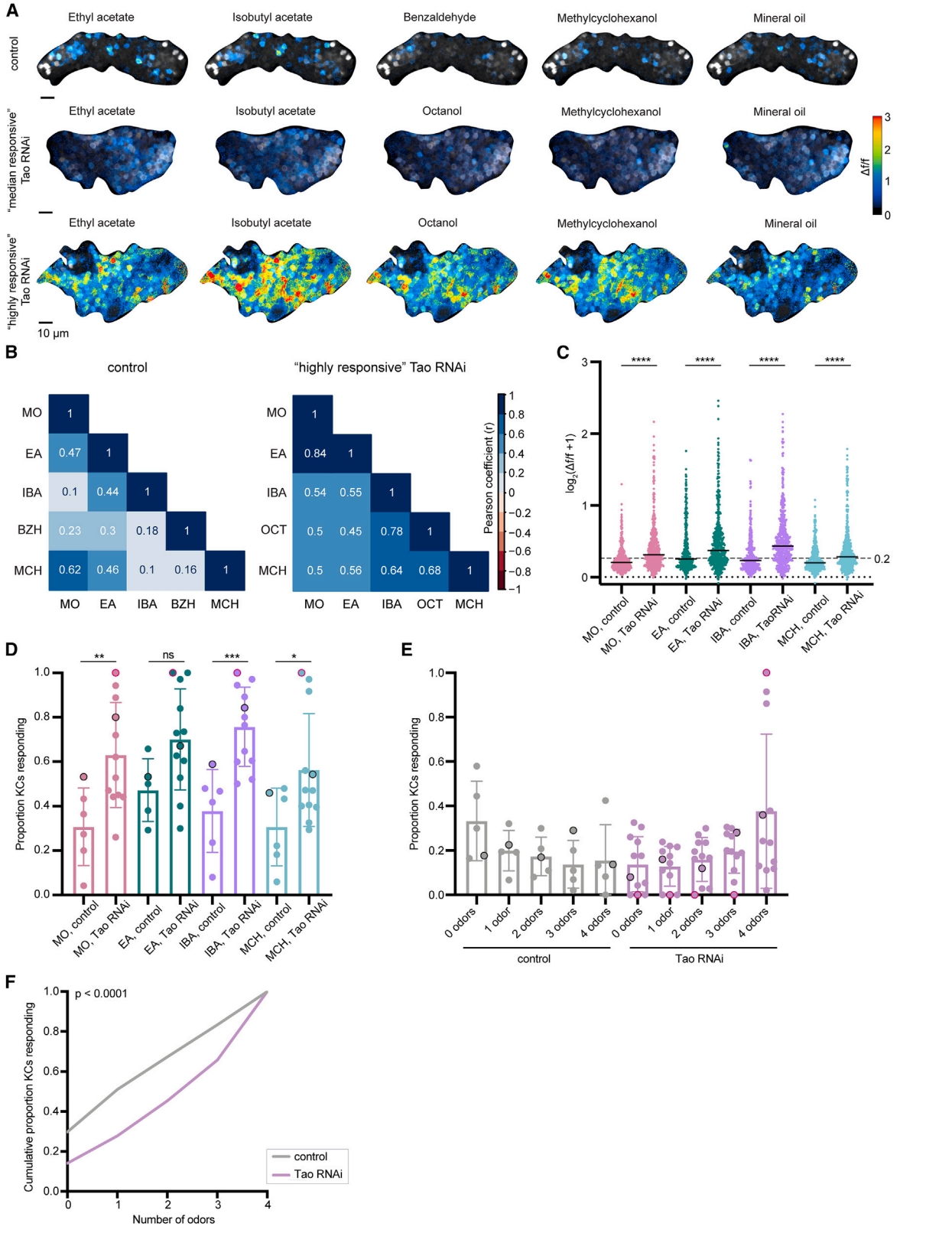

(legend on next page)

Please cite this article in press as: Ahmed et al., Input density tunes Kenyon cell sensory responses in the *Drosophila* mushroom body, Current Biology (2023), https://doi.org/10.1016/j.cub.2023.05.064

responsive to odors, leading to population-level KC responses becoming sparser than controls.

Animals with reduced Kenyon cell numbers learn a two-choice odor association task

To allow association of odor information with contingent events, KCs connect with dopaminergic neurons (DANs) and MBONs in the mushroom body lobes. DANs convey environmental context and can signal positive and negative events; coincident firing of KCs and DANs results in alteration of KC-MBON synaptic weight and modulates future behavioral responses to the same odor.[45,46,64–68] Previous work found that animals without any KCs cannot learn, whereas groups of animals with heterogeneous reductions in KCs have reduced odor learning.[69] We asked how the number of KCs influences associative learning abilities of individual animals.

To generate flies with variably reduced KC numbers, we use mild hydroxyurea (HU) treatment to ablate stochastic sets of KC neuroblasts shortly after larval hatching.[29,69,70] We tested individual HU-treated flies in a recently described Y-maze two-alternative forced-choice task (2AFC),[71] assaying preference for 3-octanol versus 4-methylcyclohexanol before and after one odor was randomly paired with optogenetic reward via stimulation of protocerebral anterior medial (PAM)-DANs (Figure 6A).[72,73] Animals performed 40–60 choices for the naive and rewarded trials. Each fly was dissected post-hoc and immunostained (Figures 6B and S5A). This allowed us to take advantage of the range of phenotypes produced by our manipulations, instead of merging animals with heterogeneous circuit anatomy in a group assay. We labeled the latest born "αβ core" KCs, allowing us to score KC clone number by counting the groups of labeled soma or axon tracts.[29] As HU ablation sometimes affects the neuroblast that gives rise to lateral PNs, we included the Mz19 marker to track the lateral DA1 glomerulus (Figure 6C).[74,75] Almost all animals retained the lateral PN neuroblast in at least one hemisphere (Figures S5C and S5D), whereas the number of KC clonal units varied.

With PAM-DAN reinforcement, sham-treated control animals chose the rewarded odor in 59% of trials on average, compared with 51% prior to training (Figures 6D and S5B).[71] HU-treated but unaffected animals ("[4,4]" set) learned similarly to controls, whereas animals with all 8 clones lost ("[0,0]") failed to learn (Figures 6D and S5B). To our surprise, flies with at least one remaining KC clone ("[1,0]") were still able to increase their preference for the odor paired with PAM-DAN reward. As a result, learning performance did not correlate with number of KC clones (Figure 6E). This is consistent with results that indicate that as few as 25 KCs can be adequate for computationally distinguishing different odors, as well as behavioral effects of partial mushroom body loss in honeybees.[76,77]

Synaptic density remained consistent across animals with different numbers of KCs (Figures 6F and S5E). This supports our previous findings that population-level odor responses in these animals are similar to controls.[29] We note that the odor choices we used for this task were very distinct. Because PAM-DAN optogenetic reinforcement produced relatively weak learning scores in control animals, we did not attempt to subject KC-ablated animals to more difficult discrimination tasks.

Anatomic and functional properties of downstream circuitry in flies with reduced Kenyon cell numbers

As animals with reduced KCs retain the ability to associate odors with rewards, we investigated KC connections to MBONs and DANs in these animals. The axon bundles of KCs form "L"-shaped mushroom body lobes (Figure 6G), including vertical α and α' lobes and horizontal β, β′, and γ lobes. Individual MBONs and DANs innervate discrete, characteristic compartments within these lobes, where individual MBONs receive inputs from KCs and DANs modulate KC-MBON connection strength.[43,50,65] These precise compartmental divisions are expected to allow precise behavioral responses to conditioned stimuli.[44,78,79]

The Mz19 driver labels PAM-DANs that project their axons to the β′2γ5 compartment of the mushroom body (Figure S5A).[80] In flies with reduced KC numbers, and even those that retain only embryonically born γd KCs, we found that β′2γ5 PAM-DANs project to the same region as controls. To examine MBON anatomy and function, we chose the γ2,α′1 MBON, which drives approach behavior when activated,[44] is anatomically compatible with all our KC manipulations (described further below) and can be labeled with R25D01-LexA (Figure 6G). Dendrites of γ2,α′1 MBON arborize at the intersection of vertical and horizontal lobes of the mushroom body and receive inputs from both γ and α' lobes.[50] This position was retained in KC-reduced, shrunken lobes (Figure 6G, inset). In HU-fully ablated animals, embryonic-born γd KCs are retained to form part of the γ lobe.[81] γ2,α′1 MBON dendrites were seen throughout the γ lobe in the transverse plane and slightly extended along the lobe in the coronal Z-projection (Figure 6G). Consistent with a recent study of MBON morphology in

Figure 3. Odor selectivity is reduced in Kenyon cells with increased dendritic claw numbers

(A) Example KC somatic odor responses in control, median-responsive KC>*Tao* RNAi, and extremely responsive KC>*Tao* RNAi hemispheres. Grayscale backdrop indicates the cells. Control dataset throughout this figure is the same data as controls for *mud* RNAi condition in Figure 1, and the sample shown in (A) is rescaled from Figure 1G. We discuss use of octanol versus benzaldehyde in the STAR Methods.

(B) Pearson correlation matrix shows the linear relation between each pairwise odor comparison across the cells for the control and "highly responsive" KC>*Tao* RNAi image shown in (A). r can range from −1 to +1, but we did not observe negative correlations.

(C) Peak odor responses of aggregated cells. Dashed line: 0.2 Δf/f threshold. Black horizontal bars: medians. Significance: Mann-Whitney test. n = 349–404 control cells, 496 *Tao* RNAi cells for each stimulus.

(D) Proportion of cells in each hemisphere responding to each odor above 0.2 Δf/f threshold. Significance: unpaired t test.

(E) Proportion cells responding to 0–4 odors. Bar plots in (D) and (E) show mean ± SD, black circled points correspond to the control, and "median responsive" *Tao* RNAi images shown in (A), red circled points correspond to highly responsive image in (A).

(F) Mean cumulative proportion of cells responding from 0 up to 4 odors, pooled from all control (gray; n = 349) and *Tao* RNAi cells (purple; n = 496). Significance: Kruskal-Wallis test; K-S distance = 0.2318. Distributions for each hemisphere shown in Figure S3B.

See also Table S2.

Please cite this article in press as: Ahmed et al., Input density tunes Kenyon cell sensory responses in the *Drosophila* mushroom body, Current Biology (2023), https://doi.org/10.1016/j.cub.2023.05.064

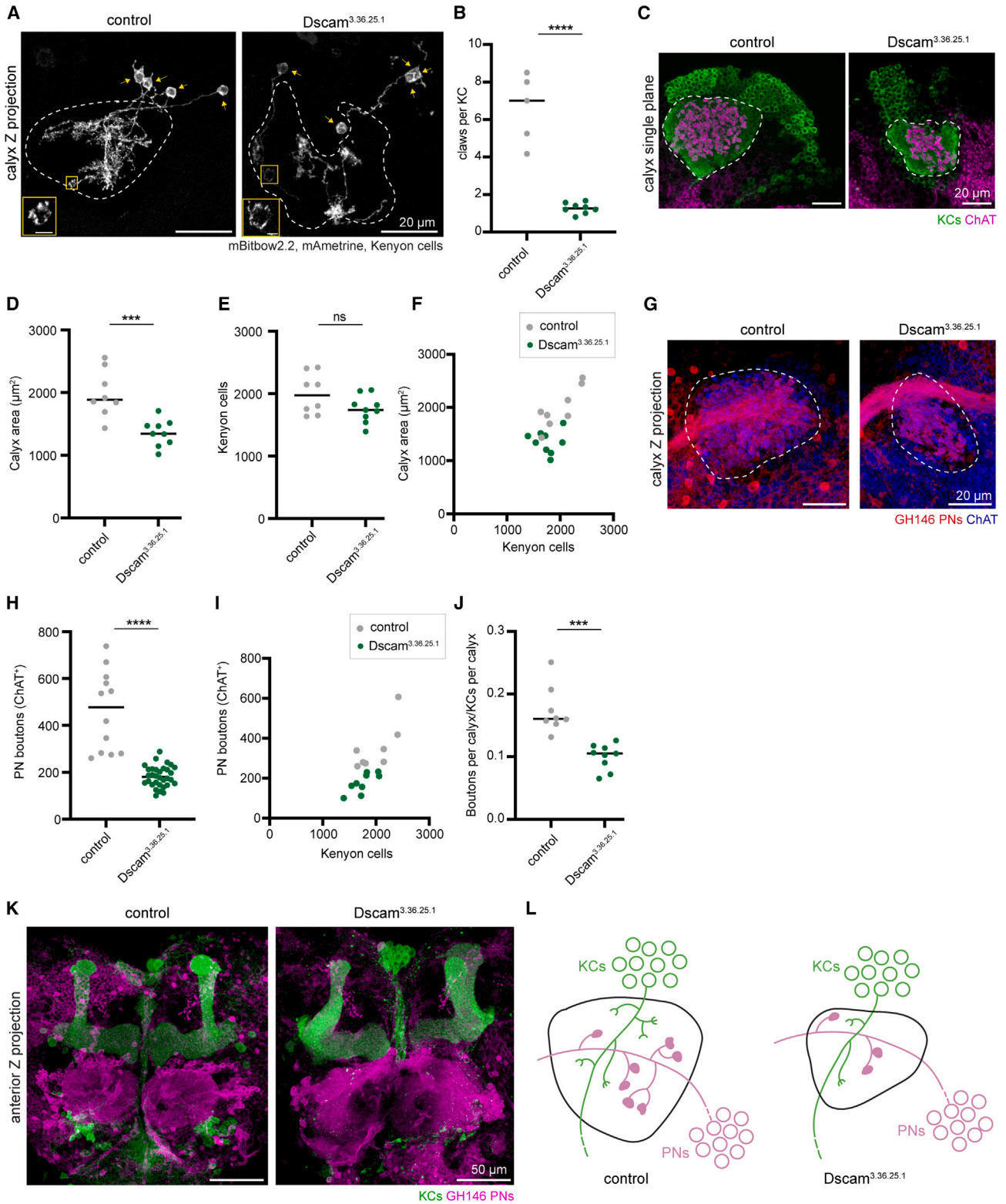

Figure 4. Overexpressing dendritically targeted Dscam1 in Kenyon cells decreases dendritic claws per cell

(A) Maximum intensity Z-projections of mBitbow2.2-labeled KCs in control and KC>*Dscam*$^{3.36.25.1}$ calyces. Dashed lines: calyx. Arrows: KC somata. Insets: claw structure, brightened for visualization (scale bars, 2 µm).

(legend continued on next page)

Please cite this article in press as: Ahmed et al., Input density tunes Kenyon cell sensory responses in the *Drosophila* mushroom body, Current Biology (2023), https://doi.org/10.1016/j.cub.2023.05.064

HU-fully ablated animals, we also observed sparser innervation of γ2,α′1 MBON dendrites in the lobes, with slight extension outside the lobes.[82]

We imaged odor responses of γ2,α′1 MBON axonal arbor in animals with partial KC ablation (Figure 6H). Peak responses were comparable between sham and partially ablated animals (Figures 6H, 6I, and S5F). There was no correlation between peak odor response and calyx area (Figure S5G).[29] This indicates that a reduced population of KCs can successfully transmit signals to the γ2,α′1 MBONs.

Associative learning abilities of animals with increased Kenyon cell numbers or altered dendrite numbers

We next tested the learning capabilities of individual OK107> *mud* RNAi and *Tao* RNAi flies, with expanded KC repertoire or claw number, respectively. Again, mushroom body anatomy was evaluated by post-hoc staining. In this set of experiments, we provided optogenetic reward using Gr64f$^+$, sugar-sensing gustatory neurons, which improved learning in controls (Figure 7A); we discuss this difference in Rajagopalan et al.[71] All three genotypes showed robust, odor-specific learning (Figures 7B and 7C). Surprisingly, learning improved with increasing calyx size in the *mud* RNAi animals, suggesting that increasing the size of the KC repertoire gives animals more power to discriminate odors, form learned associations, or use learned associations to guide decisions (Figure 7D). The robust odor associations formed by flies with excess KC claws are also surprising, as the weakened KC odor selectivity in these animals should make odor discrimination more difficult. One possibility is that these two odors are still sufficiently different at the level of KCs to be decodable.

We therefore sought to test fine odor discrimination ability in animals with excess or diminished claws on each KC. As *Tao* RNAi and Dscam[TM1] overexpressing animals have relatively consistent calyx anatomy, we used a group learning assay, the circular arena.[64,83] We chose two chemically similar odors that activate overlapping sets of KCs, pentyl acetate and butyl acetate. During the learning phase, one odor was paired with optogenetic reward via Gr64f neuron stimulation (Figure 7E, top). In test trials, the distribution of animals in the quadrants of the arena was measured before and after the odors were presented (Figure 7E, bottom). Upon odor onset, control animals redistributed into quadrants containing the rewarded odor, demonstrating that they can discriminate it from the similar odor in the other quadrants, as observed previously. Animals with excess claws per KC were distributed randomly among odor quadrants, whereas animals with fewer claws per KC moved into quadrants containing the rewarded odor in proportions similar to controls but showed delayed choice kinetics (Figures 7E and S6A). The chance-level performance of excess-claw, *Tao* RNAi animals is consistent with the expectation that increased representation overlap will degrade discrimination behavior, whereas the slow responses of animals with diminished claws suggest these animals may have dampened odor detection.

MBON odor responses are robust to increasing Kenyon cell number or claw number

To examine functional connections downstream of KCs, we chose the γ2,α′1 MBON because the γ lobe is retained in both OK107>*Tao* RNAi and *mud* RNAi animals in our behavioral strain background (Figure 2N).[59] Dendrites of the γ2,α′1 MBON projected to the same compartment in the *mud* RNAi and *Tao* RNAi animals as in controls (Figure 7F). In *Tao* RNAi animals, γ2,α′1 MBON dendrites were seen throughout the remaining γ lobe (Figure 7F, inset). In both genotypes, this MBON responded to all four odors (Figure 7G). Peak odor responses were comparable between control and *mud* RNAi animals, and odor responses did not correlate with calyx size (Figures 7G, 7H, S6B, and S6C). Peak odor responses to EA and IBA were significantly higher in *Tao* RNAi animals compared with control animals (Figures 7H and S6B), consistent with our result above that *Tao* RNAi KCs receive increased input from PNs (Figure 3). In conclusion, γ2,α′1 MBON shows robust functional input from KCs, regardless of manipulation of KC number or claw number. This provides an anatomical basis for the robust learning we reported in these conditions.

DISCUSSION

Here, we have initiated a new method, developmental hacking of circuit wiring, to test how specific circuit parameters of the arthropod expansion layer influence cognitive computations. Using chemical and genetic approaches, we increase and decrease KC number and KC input density. This approach adds to a growing body of literature in which researchers engineer cell biological changes to neurons in order to probe developmental algorithms or change circuit function.[84–92] We find that changing KC number, and thus expansion ratio, has minimal effect on KC odor representation. Moreover, animals with diminished KC repertoires can still make simple learned associations, and animals with larger numbers of KCs show improved two-choice odor learning. These findings suggest that the developmental algorithms we and others identified previously, which prioritize relationships among circuit layers rather than cellular precision, allow nervous systems to be computationally robust.[29,93,94] Second, we confirm the Marr-Albus theory *in vivo*,

(B) Quantification of KC claws in control (gray) and KC>*Dscam*$^{3.36.25.1}$ (green) hemispheres.
(C) Representative confocal slices of control and KC>*Dscam*$^{3.36.25.1}$ calyx. OK107 labels KCs (green) and ChAT labels PN boutons (magenta). Dashed lines: calyx.
(D–F) Maximum calyx cross-sectional area (D), number of KCs (E), and the relationship between KC number and maximum calyx cross-sectional area (F) in control (gray) and KC>*Dscam*$^{3.36.25.1}$ hemispheres (green).
(G) Maximum intensity projection of calyx bouton production by GH146$^+$ PNs (red) in control and KC>*Dscam*$^{3.36.25.1}$ hemispheres. ChAT immunostaining (blue) highlights calyx extent (circled).
(H–J) PN bouton number (H and I), and ratio of ChAT$^+$ boutons per KC (J) in control (gray) and KC>*Dscam*$^{3.36.25.1}$ hemispheres (green).
(K) Maximum intensity projection of confocal stacks taken from anterior side of control and KC>*Dscam*$^{3.36.25.1}$ brains. KCs (green) show the mushroom body lobes, GH146$^+$ PNs (magenta) show the antennal lobe and PN cell bodies.
(L) Model of KC>*Dscam*$^{3.36.25.1}$ calyx. Throughout this figure, significance: unpaired t test, black horizontal bars: medians.
See also Table S2.

Please cite this article in press as: Ahmed et al., Input density tunes Kenyon cell sensory responses in the *Drosophila* mushroom body, Current Biology (2023), https://doi.org/10.1016/j.cub.2023.05.064

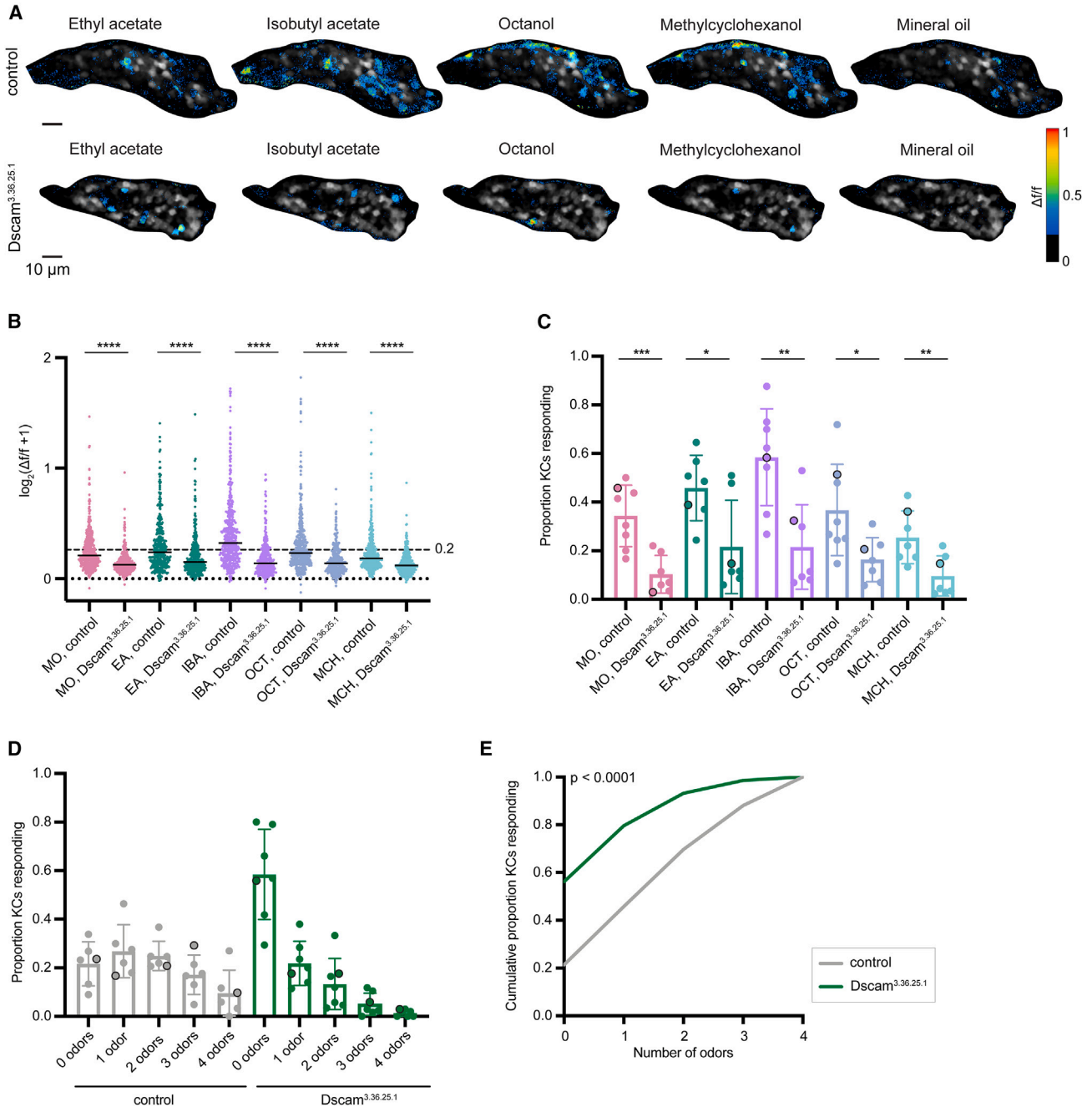

Figure 5. Kenyon cells with fewer claws are less responsive to odors

(A) KC somatic odor responses in control and KC>*Dscam*$^{3.36.25.1}$ hemispheres. Grayscale backdrop indicates the cells.

(B) Peak odor responses of aggregated cells. Dashed line: 0.2 Δf/f threshold. Black horizontal bars: medians. Significance: Mann-Whitney test. n = 380–428 control cells, 372 Dscam$^{3.36.25.1}$ cells for each odor.

(C) Proportion of cells in each hemisphere responding to each odor above 0.2 Δf/f threshold. Significance: unpaired t test.

(D) Proportion of cells in each hemisphere responding to 0, 1, or multiple odors. Bar plots in (C) and (D) show mean ± SD, and black circled data points correspond to the images shown in (A).

(E) Mean cumulative proportion of cells responding from 0 up to 4 odors from all control (gray; n = 369) and Dscam$^{3.36.25.1}$ cells (green; n = 338). Significance: Kruskal-Wallis test; K-S distance = 0.348. Distributions for each hemisphere shown in Figure S4B.

See also Table S2.

Please cite this article in press as: Ahmed et al., Input density tunes Kenyon cell sensory responses in the *Drosophila* mushroom body, Current Biology (2023), https://doi.org/10.1016/j.cub.2023.05.064

CellPress

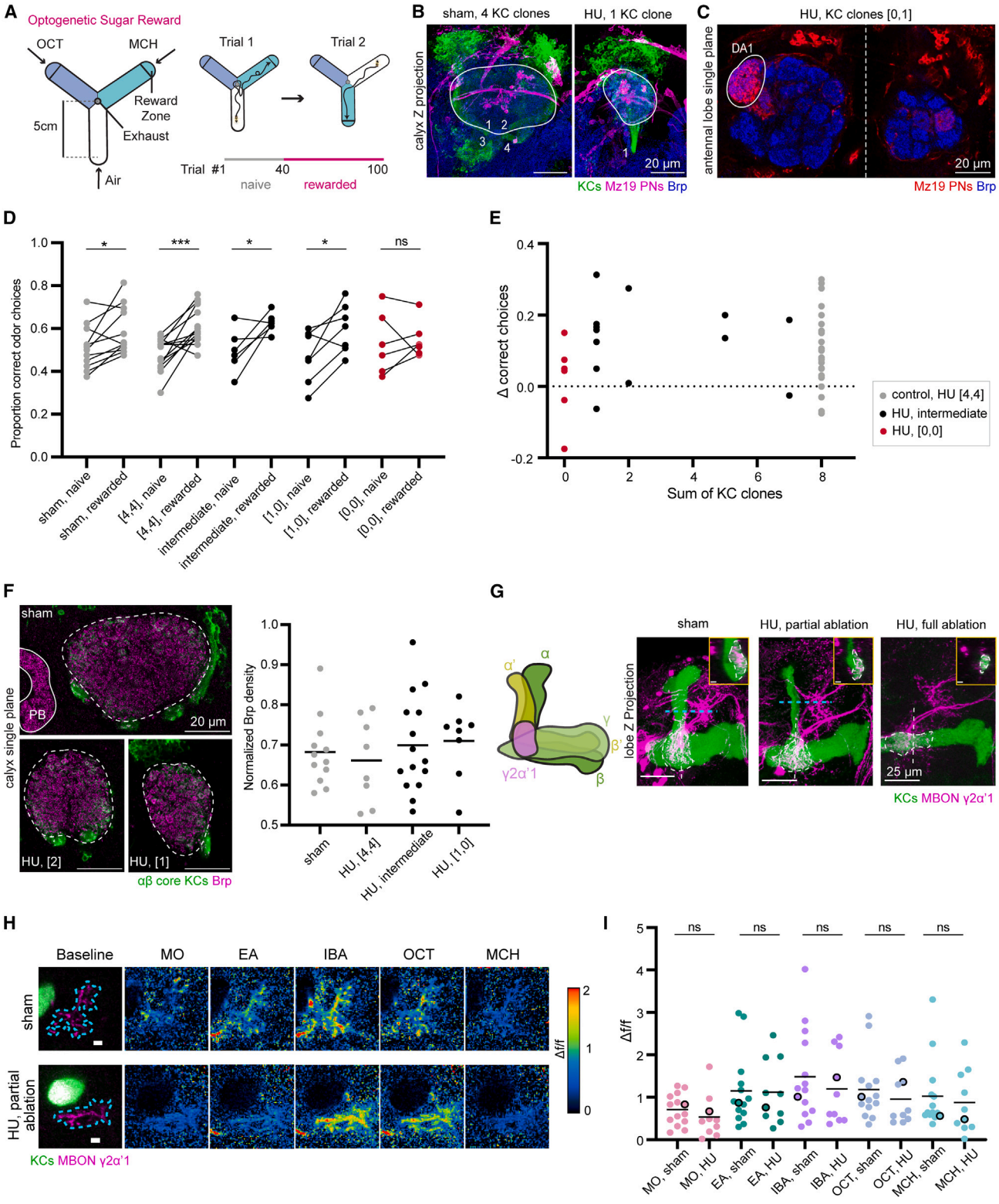

Figure 6. Associative learning and feedforward functional responses in flies with reduced Kenyon cell numbers

(A) Schematic of Y-arena and 2AFC task. Entering the reward zone is considered a choice; then the two odors are randomly re-assigned to the arms for the next trial. During rewarded trials, entering reward zone for a specific odor triggers a 500 ms pulse of red light (optogenetic reward).

(legend continued on next page)

Please cite this article in press as: Ahmed et al., Input density tunes Kenyon cell sensory responses in the *Drosophila* mushroom body, Current Biology (2023), https://doi.org/10.1016/j.cub.2023.05.064

finding that lowering KC input density makes KCs more stringent in their odor responses, whereas raising input density makes them more promiscuous. Finally, animals with *Tao* knocked down in KCs, which results in excess KC claws, promiscuous KC odor responses, and disrupted KC axons, remain adept at two-choice odor learning if the stimuli are very distinct. However, these animals fail at discriminating chemically similar odors, whereas animals with fewer claws per KC were able to achieve this discrimination. This highlights the significance of having a low overlap of odor representations in KCs in order to allow odor discrimination at the behavioral level. Future behavioral analyses of animals with these diverse mushroom body architectures will allow us to assess in detail the effects on sensory sensitivity, discrimination, generalization, and memory storage.

Characteristics of expansion layer neurons govern both input and output weights

Although neurons of all expansion layers receive multiple inputs, KCs of the mushroom body have the special "keystone" property of connecting all local sensory inputs to a multitude of neurons that govern behavioral outputs. In previous work, we showed that the connectivity relationship between presynaptic olfactory PNs and postsynaptic KCs is set by the KCs. When we varied KC number and PN number, the number of inputs to individual KCs always averaged 5–6 per cell.[29] This wiring algorithm requires developmental flexibility from PNs and maintains odor coding across variable KC repertoires. Just as PNs adjust to KC numbers, we find that MBONs adjust to KC numbers. MBONs were able to be activated to a similar level by KC repertoires varying by almost an order of magnitude. Previous work on the $\alpha'2$ MBON showed that this cell can seek input from alternative KC partners when its preferred KCs are lost.[82] The functional robustness we observe could result from developmental compensation, if MBONs seek a particular complement of input synapses from KCs regardless of cell number. MBON response scaling to KC number could also be produced by APL, an inhibitory neuron that feeds back on KCs to sparsen their firing.[41] Recent work suggests that APL provides local feedback inhibition.[95–97] Successful functional compensation by APL would require that APL scaling is itself either developmentally or functionally robust to changes in KC number.

In contrast to the developmental accommodation that MBONs make for KC number, excess KC activity in the *Tao* knockdown case propagates forward and produces excess MBON activity in response to some odors. This compensation failure could point to developmental mechanisms at the KC-MBON synapse that are not influenced by sensory activity.[98,99] In this condition, APL scaling is clearly unable to "fix" either KC population responses to odors or propagation of these odor responses to MBONs. Whether the functional promiscuity induced by *Tao* knockdown is beyond APL's capability to fix, or whether APL's innervation of the mushroom body is altered in this case will require additional research.

Effect of *Tao* knockdown and ectopic *Dscam1* expression on Kenyon cell anatomy and function

Different kinds of neurons have diverse dendritic branching patterns; these patterns are specified as an aspect of cell identity and are consistent for the same neuron types across animals.[100] We found that *Tao* may universally restrain dendritic branching: just as reducing *Tao* expression in the sensory periphery results in arbor overgrowth, reducing *Tao* in KCs allows their dendrites to grow more complex.[58] It is possible that *Tao* levels naturally vary across cells of different dendritic complexity, as do levels of *cut* and *knot*.[100]

In our experiments, we ectopically expressed a single Dscam1 [TM1] isoform, which traffics to dendrites, across all KCs. We assume that when KC dendrites all carry the same Dscam ectodomain, inter-neuronal repulsion limits arbor growth.[101–103] In this condition, elongating dendritic neurites of KCs might experience a terrain similar to that encountered by the train Tootle when he jumps off the tracks: everywhere he turns, he sees a stop sign.[104] KC claws that form appear to make anatomically normal connections with PNs, and KCs still respond functionally to odors. Just as the expansion of KC dendrites in the *Tao* knockdown condition prompts PNs to produce more boutons than is typical for

(B) Maximum intensity Z-projections of calyces from sham- and HU-treated animals. 58F02 labels $\alpha\beta$ core KCs (green). Mz19 labels ~16 PNs (magenta). Brp (blue) marks synapses. White outline: calyx. Numbers count 58F02$^+$ neurite bundles (i.e., KC clones) innervating the pedunculus when traced through the stack.
(C) Single slice of the antennal lobes from a HU-treated brain with 1 KC clone in the left hemisphere, and no clones in the right hemisphere. Dotted line: midline of the central brain. Mz19 labels the DA1 glomerulus (circled), allowing scoring of the lNB/BAlc PN neuroblast; it is ablated in the right hemisphere and DA1 glomerulus is lost.
(D) Proportion of correct odor choices in naive and rewarded trials. Each data point is one fly. Sham-treated and unaffected, HU-treated animals are displayed in gray, intermediate HU-treated clone numbers in black, and fully ablated "[0,0]" HU-treated animals in red. Jitter added in this plot and (E) to display all the data points. Significance: paired t test. See also Figure S5B.
(E) Relationship between Δ correct choices between rewarded versus naive trails, and sum of KC clones from both hemispheres (0–8). No correlation was observed. See Figures S5C and S5D for relation with lNB/BAlc ablation.
(F) Left: confocal slice with maximum calyx cross-sectional area of sham and HU-treated calyces (bottom left, 2 KC clones; bottom right, 1 KC clone). Dashed lines: calyx. Part of the protocerebral bridge (PB) is included in the sham image. Right: quantification of Bruchpilot density, normalized to protocerebral bridge. Black bars: medians. All pairwise comparisons are non-significant by unpaired t test. See also Figure S5E.
(G) Left: schematic of the mushroom body lobe anatomy with KCs (green) and $\gamma2\alpha'1$ MBON dendrite compartment (magenta). Right: maximum intensity Z-projections of MB lobe with KCs (green) and $\gamma2\alpha'1$ MBON (magenta) in sham and HU-treated animals. MBON compartment is circled with a dashed line. Inset: lateral view of MBON compartment (scale bars, 5 μm). Corresponding location is indicated by white dashed vertical line. Blue dashed line: focal plane for calcium imaging of MBON axonal terminals in (H) and (I). See Figure S5A for effect on PAM-DAN arbors.
(H) Example $\gamma2\alpha'1$ MBON axonal odor responses in sham and HU-treated hemispheres. Left: focal plane of KC vertical lobe (green) and baseline GCaMP6s signal in MBON axonal terminals (magenta). Blue dashes: ROI used to measure odor responses. Scale bars, 5 μm. Right: responses to odors. See also Figure S5F.
(I) Peak odor responses of all MBON axonal ROIs. Each dot is one hemisphere. Only treated hemispheres with maximum cross-sectional calyx area less than every control (<2,100 μm^2) are included (Figure S5G). Black horizontal bars: mean. Significance: unpaired t test. Black circled points: samples shown in (H). See also Table S2.

Please cite this article in press as: Ahmed et al., Input density tunes Kenyon cell sensory responses in the *Drosophila* mushroom body, Current Biology (2023), https://doi.org/10.1016/j.cub.2023.05.064

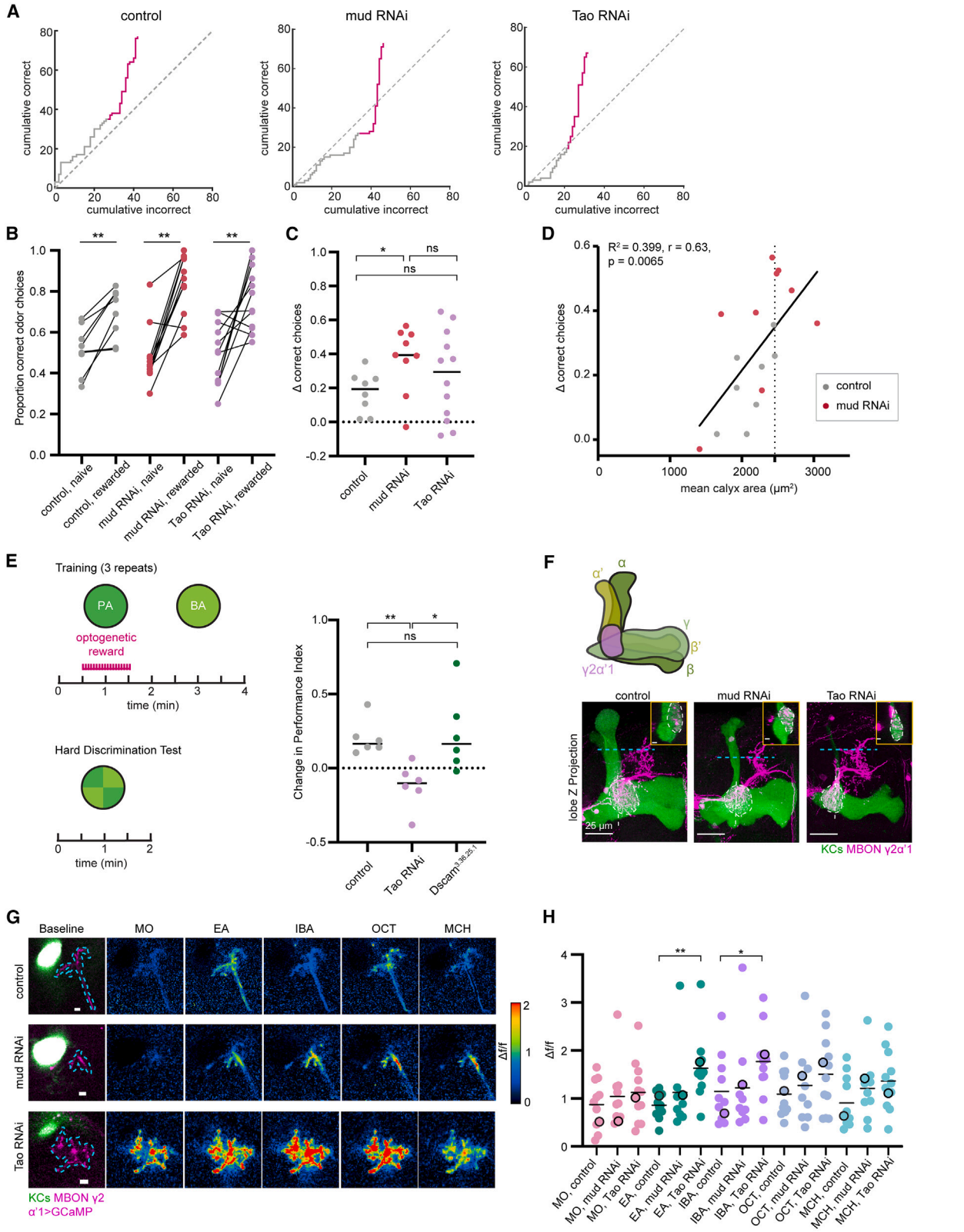

(legend on next page)

that number of KCs, claw reduction via ectopic Dscam1[TM1] expression results in PNs producing fewer boutons per KC. Together, these results suggest that PN bouton development is quantitatively matched to the KC claw number.

Claw number and strength are independent variables determining the sparsity of Kenyon cell odor responses

In wild-type animals, KCs are more stringent in their firing than PNs, which is thought to allow them to encode glomerular combinations and thus separate olfactory patterns.[39,105–108] When we forced KCs to make fewer claws, a smaller proportion of cells responded to each odor than in wild type; when we forced KCs to make more claws, a larger fraction of cells responded to each odor, and some cells responded to all odors. Although an altered number of active inputs will reasonably change the responsiveness of individual KCs and the sparsity of odor responses on the population level, these results suggest a consistent KC firing threshold. In our prior work, we found that KCs in wild-type animals were very likely to be activated when at least three of their inputs were active, that two active inputs often sufficed, and that one active input could activate a KC in certain conditions.[39] We considered two models for how KC spike threshold would be affected in our manipulations: (1) the number of active claws needed to spike the KC is proportional to the total number of claws or (2) the number of active claws needed to spike the KC is constant. Our Brp staining results suggest that synaptic input per claw does not vary with claw number in our manipulations. Moreover, in model (1), KCs would become less responsive to odors as the claw number grows, which is the opposite of what we observe. Our results thus favor model (2), as described further in Tables S1 and S2 and the preprint version of this paper.[109]

Therefore, claw number and claw strength appear to be developmentally uncoupled. Our results highlight that the evolutionary optimization of combinatorial coding requires a precise relationship between the dendrite structure of expansion layer neurons and their spike threshold, which are likely controlled by distinct developmental mechanisms.

STAR★METHODS

Detailed methods are provided in the online version of this paper and include the following:

- KEY RESOURCES TABLE
- RESOURCE AVAILABILITY
  - Lead contact
  - Materials availability
  - Data and code availability
- EXPERIMENTAL MODEL AND SUBJECT DETAILS
  - Flies
- METHOD DETAILS
  - Immunostainings
  - Molecular cloning of mBitbow2.2
  - HU ablation
  - Identification of relevant MBON driver lines
  - *In vivo* functional imaging
  - Analysis of KC somatic odor responses
  - Analysis of MBON odor responses
  - Y-arena
  - Behavioral Protocol
- QUANTIFICATION AND STATISTICAL ANALYSIS
  - Image analysis
  - Behavior analysis
  - Statistical considerations

SUPPLEMENTAL INFORMATION

Supplemental information can be found online at https://doi.org/10.1016/j.cub.2023.05.064.

ACKNOWLEDGMENTS

We thank BDSC, Bing Ye, and Tzumin Lee for stocks; MCDB Imaging Facility and Gregg Sobocinski for confocal microscopy assistance; and Clowney lab members for comments on the manuscript. Funding provided by NIDCD R01DC018032 and Sloan Research Fellowship to E.J.C., Janelia Visiting

Figure 7. Effect of increasing Kenyon cell number or claw number on associative learning and feedforward functional responses

(A) Example learning curves of individual flies are plotted to show cumulative correct and incorrect odor choices across all trials. Gray and pink lines indicate naive and rewarded trials respectively (40–60 trials each). Dotted line (y = x) displays equal preference.

(B) Proportion of correct odor choices made in naive and rewarded trials, in control (gray), KC>*mud* RNAi (red), and KC>*Tao* RNAi (purple) animals. Each data point is an individual fly. Jitter added in this plot and (C) to display all the data points. Significance: paired t test.

(C) Difference (Δ) in correct choices made in rewarded versus naive trials in control (gray), KC>*mud* RNAi (red), and KC>*Tao* RNAi (purple) animals. Black horizontal bars: median. Significance: unpaired t test.

(D) Δ correct choices plotted against inter-hemisphere mean calyx area for each animal in control and KC>*mud* RNAi conditions. Black line: linear fit. Dotted line: largest control calyx.

(E) Left: schematic of circular arena and hard discrimination task. In training, one of the odors (PA, pentyl acetate or BA, butyl acetate) is paired with an optogenetic reward. During test trials, the positions of all animals (15–20 animals/assay) are recorded before and during odor presentation. Right: change in performance index is calculated by comparing distribution of animals in rewarded-odor quadrants to their distribution before odor onset, as described.[64,83] Each dot is one group assay. Behavior traces over time are provided in Figure S6A.

(F) Maximum intensity Z-projections of MB lobe with KCs (green) and MBONs γ2α′1 (magenta) in control, *mud* RNAi and *Tao* RNAi animals. Dashed circle: MBON compartment. Inset: lateral view of MBON compartment at the location of the white dashed vertical line (scale bars, 5 μm). Blue dashed line: focal plane for MBON axonal terminals in (G) and (H).

(G) Example MBON axonal odor responses in control, *mud* RNAi, and *Tao* RNAi animals. Left: focal plane of KC vertical lobe (green) and baseline GCaMP6s signal in MBON axonal terminals (magenta). Blue dashes outline the ROI used to measure odor responses. Scale bars, 5 μm. Right: responses to odors. See also Figure S6B.

(H) Peak odor responses of all MBON axonal ROIs; each dot is one hemisphere. For *mud* RNAi, only hemispheres greater than every control (>2,200 μm^2) are included (Figure S6C). Black horizontal bars: mean peak responses. Peak responses of *mud* RNAi and *Tao* RNAi are compared with control using unpaired t tests. Non-significant comparisons are not shown. Black circled points: samples shown in (G).

See also Table S2.

Scientist Program and Rackham Predoctoral Fellowship to M.A., NIMH R01MH110932 to D.C., and HHMI to G.C.T. E.J.C. is the Rita Allen Foundation Milton Cassel Scholar, a McKnight Scholar, and a Pew Biomedical Scholar.

AUTHOR CONTRIBUTIONS

M.A. and E.J.C. conceived the project and coordinated all authors. M.A. performed genetic discovery experiments, anatomic analyses, and Kenyon cell functional imaging with assistance of D.L.W., M.T., and E.A.P. A.E.R. designed and performed behavioral analyses with M.A. under supervision of G.C.T. Y.P. designed and performed MBON experiments. Y.L. and D.C. created mBitbow 2.2. The Janelia Project Technical Resources team led by Gudrun Ihrke performed histology and imaging for behavioral analyses (K.C.C., C.P.C., and Yisheng He). A.P. improved HU ablation methods. M.A., E.J.C., and Y.P. wrote the manuscript with contributions from Y.L. and A.E.R.

DECLARATION OF INTERESTS

The authors declare no competing interests.

INCLUSION AND DIVERSITY

One or more of the authors of this paper self-identifies as an underrepresented ethnic minority in science. We support inclusive, diverse, and equitable conduct of research.

Received: February 5, 2023
Revised: May 2, 2023
Accepted: May 26, 2023
Published: June 21, 2023

REFERENCES

1. Wong, A.M., Wang, J.W., and Axel, R. (2002). Spatial representation of the glomerular map in the Drosophila protocerebrum. Cell *109*, 229–241.
2. Sosulski, D.L., Bloom, M.L., Cutforth, T., Axel, R., and Datta, S.R. (2011). Distinct representations of olfactory information in different cortical centres. Nature *472*, 213–216. https://doi.org/10.1038/nature09868.
3. Miyamichi, K., Amat, F., Moussavi, F., Wang, C., Wickersham, I., Wall, N.R., Taniguchi, H., Tasic, B., Huang, Z.J., He, Z., et al. (2011). Cortical representations of olfactory input by trans-synaptic tracing. Nature *472*, 191–196. https://doi.org/10.1038/nature09714.
4. Marin, E.C., Jefferis, G.S.X.E., Komiyama, T., Zhu, H., and Luo, L. (2002). Representation of the glomerular olfactory map in the Drosophila brain. Cell *109*, 243–255.
5. Ghosh, S., Larson, S.D., Hefzi, H., Marnoy, Z., Cutforth, T., Dokka, K., and Baldwin, K.K. (2011). Sensory maps in the olfactory cortex defined by long-range viral tracing of single neurons. Nature *472*, 217–220. https://doi.org/10.1038/nature09945.
6. Tanaka, N.K., Awasaki, T., Shimada, T., and Ito, K. (2004). Integration of chemosensory pathways in the Drosophila second-order olfactory centers. Curr. Biol. *14*, 449–457. https://doi.org/10.1016/j.cub.2004.03.006.
7. Chin, S.G., Maguire, S.E., Huoviala, P., Jefferis, G.S.X.E., and Potter, C.J. (2018). Olfactory neurons and brain centers directing oviposition decisions in Drosophila. Cell Rep. *24*, 1667–1678. https://doi.org/10.1016/j.celrep.2018.07.018.
8. Clowney, E.J., Iguchi, S., Bussell, J.J., Scheer, E., and Ruta, V. (2015). Multimodal chemosensory circuits controlling male courtship in Drosophila. Neuron *87*, 1036–1049. https://doi.org/10.1016/j.neuron.2015.07.025.
9. Fişek, M., and Wilson, R.I. (2014). Stereotyped connectivity and computations in higher-order olfactory neurons. Nat. Neurosci. *17*, 280–288. https://doi.org/10.1038/nn.3613.
10. Jefferis, G.S.X.E., Potter, C.J., Chan, A.M., Marin, E.C., Rohlfing, T., Maurer, C.R., and Luo, L. (2007). Comprehensive maps of Drosophila higher olfactory centers: spatially segregated fruit and pheromone representation. Cell *128*, 1187–1203. https://doi.org/10.1016/j.cell.2007.01.040.
11. Kobayakawa, K., Kobayakawa, R., Matsumoto, H., Oka, Y., Imai, T., Ikawa, M., Okabe, M., Ikeda, T., Itohara, S., Kikusui, T., et al. (2007). Innate versus learned odour processing in the mouse olfactory bulb. Nature *450*, 503–508. https://doi.org/10.1038/nature06281.
12. Lin, D., Boyle, M.P., Dollar, P., Lee, H., Lein, E.S., Perona, P., and Anderson, D.J. (2011). Functional identification of an aggression locus in the mouse hypothalamus. Nature *470*, 221–226. https://doi.org/10.1038/nature09736.
13. Root, C.M., Denny, C.A., Hen, R., and Axel, R. (2014). The participation of cortical amygdala in innate, odor-driven behavior. Nature *515*, 269–273. https://doi.org/10.1038/nature13897.
14. Troemel, E.R., Kimmel, B.E., and Bargmann, C.I. (1997). Reprogramming chemotaxis responses: sensory neurons define olfactory preferences in C. elegans. Cell *91*, 161–169. https://doi.org/10.1016/S0092-8674(00)80399-2.
15. Wang, L., Gillis-Smith, S., Peng, Y., Zhang, J., Chen, X., Salzman, C.D., Ryba, N.J.P., and Zuker, C.S. (2018). The coding of valence and identity in the mammalian taste system. Nature *558*, 127–131. https://doi.org/10.1038/s41586-018-0165-4.
16. Albus, J.S. (1971). A theory of cerebellar function. Math. Biosci. *10*, 25–61. https://doi.org/10.1016/0025-5564(71)90051-4.
17. Ito, M. (1972). Neural design of the cerebellar motor control system. Brain Res. *40*, 81–84.
18. Marr, D. (1969). A theory of cerebellar cortex. J. Physiol. *202*, 437–470. https://doi.org/10.1113/jphysiol.1969.sp008820.
19. Minsky, M. (1952). A neural-analogue calculator based upon a probability model of reinforcement. Harvard University Pychological Laboratories Internal Report.
20. Minsky, M.. Building my randomly wired neural network machine. https://www.webofstories.com/play/marvin.minsky/136.
21. Babadi, B., and Sompolinsky, H. (2014). Sparseness and expansion in sensory representations. Neuron *83*, 1213–1226. https://doi.org/10.1016/j.neuron.2014.07.035.
22. Cayco-Gajic, N.A., and Silver, R.A. (2019). Re-evaluating circuit mechanisms underlying pattern separation. Neuron *101*, 584–602. https://doi.org/10.1016/j.neuron.2019.01.044.
23. Hiratani, N., and Latham, P.E. (2022). Developmental and evolutionary constraints on olfactory circuit selection. Proc. Natl. Acad. Sci. USA *119*. e2100600119. https://doi.org/10.1073/pnas.2100600119.
24. Jortner, R.A., Farivar, S.S., and Laurent, G. (2007). A simple connectivity scheme for sparse coding in an olfactory system. J. Neurosci. *27*, 1659–1669. https://doi.org/10.1523/JNEUROSCI.4171-06.2007.
25. Litwin-Kumar, A., Harris, K.D., Axel, R., Sompolinsky, H., and Abbott, L.F. (2017). Optimal degrees of synaptic connectivity. Neuron *93*, 1153–1164.e7. https://doi.org/10.1016/j.neuron.2017.01.030.
26. Luo, S.X., Axel, R., and Abbott, L.F. (2010). Generating sparse and selective third-order responses in the olfactory system of the fly. Proc. Natl. Acad. Sci. USA *107*, 10713–10718. https://doi.org/10.1073/pnas.1005635107.
27. Modi, M.N., Shuai, Y., and Turner, G.C. (2020). The Drosophila mushroom body: from architecture to algorithm in a learning circuit. Annu. Rev. Neurosci. *43*, 465–484. https://doi.org/10.1146/annurev-neuro-080317-0621333.
28. Rajagopalan, A., and Assisi, C. (2020). Effect of circuit structure on odor representation in the insect olfactory system. eNeuro *7*. ENEURO.0130-19.2020. https://doi.org/10.1523/ENEURO.0130-19.2020.
29. Elkahlah, N.A., Rogow, J.A., Ahmed, M., and Clowney, E.J. (2020). Presynaptic developmental plasticity allows robust sparse wiring of the Drosophila mushroom body. eLife *9*, e52278. https://doi.org/10.7554/eLife.52278.
30. Puñal, V.M., Ahmed, M., Thornton-Kolbe, E.M., and Clowney, E.J. (2021). Untangling the wires: development of sparse, distributed connectivity in

the mushroom body calyx. Cell Tissue Res. *383*, 91–112. https://doi.org/10.1007/s00441-020-03386-4.

31. Butcher, N.J., Friedrich, A.B., Lu, Z., Tanimoto, H., and Meinertzhagen, I.A. (2012). Different classes of input and output neurons reveal new features in microglomeruli of the adult Drosophila mushroom body calyx. J. Comp. Neurol. *520*, 2185–2201. https://doi.org/10.1002/cne.23037.
32. Leiss, F., Groh, C., Butcher, N.J., Meinertzhagen, I.A., and Tavosanis, G. (2009). Synaptic organization in the adult Drosophila mushroom body calyx. J. Comp. Neurol. *517*, 808–824. https://doi.org/10.1002/cne.22184.
33. Yang, K., Liu, T., Wang, Z., Liu, J., Shen, Y., Pan, X., Wen, R., Xie, H., Ruan, Z., Tan, Z., et al. (2022). Classifying Drosophila olfactory projection neuron boutons by quantitative analysis of electron microscopic reconstruction. iScience *25*, 104180. https://doi.org/10.1016/j.isci.2022.104180.
34. Caron, S.J.C., Ruta, V., Abbott, L.F., and Axel, R. (2013). Random convergence of olfactory inputs in the Drosophila mushroom body. Nature *497*, 113–117. https://doi.org/10.1038/nature12063.
35. Zheng, Z., Lauritzen, J.S., Perlman, E., Robinson, C.G., Nichols, M., Milkie, D., Torrens, O., Price, J., Fisher, C.B., Sharifi, N., et al. (2018). A complete electron microscopy volume of the brain of adult Drosophila melanogaster. Cell *174*, 730–743.e22. https://doi.org/10.1016/j.cell.2018.06.019.
36. Eichler, K., Li, F., Litwin-Kumar, A., Park, Y., Andrade, I., Schneider-Mizell, C.M., Saumweber, T., Huser, A., Eschbach, C., Gerber, B., et al. (2017). The complete connectome of a learning and memory centre in an insect brain. Nature *548*, 175–182. https://doi.org/10.1038/nature23455.
37. Zheng, Z., Li, F., Fisher, C., Ali, I.J., Sharifi, N., Calle-Schuler, S., Hsu, J., Masoodpanah, N., Kmecova, L., Kazimiers, T., et al. (2022). Structured sampling of olfactory input by the fly mushroom body. Curr. Biol. *32*, 3334–3349.e6. https://doi.org/10.1016/j.cub.2022.06.031.
38. Groschner, L.N., Hak, C.W., L, Bogacz, R., DasGupta, S., and Miesenböck, G. (2018). Dendritic integration of sensory evidence in perceptual decision-making. Cell *173*, 894–905.e13. https://doi.org/10.1016/j.cell.2018.03.075.
39. Gruntman, E., and Turner, G.C. (2013). Integration of the olfactory code across dendritic claws of single mushroom body neurons. Nat. Neurosci. *16*, 1821–1829. https://doi.org/10.1038/nn.3547.
40. Li, H., Li, Y., Lei, Z., Wang, K., and Guo, A. (2013). Transformation of odor selectivity from projection neurons to single mushroom body neurons mapped with dual-color calcium imaging. Proc. Natl. Acad. Sci. USA *110*, 12084–12089. https://doi.org/10.1073/pnas.1305857110.
41. Lin, A.C., Bygrave, A.M., de Calignon, A., Lee, T., and Miesenböck, G. (2014). Sparse, decorrelated odor coding in the mushroom body enhances learned odor discrimination. Nat. Neurosci. *17*, 559–568. https://doi.org/10.1038/nn.3660.
42. Tully, T., Preat, T., Boynton, S.C., and Del Vecchio, M. (1994). Genetic dissection of consolidated memory in Drosophila. Cell *79*, 35–47. https://doi.org/10.1016/0092-8674(94)90398-0.
43. Aso, Y., Hattori, D., Yu, Y., Johnston, R.M., Iyer, N.A., Ngo, T.T., Dionne, H., Abbott, L.F., Axel, R., Tanimoto, H., et al. (2014). The neuronal architecture of the mushroom body provides a logic for associative learning. eLife *3*, e04577. https://doi.org/10.7554/eLife.04577.
44. Aso, Y., Sitaraman, D., Ichinose, T., Kaun, K.R., Vogt, K., Belliart-Guérin, G., Plaçais, P.Y., Robie, A.A., Yamagata, N., Schnaitmann, C., et al. (2014). Mushroom body output neurons encode valence and guide memory-based action selection in Drosophila. eLife *3*, e04580. https://doi.org/10.7554/eLife.04580.
45. Cohn, R., Morantte, I., and Ruta, V. (2015). Coordinated and compartmentalized neuromodulation shapes sensory processing in Drosophila. Cell *163*, 1742–1755. https://doi.org/10.1016/j.cell.2015.11.019.
46. Hige, T., Aso, Y., Rubin, G.M., and Turner, G.C. (2015). Plasticity-driven individualization of olfactory coding in mushroom body output neurons. Nature *526*, 258–262. https://doi.org/10.1038/nature15396.
47. Owald, D., Felsenberg, J., Talbot, C.B., Das, G., Perisse, E., Huetteroth, W., and Waddell, S. (2015). Activity of defined mushroom body output neurons underlies learned olfactory behavior in Drosophila. Neuron *86*, 417–427. https://doi.org/10.1016/j.neuron.2015.03.025.
48. Aso, Y., Grübel, K., Busch, S., Friedrich, A.B., Siwanowicz, I., and Tanimoto, H. (2009). The mushroom body of adult Drosophila characterized by GAL4 drivers. J. Neurogenet. *23*, 156–172. https://doi.org/10.1080/01677060802471718.
49. Bates, A.S., Schlegel, P., Roberts, R.J.V., Drummond, N., Tamimi, I.F.M., Turnbull, R., Zhao, X., Marin, E.C., Popovici, P.D., Dhawan, S., et al. (2020). Complete connectomic reconstruction of olfactory projection neurons in the fly brain. Curr. Biol. *30*, 3183–3199.e6. https://doi.org/10.1016/j.cub.2020.06.042.
50. Li, F., Lindsey, J.W., Marin, E.C., Otto, N., Dreher, M., Dempsey, G., Stark, I., Bates, A.S., Pleijzier, M.W., Schlegel, P., et al. (2020). The connectome of the adult Drosophila mushroom body provides insights into function. eLife *9*, e62576. https://doi.org/10.7554/eLife.62576.
51. Schlegel, P., Bates, A.S., Stürner, T., Jagannathan, S.R., Drummond, N., Hsu, J., Serratosa Capdevila, L., Javier, A., Marin, E.C., Barth-Maron, A., et al. (2021). Information flow, cell types and stereotypy in a full olfactory connectome. eLife *10*, e66018. https://doi.org/10.7554/eLife.66018.
52. Takemura, S.Y., Aso, Y., Hige, T., Wong, A., Lu, Z., Xu, C.S., Rivlin, P.K., Hess, H., Zhao, T., Parag, T., et al. (2017). A connectome of a learning and memory center in the adult Drosophila brain. eLife *6*, e26975. https://doi.org/10.7554/eLife.26975.
53. Lillvis, J.L., Otsuna, H., Ding, X., Pisarev, I., Kawase, T., Colonell, J., Rokicki, K., Goina, C., Gao, R., Hu, A., et al. (2022). Rapid reconstruction of neural circuits using tissue expansion and light sheet microscopy. eLife *11*, e81248. https://doi.org/10.7554/eLife.81248.
54. Wagh, D.A., Rasse, T.M., Asan, E., Hofbauer, A., Schwenkert, I., Dürrbeck, H., Buchner, S., Dabauvalle, M.C., Schmidt, M., Qin, G., et al. (2006). Bruchpilot, a protein with homology to ELKS/CAST, is required for structural integrity and function of synaptic active zones in Drosophila. Neuron *49*, 833–844. https://doi.org/10.1016/j.neuron.2006.02.008.
55. Pachitariu, M., Stringer, C., Dipoppa, M., Schröder, S., Rossi, L.F., Dalgleish, H., Carandini, M., and Harris, K.D. (2017). Suite2p: beyond 10,000 neurons with standard two-photon microscopy. Preprint at bioRxiv. https://doi.org/10.1101/061507.
56. Dan, I., Watanabe, N.M., and Kusumi, A. (2001). The Ste20 group kinases as regulators of MAP kinase cascades. Trends Cell Biol. *11*, 220–230. https://doi.org/10.1016/s0962-8924(01)01980-8.
57. Hu, C., Feng, P., Chen, M., Tang, Y., and Soba, P. (2022). Spatiotemporal changes in microtubule dynamics during dendritic morphogenesis. Fly *16*, 13–23. https://doi.org/10.1080/19336934.2021.1976033.
58. Hu, C., Kanellopoulos, A.K., Richter, M., Petersen, M., Konietzny, A., Tenedini, F.M., Hoyer, N., Cheng, L., Poon, C.L.C., Harvey, K.F., et al. (2020). Conserved Tao kinase activity regulates dendritic arborization, cytoskeletal dynamics, and sensory function in Drosophila. J. Neurosci. *40*, 1819–1833. https://doi.org/10.1523/JNEUROSCI.1846-19.2020.
59. King, I., Tsai, L.T.-Y., Pflanz, R., Voigt, A., Lee, S., Jäckle, H., Lu, B., and Heberlein, U. (2011). Drosophila Tao controls mushroom body development and ethanol-stimulated behavior through par-1. J. Neurosci. *31*, 1139–1148. https://doi.org/10.1523/JNEUROSCI.4416-10.2011.
60. Mitsopoulos, C., Zihni, C., Garg, R., Ridley, A.J., and Morris, J.D.H. (2003). The prostate-derived sterile 20-like kinase (PSK) regulates microtubule organization and stability. J. Biol. Chem. *278*, 18085–18091. https://doi.org/10.1074/jbc.M213064200.
61. Li, Y., Walker, L.A., Zhao, Y., Edwards, E.M., Michki, N.S., Cheng, H.P.J., Ghazzi, M., Chen, T.Y., Chen, M., Roossien, D.H., et al. (2021). Bitbow enables highly efficient neuronal lineage tracing and morphology reconstruction in single Drosophila brains. Front. Neural Circuits *15*, 732183. https://doi.org/10.3389/fncir.2021.732183.
62. Veling, M.W., Li, Y., Veling, M.T., Litts, C., Michki, N., Liu, H., Ye, B., and Cai, D. (2019). Identification of neuronal lineages in the Drosophila

peripheral nervous system with a "digital" multi-spectral lineage tracing system. Cell Rep. *29*, 3303–3312.e3. https://doi.org/10.1016/j.celrep.2019.10.124.

63. Wang, J., Ma, X., Yang, J.S., Zheng, X., Zugates, C.T., Lee, C.H., and Lee, T. (2004). Transmembrane/juxtamembrane domain-dependent Dscam distribution and function during mushroom body neuronal morphogenesis. Neuron *43*, 663–672. https://doi.org/10.1016/j.neuron.2004.06.033.
64. Aso, Y., and Rubin, G.M. (2016). Dopaminergic neurons write and update memories with cell-type-specific rules. eLife *5*, e16135. https://doi.org/10.7554/eLife.16135.
65. Handler, A., Graham, T.G.W., Cohn, R., Morantte, I., Siliciano, A.F., Zeng, J., Li, Y., and Ruta, V. (2019). Distinct dopamine receptor pathways underlie the temporal sensitivity of associative learning. Cell *178*, 60–75.e19. https://doi.org/10.1016/j.cell.2019.05.040.
66. Owald, D., and Waddell, S. (2015). Olfactory learning skews mushroom body output pathways to steer behavioral choice in Drosophila. Curr. Opin. Neurobiol. *35*, 178–184. https://doi.org/10.1016/j.conb.2015.10.002.
67. Séjourné, J., Plaçais, P.Y., Aso, Y., Siwanowicz, I., Trannoy, S., Thoma, V., Tedjakumala, S.R., Rubin, G.M., Tchénio, P., Ito, K., et al. (2011). Mushroom body efferent neurons responsible for aversive olfactory memory retrieval in Drosophila. Nat. Neurosci. *14*, 903–910. https://doi.org/10.1038/nn.2846.
68. Tomchik, S.M., and Davis, R.L. (2009). Dynamics of learning-related cAMP signaling and stimulus integration in the Drosophila olfactory pathway. Neuron *64*, 510–521. https://doi.org/10.1016/j.neuron.2009.09.029.
69. de Belle, J.S., and Heisenberg, M. (1994). Associative odor learning in Drosophila abolished by chemical ablation of mushroom bodies. Science *263*, 692–695.
70. Sweeney, S.T., Hidalgo, A., de Belle, J.S., and Keshishian, H. (2012). Hydroxyurea ablation of mushroom bodies in Drosophila. Cold Spring Harb. Protoc. *2012*, 231–234. https://doi.org/10.1101/pdb.prot067777.
71. Rajagopalan, A.E., Darshan, R., Hibbard, K.L., Fitzgerald, J.E., and Turner, G.C. (2022). Reward expectations direct learning and drive operant matching in Drosophila. Preprint at bioRxiv. https://doi.org/10.1101/2022.05.24.493252.
72. Burke, C.J., Huetteroth, W., Owald, D., Perisse, E., Krashes, M.J., Das, G., Gohl, D., Silies, M., Certel, S., and Waddell, S. (2012). Layered reward signalling through octopamine and dopamine in Drosophila. Nature *492*, 433–437. https://doi.org/10.1038/nature11614.
73. Liu, C., Plaçais, P.Y., Yamagata, N., Pfeiffer, B.D., Aso, Y., Friedrich, A.B., Siwanowicz, I., Rubin, G.M., Preat, T., and Tanimoto, H. (2012). A subset of dopamine neurons signals reward for odour memory in Drosophila. Nature *488*, 512–516. https://doi.org/10.1038/nature11304.
74. Lai, S.L., Awasaki, T., Ito, K., and Lee, T. (2008). Clonal analysis of Drosophila antennal lobe neurons: diverse neuronal architectures in the lateral neuroblast lineage. Development *135*, 2883–2893. https://doi.org/10.1242/dev.024380.
75. Stocker, R.F., Heimbeck, G., Gendre, N., and de Belle, J.S. (1997). Neuroblast ablation in Drosophila P[GAL4] lines reveals origins of olfactory interneurons. J. Neurobiol. *32*, 443–456.
76. Campbell, R.A.A., Honegger, K.S., Qin, H., Li, W., Demir, E., and Turner, G.C. (2013). Imaging a population code for odor identity in the Drosophila mushroom body. J. Neurosci. *33*, 10568–10581. https://doi.org/10.1523/JNEUROSCI.0682-12.2013.
77. Malun, D., Giurfa, M., Galizia, C.G., Plath, N., Brandt, R., Gerber, B., and Eisermann, B. (2002). Hydroxyurea-induced partial mushroom body ablation does not affect acquisition and retention of olfactory differential conditioning in honeybees. J. Neurobiol. *53*, 343–360. https://doi.org/10.1002/neu.10119.
78. Eschbach, C., Fushiki, A., Winding, M., Schneider-Mizell, C.M., Shao, M., Arruda, R., Eichler, K., Valdes-Aleman, J., Ohyama, T., Thum, A.S., et al. (2020). Recurrent architecture for adaptive regulation of learning in the insect brain. Nat. Neurosci. *23*, 544–555. https://doi.org/10.1038/s41593-020-0607-9.
79. Scaplen, K.M., Talay, M., Fisher, J.D., Cohn, R., Sorkaç, A., Aso, Y., Barnea, G., and Kaun, K.R. (2021). Transsynaptic mapping of Drosophila mushroom body output neurons. eLife *10*, e63379. https://doi.org/10.7554/eLife.63379.
80. Aso, Y., Herb, A., Ogueta, M., Siwanowicz, I., Templier, T., Friedrich, A.B., Ito, K., Scholz, H., and Tanimoto, H. (2012). Three dopamine pathways induce aversive odor memories with different stability. PLoS Genet. *8*, e1002768. https://doi.org/10.1371/journal.pgen.1002768.
81. Armstrong, J.D., de Belle, J.S., Wang, Z., and Kaiser, K. (1998). Metamorphosis of the mushroom bodies; large-scale rearrangements of the neural substrates for associative learning and memory in Drosophila. Learn. Mem. *5*, 102–114.
82. Lin, C.H., Senapati, B., Chen, W.J., Bansal, S., and Lin, S. (2022). Semaphorin 1a-mediated dendritic wiring of the Drosophila mushroom body extrinsic neurons. Proc. Natl. Acad. Sci. USA *119*. e2111283119. https://doi.org/10.1073/pnas.2111283119.
83. Tully, T., and Quinn, W.G. (1985). Classical conditioning and retention in normal and mutant Drosophila melanogaster. J. Comp. Physiol. A *157*, 263–277. https://doi.org/10.1007/BF01350033.
84. Dzirasa, K., Ransey, E., Chesnov, K., Wisdom, E., Bowman, R., Rodriguez, T., Adamson, E., Thomas, G., Almoril-Porras, A., Schwennesen, H., et al. (2022). Long-term precision editing of neural circuits using engineered gap junction hemichannels. Biol. Psychiatry *91*, S14–S15. https://doi.org/10.1016/j.biopsych.2022.02.055.
85. Hawk, J.D., Wisdom, E.M., SenGupta, T., Kashlan, Z.D., and Colón-Ramos, D.A. (2021). A genetically encoded tool for reconstituting synthetic modulatory neurotransmission and reconnect neural circuits in vivo. Nat. Commun. *12*, 4795. https://doi.org/10.1038/s41467-021-24690-9.
86. Heckman, E.L., and Doe, C.Q. (2022). Presynaptic contact and activity opposingly regulate postsynaptic dendrite outgrowth. eLife *11*, e82093. https://doi.org/10.7554/eLife.82093.
87. Linneweber, G.A., Andriatsilavo, M., Dutta, S.B., Bengochea, M., Hellbruegge, L., Liu, G., Ejsmont, R.K., Straw, A.D., Wernet, M., Hiesinger, P.R., et al. (2020). A neurodevelopmental origin of behavioral individuality in the Drosophila visual system. Science *367*, 1112–1119. https://doi.org/10.1126/science.aaw7182.
88. Meng, J.L., Marshall, Z.D., Lobb-Rabe, M., and Heckscher, E.S. (2019). How prolonged expression of Hunchback, a temporal transcription factor, re-wires locomotor circuits. eLife *8*, e46089. https://doi.org/10.7554/eLife.46089.
89. Pechuk, V., Goldman, G., Salzberg, Y., Chaubey, A.H., Bola, R.A., Hoffman, J.R., Endreson, M.L., Miller, R.M., Reger, N.J., Portman, D.S., et al. (2022). Reprogramming the topology of the nociceptive circuit in C. elegans reshapes sexual behavior. Curr. Biol. *32*, 4372–4385.e7. https://doi.org/10.1016/j.cub.2022.08.038.
90. Pop, S., Chen, C.L., Sproston, C.J., Kondo, S., Ramdya, P., and Williams, D.W. (2020). Extensive and diverse patterns of cell death sculpt neural networks in insects. eLife *9*, e59566. https://doi.org/10.7554/eLife.59566.
91. Prieto-Godino, L.L., Silbering, A.F., Khallaf, M.A., Cruchet, S., Bojkowska, K., Pradervand, S., Hansson, B.S., Knaden, M., and Benton, R. (2020). Functional integration of "undead" neurons in the olfactory system. Sci. Adv. *6*, eaaz7238. https://doi.org/10.1126/sciadv.aaz7238.
92. Valdes-Aleman, J., Fetter, R.D., Sales, E.C., Heckman, E.L., Venkatasubramanian, L., Doe, C.Q., Landgraf, M., Cardona, A., and Zlatic, M. (2021). Comparative connectomics reveals how partner identity, location, and activity specify synaptic connectivity in Drosophila. Neuron *109*, 105–122.e7. https://doi.org/10.1016/j.neuron.2020.10.004.
93. Kiral, F.R., Dutta, S.B., Linneweber, G.A., Hilgert, S., Poppa, C., Duch, C., von Kleist, M., Hassan, B.A., and Hiesinger, P.R. (2021). Brain

connectivity inversely scales with developmental temperature in Drosophila. Cell Rep. *37*, 110145. https://doi.org/10.1016/j.celrep.2021.110145.

94. Otopalik, A.G., Goeritz, M.L., Sutton, A.C., Brookings, T., Guerini, C., and Marder, E. (2017). Sloppy morphological tuning in identified neurons of the crustacean stomatogastric ganglion. eLife *6*, e22352. https://doi.org/10.7554/eLife.22352.

95. Inada, K., Tsuchimoto, Y., and Kazama, H. (2017). Origins of cell-type-specific olfactory processing in the Drosophila mushroom body circuit. Neuron *95*, 357–367.e4. https://doi.org/10.1016/j.neuron.2017.06.039.

96. Amin, H., Apostolopoulou, A.A., Suárez-Grimalt, R., Vrontou, E., and Lin, A.C. (2020). Localized inhibition in the Drosophila mushroom body. eLife *9*, e56954. https://doi.org/10.7554/eLife.56954.

97. Prisco, L., Deimel, S.H., Yeliseyeva, H., Fiala, A., and Tavosanis, G. (2021). The anterior paired lateral neuron normalizes odour-evoked activity in the Drosophila mushroom body calyx. eLife *10*, e74172. https://doi.org/10.7554/eLife.74172.

98. Hayashi, T.T., MacKenzie, A.J., Ganguly, I., Ellis, K.E., Smihula, H.M., Jacob, M.S., Litwin-Kumar, A., and Caron, S.J.C. (2022). Mushroom body input connections form independently of sensory activity in Drosophila melanogaster. Curr. Biol. *32*, 4000–4012.e5. https://doi.org/10.1016/j.cub.2022.07.055.

99. Bajar, B.T., Phi, N.T., Isaacman-Beck, J., Reichl, J., Randhawa, H., and Akin, O. (2022). A discrete neuronal population coordinates brain-wide developmental activity. Nature *602*, 639–646. https://doi.org/10.1038/s41586-022-04406-9.

100. Jan, Y.N., and Jan, L.Y. (2010). Branching out: mechanisms of dendritic arborization. Nat. Rev. Neurosci. *11*, 316–328. https://doi.org/10.1038/nrn2836.

101. Hattori, D., Chen, Y., Matthews, B.J., Salwinski, L., Sabatti, C., Grueber, W.B., and Zipursky, S.L. (2009). Robust discrimination between self and non-self neurites requires thousands of Dscam1 isoforms. Nature *461*, 644–648. https://doi.org/10.1038/nature08431.

102. Matthews, B.J., Kim, M.E., Flanagan, J.J., Hattori, D., Clemens, J.C., Zipursky, S.L., and Grueber, W.B. (2007). Dendrite self-avoidance is controlled by Dscam. Cell *129*, 593–604. https://doi.org/10.1016/j.cell.2007.04.013.

103. Soba, P., Zhu, S., Emoto, K., Younger, S., Yang, S.J., Yu, H.H., Lee, T., Jan, L.Y., and Jan, Y.N. (2007). Drosophila sensory neurons require Dscam for dendritic self avoidance and proper dendritic field organization. Neuron *54*, 403–416. https://doi.org/10.1016/j.neuron.2007.03.029.

104. Crampton, G., Gergely, T., Crampton, G., and Gergely, T. (1946). Tootle (Golden Press).

105. Honegger, K.S., Campbell, R.A.A., and Turner, G.C. (2011). Cellular-resolution population imaging reveals robust sparse coding in the Drosophila mushroom body. J. Neurosci. *31*, 11772–11785. https://doi.org/10.1523/JNEUROSCI.1099-11.2011.

106. Murthy, M., Fiete, I., and Laurent, G. (2008). Testing odor response stereotypy in the Drosophila mushroom body. Neuron *59*, 1009–1023. https://doi.org/10.1016/j.neuron.2008.07.040.

107. Turner, G.C., Bazhenov, M., and Laurent, G. (2008). Olfactory representations by Drosophila mushroom body neurons. J. Neurophysiol. *99*, 734–746. https://doi.org/10.1152/jn.01283.2007.

108. Wilson, R.I., Turner, G.C., and Laurent, G. (2004). Transformation of olfactory representations in the Drosophila antennal lobe. Science *303*, 366–370. https://doi.org/10.1126/science.1090782.

109. Ahmed, M., Rajagopalan, A.E., Pan, Y., Li, Y., Williams, D.L., Pedersen, E.A., Thakral, M., Previero, A., Close, K.C., Christoforou, C.P., et al. (2023). Hacking brain development to test models of sensory coding. Preprint at bioRxiv. https://doi.org/10.1101/2023.01.25.525425.

110. Lee, T., and Luo, L. (1999). Mosaic analysis with a repressible cell marker for studies of gene function in neuronal morphogenesis. Neuron *22*, 451–461.

111. Perkins, L.A., Holderbaum, L., Tao, R., Hu, Y., Sopko, R., McCall, K., Yang-Zhou, D., Flockhart, I., Binari, R., Shim, H.S., et al. (2015). The transgenic RNAi Project at Harvard Medical School: resources and validation. Genetics *201*, 843–852. https://doi.org/10.1534/genetics.115.180208.

112. Connolly, J.B., Roberts, I.J.H., Armstrong, J.D., Kaiser, K., Forte, M., Tully, T., and O'Kane, C.J. (1996). Associative learning disrupted by impaired gs signaling in Drosophila mushroom bodies. Science *274*, 2104–2107. https://doi.org/10.1126/science.274.5295.2104.

113. Akerboom, J., Chen, T.W., Wardill, T.J., Tian, L., Marvin, J.S., Mutlu, S., Calderón, N.C., Esposti, F., Borghuis, B.G., Sun, X.R., et al. (2012). Optimization of a GCaMP calcium indicator for neural activity imaging. J. Neurosci. *32*, 13819–13840. https://doi.org/10.1523/JNEUROSCI.2601-12.2012.

114. Hong, W., Mosca, T.J., and Luo, L. (2012). Teneurins instruct synaptic partner matching in an olfactory map. Nature *484*, 201–207. https://doi.org/10.1038/nature10926.

115. Potter, C.J., Tasic, B., Russler, E.V., Liang, L., and Luo, L. (2010). The Q system: a repressible binary system for transgene expression, lineage tracing, and mosaic analysis. Cell *141*, 536–548. https://doi.org/10.1016/j.cell.2010.02.025.

116. Stringer, C., Wang, T., Michaelos, M., and Pachitariu, M. (2021). Cellpose: a generalist algorithm for cellular segmentation. Nat. Methods *18*, 100–106. https://doi.org/10.1038/s41592-020-01018-x.

117. Jenett, A., Rubin, G.M., Ngo, T.T., Shepherd, D., Murphy, C., Dionne, H., Pfeiffer, B.D., Cavallaro, A., Hall, D., Jeter, J., et al. (2012). A GAL4-driver line resource for Drosophila neurobiology. Cell Rep. *2*, 991–1001. https://doi.org/10.1016/j.celrep.2012.09.011.

118. Pfeiffer, B.D., Ngo, T.T., Hibbard, K.L., Murphy, C., Jenett, A., Truman, J.W., and Rubin, G.M. (2010). Refinement of tools for targeted gene expression in Drosophila. Genetics *186*, 735–755. https://doi.org/10.1534/genetics.110.119917.

119. Yu, H.H., Yang, J.S., Wang, J., Huang, Y., and Lee, T. (2009). Endodomain diversity in the Drosophila Dscam and its roles in neuronal morphogenesis. J. Neurosci. *29*, 1904–1914. https://doi.org/10.1523/JNEUROSCI.5743-08.2009.

120. Awasaki, T., Kao, C.F., Lee, Y.J., Yang, C.P., Huang, Y., Pfeiffer, B.D., Luan, H., Jing, X., Huang, Y.F., He, Y., et al. (2014). Making *Drosophila* lineage–restricted drivers via patterned recombination in neuroblasts. Nat. Neurosci. *17*, 631–637. https://doi.org/10.1038/nn.3654.

121. Schindelin, J., Arganda-Carreras, I., Frise, E., Kaynig, V., Longair, M., Pietzsch, T., Preibisch, S., Rueden, C., Saalfeld, S., Schmid, B., et al. (2012). Fiji: an open-source platform for biological-image analysis. Nat. Methods *9*, 676–682. https://doi.org/10.1038/nmeth.2019.

122. Ito, K., Awano, W., Suzuki, K., Hiromi, Y., and Yamamoto, D. (1997). The Drosophila mushroom body is a quadruple structure of clonal units each of which contains a virtually identical set of neurones and glial cells. Development *124*, 761–771.

123. Ruta, V., Datta, S.R., Vasconcelos, M.L., Freeland, J., Looger, L.L., and Axel, R. (2010). A dimorphic pheromone circuit in Drosophila from sensory input to descending output. Nature *468*, 686–690. https://doi.org/10.1038/nature09554.

124. Mamiya, A., Beshel, J., Xu, C., and Zhong, Y. (2008). Neural representations of airflow in Drosophila mushroom body. PLoS One *3*, e4063. https://doi.org/10.1371/journal.pone.0004063.

125. Stopfer, M., and Laurent, G. (1999). Short-term memory in olfactory network dynamics. Nature *402*, 664–668. https://doi.org/10.1038/45244.

126. Barnstedt, O., Owald, D., Felsenberg, J., Brain, R., Moszynski, J.P., Talbot, C.B., Perrat, P.N., and Waddell, S. (2016). Memory-relevant mushroom body output synapses are cholinergic. Neuron *89*, 1237–1247. https://doi.org/10.1016/j.neuron.2016.02.015.

127. Brovkina, M.V., Duffié, R., Burtis, A.E.C., and Clowney, E.J. (2021). Fruitless decommissions regulatory elements to implement cell-type-specific neuronal masculinization. PLoS Genet. *17*, e1009338. https://doi.org/10.1371/journal.pgen.1009338.

128. Jefferis, G.S.X.E., Vyas, R.M., Berdnik, D., Ramaekers, A., Stocker, R.F., Tanaka, N.K., Ito, K., and Luo, L. (2004). Developmental origin of wiring specificity in the olfactory system of Drosophila. Development *131*, 117–130. https://doi.org/10.1242/dev.00896.

129. Ito, K., Suzuki, K., Estes, P., Ramaswami, M., and Yamamoto, D. (1998). The organization of extrinsic neurons and their implications in the functional roles of the mushroom bodies in Drosophila melanogaster Meigen. Learn Mem. *5*, 52–77.

130. Yu, H.H., Kao, C.F., He, Y., Ding, P., Kao, J.C., and Lee, T. (2010). A complete developmental sequence of a Drosophila neuronal lineage as revealed by twin-spot MARCM. PLoS Biol. *8*, https://doi.org/10.1371/journal.pbio.1000461.

131. Jefferis, G.S.X.E., Marin, E.C., Stocker, R.F., and Luo, L. (2001). Target neuron prespecification in the olfactory map of Drosophila. Nature *414*, 204–208. https://doi.org/10.1038/35102574.

Please cite this article in press as: Ahmed et al., Input density tunes Kenyon cell sensory responses in the *Drosophila* mushroom body, Current Biology (2023), https://doi.org/10.1016/j.cub.2023.05.064

STAR★METHODS

KEY RESOURCES TABLE

REAGENT or RESOURCE	SOURCE	IDENTIFIER
Antibodies		
anti-ChAT (mouse monoclonal)	Developmental Studies Hybridoma Bank	Cat# chat4b1; RRID: AB_528122
anti-DsRed (rabbit polyclonal)	Clontech/Takara Bio	Cat# 632496; RRID: AB_10013483
anti-GFP (sheep polyclonal)	Bio-Rad	Cat# 4745-1051; RRID: AB_619712
anti-GFP (chicken polyclonal) Umich (also used to stain mAmetrine, GCaMP, C3PA)	Cai Lab	N/A
anti-GFP (chicken) Janelia	Fisher	Cat# A10262; RRID: AB_2534023
CyTM3 anti-rabbit (goat)	Jackson Immunoresearch	Cat# 111-165-144; RRID: AB_2338006
CyTM5-anti-mouse (goat)	Jackson Immunoresearch	Cat# 115-175-166; RRID: AB_2338714
Alexa 488 anti-chicken (goat polyclonal) Janelia	Fisher	Cat# A32931; RRID: AB_2762843
Alexa 488 anti-mouse (goat polyclonal)	Fisher	Cat# A-11029; RRID: AB_2534088
Alexa 647 anti-mouse (goat polyclonal)	Fisher	Cat# A-21236; RRID: AB_2535805
Alexa 488 anti-sheep (donkey polyclonal)	Fisher	Cat# A-11015; RRID: AB_2534082
Alexa 488 anti-chicken (goat polyclonal) Umich	Fisher	Cat# A-11039; RRID: AB_2534096
Alexa 568 anti-rabbit (goat polyclonal)	Fisher	Cat# A-11036; RRID: AB_10563566
anti-brp (mouse monoclonal)	Developmental Studies Hybridoma Bank	Cat# nc82; RRID: AB_2314866
anti-mTFP (rat)	Cai Lab	N/A
anti-mNeonGreen (rabbit)	Cai Lab	N/A
anti-mKusabiraOrange2 (mouse)	Cai Lab	N/A
anti-mKate2 (guinea pig)	Cai Lab	N/A
Alexa 594 anti-rat (donkey polyclonal)	Fisher	Cat# A-21209; RRID: AB_2535795
CF 555 anti-mouse (donkey polyclonal)	Sigma	SAB4600060
CF 633 ant-guinea pig (donkey polyclonal)	Sigma	Cat# SAB4600129; RRID: AB_2890636
Atto490 LS anti-rabbit	Hypermol	2309
Chemicals, peptides, and recombinant proteins		
Paraformaldehyde (Clowney Lab)	EMS	15710
Paraformaldehyde (Janelia)	EMS	15713
Paraformaldehyde (Cai Lab)	Sigma	P6148
Hydroxyurea	Sigma	H8627
Mineral oil	Sigma	330760
Paraffin oil	Sigma	18512
Benzaldehyde	Sigma	418099
Isobutyl acetate	Sigma	537470
Ethyl acetate	Sigma	270989
Methylcyclohexanol	Sigma	153095
3-Octanol	Sigma	218405
Pentyl Acetate	Sigma	109584
Butyl Acetate	Sigma	287725
Phalloidin-568 (used in stainings, though not shown in figures)	Fisher	A12380
DAPI (used in stainings, though not shown in figures)	Sigma	D9542
Retinal	Janelia Media Facility	N/A
10x PBS Gibco	Fisher	70-011-044

(*Continued on next page*)

Please cite this article in press as: Ahmed et al., Input density tunes Kenyon cell sensory responses in the *Drosophila* mushroom body, Current Biology (2023), https://doi.org/10.1016/j.cub.2023.05.064

Continued

REAGENT or RESOURCE	SOURCE	IDENTIFIER
Glycerol	Fisher	G33-500
Propyl gallate	Sigma	02370
Vectashield	Vector Laboratories	H-1000
StartingBlock	Thermo	37578
Normal goat serum (Umich)	MP biobiomedicals	8642921
Normal goat serum (Umich)	Abcam	ab7481
Triton	Sigma	X100
Sodium chloride NaCl	Sigma	S7653
Potassium chloride KCl	Fisher	P217-500
Calcium chloride CaCl2*2H2O	Fisher	C70-500
Magnesium chloride MgCl2*6H2O	Sigma	M2670
Sodium bicarbonate NaHCO3	Fisher	S233-500
Sodium phosphate NaH2PO4*H2O	Fisher	S369-500
Trehalose	Sigma	T9531
Sucrose	Sigma	84097
HEPES sodium salt	Sigma	H7006
Schneider's insect medium (Janelia)	Sigma	S01416
PBS (Janelia)	Cellgro	21-040
Normal goat serum (Janelia)	Fisher	16210-064
Poly-L-lysine hydrobromide	Sigma	P1524
Kodak Photo-Flo 200 Solution (for poly-L-lysine-coating cover slips)	EMS	74257
DPX Mountant for Microscopy	EMS	13512
Ethanol. ACS reagent, >99.5% (200 proof)	Sigma	459844
Xylenes	Fisher	X5-500
Experimental models: Organisms/strains		
UAS-CD8GFP (II)	BDSC 5130	Lee and Luo et al.[110]
$GH146^{QF}$, QUAS-mtdTomato-3xHA (II)	BL 30037	Potter et al.[116]
P(caryP) (attp2)	BL36303	Perkins et al.[111]
$OK107^{Gal4}$ (IV)	BL 854	Connolly et al.[112]
UAS-mud-RNAi (attp2)	BL 35044	Perkins et al.[111]
UAS-GCaMP6s (attp40)	BL 42746	Akerboom et al.[113]
UAS-GCaMP6s (VK0005)	BL 42749	Akerboom et al.[113]
UAS-Tao1-RNAi (attp2)	BL 35147	Perkins et al.[111]
GMR58E02-lexA (attP40)	BL 52740	Pfeiffer, Rubin LexA Collection
$MZ19^{QF}$ (II)	BL 41573	Hong et al.[114]
QUAS-mtdTomato-3xHA (II)	BL 30004	Potter et al.[115]
58F02-Gal4 (attp2)	BL 39186	Jenett et al.[117]
UAS-CD8GFP (III)	BL 5130	Lee and Luo et al.[110]
10XUAS-IVS-myr::GFP (attP2)	BL 32197	Pfeiffer et al.[118]
R25D01-lexA (attP40)	BL 53519	Pfeiffer, Rubin LexA Collection
13XLexAop2-IVS-GCaMP6s-SV40 (su(Hw)attP5)	BL 44589	FBrf0221946
10XUAS-IVS-myr::tdTomato (attP2)	BL 32221	Pfeiffer et al.[118]
R53C03-lexA (attP40)	BL 52861	Pfeiffer, Rubin LexA Collection
$UAS\text{-}Dscam^{3.36.25.1}$::RFP on II	via Vanessa Ruta	Tzumin Lee lab, made by Jacob Yang following Yu et al.[119]
LexAopChrimson::tdTomato on III	BL 55139	N/A
Gr64f-LexA on III	N/A	Rajagopalan et al.[71]
P{hs-KD}attP3	BL 56167	Awasaki et al.[120]
mBitbow 2.2 (mem5FP KDon>FLP>) VK00027	N/A	This paper

(*Continued on next page*)

Please cite this article in press as: Ahmed et al., Input density tunes Kenyon cell sensory responses in the *Drosophila* mushroom body, Current Biology (2023), https://doi.org/10.1016/j.cub.2023.05.064

Continued

REAGENT or RESOURCE	SOURCE	IDENTIFIER
UAS-Dscam$^{3.36.25.1}$::GFP on X	via Bing Ye	Wang et al.[63]
LexAopChrimson::tdTomato on X	Unknown	Janelia fly facility
UAS-CD8GFP/+; GH146^{QF}, QUAS-mtdTomato-3xHA/ P(caryP)attp2; OK107^{Gal4}/+ male, 2-3 days old	N/A	Figure 1A
LexAopChrimson::tdTomato/+; Gr64f-LexA/UAS-mud RNAi; OK107^{Gal4}/+ female, 3-7 days old	N/A	Figure 1C
LexAopChrimson::tdTomato/+; Gr64f-LexA/P(caryP) attp2; OK107^{Gal4}/+ female, 3-7 days old	N/A	Figure 1C
UAS-GCaMP6s/+; UAS-GCaMP6s/UAS-mud RNAi; OK107^{Gal4}/+ mix of males and females, 2-5 days old	N/A	Figures 1E–1J and S1
UAS-GCaMP6s/+; UAS-mud RNAi/TM2; OK107^{Gal4}/+ mix of males and females, 2-5 days old	N/A	Figures 1E–1J and S1
UAS-GCaMP6s/+; UAS-GCaMP6s/ P(caryP)attp2; OK107^{Gal4}/+ mix of males and females, 2-5 days old	N/A	Figures 1E–1J and S1
UAS-GCaMP6s/+; P(caryP)attp2/TM2; OK107^{Gal4}/+ mix of males and females, 2-5 days old	N/A	Figures 1E–1J and S1
hsKD; CyO/+; Bitbow 2.2/UAS-Tao RNAi; OK107^{Gal4}/+ males, 2-5 days old	N/A	Figures 2C, 2D, and S2B
hsKD; CyO/+; Bitbow 2.2/+; OK107^{Gal4}/+ males, 2-5 days old	N/A	Figures 2C, 2D, and S2B
UAS-CD8GFP/+; GH146^{QF}, QUAS-mtdTomato-3xHA/ UAS-Tao RNAi; OK107^{Gal4}/+ males, 3 days old	N/A	Figures 2E–2G and 2I–2N
UAS-CD8GFP/+; GH146^{QF}, QUAS-mtdTomato-3xHA/ P(caryP)attp2; OK107^{Gal4}/+ males, 3 days old	N/A	Figures 2E–2G and 2I–2N
UAS-mCD8GFP/+; Gr64f-LexA, LexAop cs-Chrimson-tdTomato/P(caryP)attp2; OK107^{Gal4}/+ females, 3-7 days old	N/A	Figure 2H
UAS-mCD8GFP/+; Gr64f-LexA, LexAop cs-Chrimson-tdTomato/UAS-Tao RNAi; OK107^{Gal4}/+ females, 3-7 days old	N/A	Figure 2H
UAS-GCaMP6s/+; UAS-GCaMP6s/UAS-Tao RNAi; OK107^{Gal4}/+ mix of males and females, 2-5 days old	N/A	Figures 3 and S3
UAS-GCaMP6s/+; UAS-Tao RNAi/TM2; OK107^{Gal4}/+ mix of males and females, 2-5 days old	N/A	Figures 3 and S3
UAS-GCaMP6s/+; UAS-GCaMP6s/ P(caryP)attp2; OK107^{Gal4}/+ mix of males and females, 2-5 days old	N/A	Figures 3 and S3
UAS-GCaMP6s/+; P(caryP)attp2/TM2; OK107^{Gal4}/+ mix of males and females, 2-5 days old	N/A	Figures 3 and S3
hsKD; Dscam$^{3.36.25.1}$:RFP/Bl; Bitbow 2.2/+; OK107^{Gal4}/+ males, 3-4 days old	N/A	Figures 4A and 4B
hsKD; Bl/+; Bitbow 2.2/+; OK107^{Gal4}/+ males, 3-4 days old	N/A	Figures 4A and 4B
Dscam$^{3.36.25.1}$:GFP; UAS-CD8GFP/Pin; GH146^{QF}, QUAS-mtdTomato-3xHA/+; OK107^{Gal4}/+ males, 2-3 days old	N/A	Figures 4C–4K
Dscam$^{3.36.25.1}$:GFP; Pin/CyO; TM2/+; OK107^{Gal4}/+ males, 2-3 days old	N/A	Figures 4C–4K
UAS-CD8GFP/Sp; GH146^{QF}, QUAS-mtdTomato-3xHA/TM2; OK107^{Gal4}/+ males, 2-3 days old	N/A	Figures 4C–4K
Bl/CyO; TM2/TM6B; OK107^{Gal4}/+ males, 2-3 days old	N/A	Figures 4C–4K
UAS-GCaMP6s/Dscam$^{3.36.25.1}$:RFP; UAS-GCaMP6s/+; OK107^{Gal4}/+ mix of males and females, 2-5 days old	N/A	Figures 5 and S4
UAS-GCaMP6s/Dscam$^{3.36.25.1}$:RFP; UAS-GCaMP6s/TM2; OK107^{Gal4}/+ mix of males and females, 2-5 days old	N/A	Figures 5 and S4
Males: UAS-GCaMP6s/+; UAS-GCaMP6s/ +; OK107^{Gal4}/+ Females: yw/+; UAS-GCaMP6s/+; UAS-GCaMP6s/ +; OK107^{Gal4}/+ 2-5 days old	N/A	Figures 5 and S4

(*Continued on next page*)

Please cite this article in press as: Ahmed et al., Input density tunes Kenyon cell sensory responses in the *Drosophila* mushroom body, Current Biology (2023), https://doi.org/10.1016/j.cub.2023.05.064

Continued

REAGENT or RESOURCE	SOURCE	IDENTIFIER
Males: UAS-GCaMP6s/+; UAS-GCaMP6s/TM2; OK107^{Gal4}/+ Females: yw/+;UAS-GCaMP6s/+; UAS-GCaMP6s/TM2; OK107^{Gal4}/+ 2-5 days old	N/A	Figures 5 and S4
13x LexAop cs-Chrimson-tdTomato/+; 58E02-LexA/Mz19^{QF}, QUAS-mtdTomato-3xHA; 58F02-Gal4, UAS-mCD8GFP/ 10xUAS-IVS-myrGFP females, 3-8 days old	N/A	Figures 6B–6F and S5A–S5E
R25D01-LexA, LexAop-GCaMP6s/CyO; UAS-tdTomato/TM6B; OK107^{Gal4}/OK107^{Gal4} mix of males and females, 2-5 days old	N/A	Figures 6G–6I, S5F, and S5G
UAS-mCD8GFP/+; Gr64f-LexA, LexAop cs-Chrimson-tdTomato/P(caryP)attp2; OK107^{Gal4}/+ females, 3-7 days old	N/A	Figures 7A–7D
UAS-mCD8GFP/+; Gr64f-LexA, LexAop cs-Chrimson-tdTomato/UAS-mud RNAi; OK107^{Gal4}/+ females, 3-7 days old	N/A	Figures 7A–7D
UAS-mCD8GFP/+; Gr64f-LexA, LexAop cs-Chrimson-tdTomato/UAS-Tao RNAi; OK107^{Gal4}/+ females, 3-7 days old	N/A	Figures 7A–7D
UAS-mCD8GFP/+; Gr64f-LexA, LexAop cs-Chrimson-tdTomato/P(caryP)attp2; OK107^{Gal4}/+ females, 4-10 days old	N/A	Figures 7E and S6A
UAS-mCD8GFP/+; Gr64f-LexA, LexAop cs-Chrimson-tdTomato/UAS-Tao RNAi; OK107^{Gal4}/+ females, 4-10 days old	N/A	Figures 7E and S6A
UAS-mCD8GFP/Dscam$^{3.36.25.1}$:RFP; Gr64f-LexA, LexAop cs-Chrimson-tdTomato/+; OK107^{Gal4}/+ females, 4-10 days old	N/A	Figures 7E and S6A
R25D01-LexA, LexAop-GCaMP6s/+; UAS-tdTomato/P(caryP) attp2; OK107^{Gal4}/+ mix of males and females, 2-5 days old	N/A	Figures 7F–7H, S6B, and S6C
R25D01-LexA, LexAop-GCaMP6s/+; UAS-tdTomato/UAS-mud RNAi; OK107^{Gal4}/+ mix of males and females, 2-5 days old	N/A	Figures 7F–7H, S6B, and S6C
R25D01-LexA, LexAop-GCaMP6s/+; UAS-tdTomato/UAS-Tao RNAi; OK107^{Gal4}/+ mix of males and females, 2-5 days old	N/A	Figures 7F–7H, S6B, and S6C
Software and algorithms		
Suite2p	HHMI Janelia Research Campus, Ashburn, VA	Pachitariu et al.[55]
FIJI	Open source	Schindelin et al.[121]
FIJI plugin “Blind Analysis Tools”	N/A	https://imagej.net/Blind_Analysis_Tools
Cellpose	HHMI Janelia Research Campus, Ashburn, VA	Stringer et al.[116]
GraphPad Prism 9	GraphPad Software, La Jolla, CA	https://www.graphpad.com/scientific-software/prism/
R	R Foundation for Statistical Computing, Vienna, Austria	https://www.R-project.org/
R package “corrplot”	N/A	https://github.com/taiyun/corrplot
Python	Centrum voor Wiskunde en Informatica Amsterdam	https://www.python.org/downloads/
MATLAB 2018b, Mathworks	The Mathworks, Natick, MA	https://www.mathworks.com/products/matlab.html
MATLAB 2020b, Mathworks	The Mathworks, Natick, MA	https://www.mathworks.com/products/matlab.html
Other		
Duck EZ Start Packaging tape	Office Depot	511879
UV Glue	Loctite	3106
JAXMAN 365nm Flashlight	Amazon	B077GPXBK1
Electra Waxer	Almore	66000
Gulfwax Paraffin	Grocery store	C0130
Hair	EJC	N/A
Umich fly food	Lab Express, Ann Arbor, MI	“B” food
Janelia fly food	HHMI Janelia Research Campus, Ashburn, VA	N/A

(*Continued on next page*)

Please cite this article in press as: Ahmed et al., Input density tunes Kenyon cell sensory responses in the *Drosophila* mushroom body, Current Biology (2023), https://doi.org/10.1016/j.cub.2023.05.064

Continued

REAGENT or RESOURCE	SOURCE	IDENTIFIER
Heat packs for mailing flies	TSKSupply	40hour Uniheat
Thermometers for mailing flies	ThermoPro	TP50
Cell strainer caps (used as colanders for stainings)	Fisher	BD 352235
Binder reinforcement stickers (for mounting brains)	Office Depot	Avery 5722
Terasaki plates Greiner Bio-One (for staining)	Fisher	07-000-623
Grape juice agar plates	Lab Express, Ann Arbor, MI	N/A
Coffee filters	Departmental coffee supplies	N/A
Caps for odor vials	Sigma	27020
Odor vials	Sigma	27088-U
Cover glass 22x22 mm Square No. 1. Corning. # (for mounting, Janelia)	Corning	CLS284522-2000EA
Cover glass 22x22 mm Square No. 2. (for spacers, Janelia)	Fisher	12-540B
Cover glass staining jar (Janelia)	EMS	72242-24
Diamond Cleaver (Janelia)	https://diatome.com/	CLE
DPX Slide Jig	Janelia Instrument Design & Fabrication	http://hhmi.flintbox.com/public/project/26605
Drosophila Mounting T-dish. 8x10 (Janelia, for adult brains)	Janelia Instrument Design & Fabrication	http://hhmi.flintbox.com/public/project/26606
Superfrost Plus Slides 25x75 mm	Fisher	12-550-15

RESOURCE AVAILABILITY

Lead contact

Further information and requests for resources and reagents should be directed to and will be fulfilled by the lead contact, E. Josephine Clowney (jclowney@umich.edu).

Materials availability

Upon publication, the mBitbow2.2 flies generated in this study will be deposited in the Bloomington Drosophila Stock Center for distribution to the research community.

Data and code availability

All data reported in this paper will be shared by the lead contact upon request. MATLAB code used to analyze the behavioral data, and any additional information required to re-analyze the data reported in this paper is available from the lead contact upon request.

EXPERIMENTAL MODEL AND SUBJECT DETAILS

Flies

All fly lines used in this study are listed in the key resources table. Flies used for anatomy and functional imaging were maintained on cornmeal ('Bloomington-B') food (Lab Express, Ann Arbor, MI) augmented with a yeast sprinkle in a humidified incubator at 25°C on a 12:12 light:dark cycle. For dense Bitbow labeling (Figure 2B), progeny of the hsKD;elav-Gal4;; and;;mBitbow2.2; flies were collected and heat shocked at the 1st instar larval stage for 30 mins in a 37°C water bath. Adults were collected 4 days after eclosion for immunostaining and imaging. For sparse Kenyon cell labeling, hsKD;;; flies were crossed with;;mBitbow2.2; OK107-Gal4. No heat shock was given. Flies used for behavioral experiments were maintained on Janelia Research Campus's standard cornmeal food supplemented with 0.2 mM all-trans-retinal. Hydroxyurea-treated ablation flies and sham-treated controls were reared in a humidified incubator at 21°C on a 12:12 light:dark cycle, while all other flies were reared at 25°C on a 12:12 light:dark cycle. Flies were kept in the dark throughout. Experimental crosses for ablation experiments were set up with large numbers of males (60-100 per cage) and females (300-500 per cage). All other behavior crosses were set up with 8 male and 8 female parents and a sprinkle of yeast was added to the food vials. Cross progeny (2-7 days old) were sorted on a cold plate at around 4°C and females of the appropriate genotype were transferred to starvation vials. Starvation vials contained nutrient-free 1% agarose to prevent desiccation. While we used mixed-sex cohorts when possible, certain genetic and experimental approaches required us to use one sex or the other, as detailed below under behavioral and image analysis (e.g. males are too small for the Y-arena).

Please cite this article in press as: Ahmed et al., Input density tunes Kenyon cell sensory responses in the *Drosophila* mushroom body, Current Biology (2023), https://doi.org/10.1016/j.cub.2023.05.064

CellPress

METHOD DETAILS

Immunostainings

This protocol is adapted from Elkahlah et al.,[29] with some modifications. Brains were dissected for up to 20 min in AHL dissection saline (108 mM NaCl, 5 mM KCl, 2 mM CaCl2, 8.2 mM MgCl2, 4 mM NaHCO3, 1 mM NaH2PO4, 5 mM trehalose, 10 mM sucrose, 5 mM HEPES pH7.5, osmolarity adjusted to 265 mOsm). For most experiments, brains were transferred to 1% paraformaldehyde in PBS on ice. All steps were performed in cell strainer baskets (caps of FACS tubes) in 24 well plates, with the brains in the baskets lifted from well to well to change solutions. Brains were fixed overnight at 4C in 1% PFA in PBS. On day 2, brains were washed 3 × 10' in PBS supplemented with 0.1% triton-x-100 on a shaker at room temperature, blocked 1 hr in PBS, 0.1% triton, 4% Normal Goat Serum, and then incubated for at least two overnights in primary antibody solution, diluted in PBS, 0.1% triton, 4% Normal Goat Serum. Primary antibody was washed 3 × 10' in PBS supplemented with 0.1% triton-x-100 on a shaker at room temperature, then brains were incubated in secondary antibodies for at least two overnights, diluted in PBS, 0.1% triton, 4% Normal Goat Serum. When used, DAPI (one μg/mL) and phalloidin 568 (1:40-1:80) were included in secondary antibody mixes. Primary antibodies used were mouse anti-ChAT 4B1 (1:200, DSHB), rabbit anti-dsRed (1:500-1:1000, Clontech), sheep anti-GFP (1:250-1:1000, Bio-Rad), chicken anti-GFP (1:5000, Dawen Cai), mouse anti-nc82 (1:30, DSHB). Secondary antibodies were Alexa 488, 568, and 647 conjugates (1:500, Invitrogen). Brains were mounted in 1x PBS, 90% glycerol supplemented with propyl gallate in binder reinforcement stickers sandwiched between two coverslips. Samples were stored at 4°C in the dark prior to imaging. The coverslip sandwiches were taped to slides, allowing us to perform confocal imaging on one side of the brain and then flip over the sandwich to allow a clear view of the other side of the brain. This allowed us to score features on the anterior and posterior sides of each sample. Scanning confocal stacks were collected along the anterior-posterior axis on a Leica SP8 with one micrometer spacing in Z and ~200 nm axial resolution.

For sparse Bitbow labeling (Figures 2C, 2D, 5I, and 5J), brains were fixed in 4% paraformaldehyde at room temperature for 30 minutes. This was followed by washing 3 × 10' in PBS supplemented with 0.1% triton-x-100 on a shaker at room temperature. The brains were blocked 1 hr in PBS, 0.1% triton, 4% Normal Goat Serum or StartingBlock. All the steps were carried out in Terasaki plates, with each well containing 2-3 brains to keep track of fixation, wash, and block timing. The brains were then moved to 24-well plates for incubation with primary antibody solution at 4C. Subsequent steps of secondary antibody incubation, mounting and imaging were the same as described above. Primary antibodies were rat anti-mTFP (1:500), chicken anti-GFP (1:5000), rabbit anti-mNeonGreen (1:500), mouse anti-mKusabira-Orange2 (1:500), guinea pig anti-mKate2 (1:500) (Dawen Cai Lab) and secondary antibodies were Alexa 488, 594, 647 conjugates (1:500, Invitrogen), CF 555, CF 633 (1:500, Sigma), and Atto490 LS (1:250, Hypermol). For dense Bitbow labeling in Figure 2A, a similar protocol was followed as described in Li et al.[61] The difference from the sparse Bitbow protocol above was that the mounting media was Vectashield. The confocal image was acquired with Zeiss LSM780 with a 40 × 1.3 NA oil immersion objective (421762-9900-000). A 32-channel GaAsP array detector was used to allow multi-track detection of five fluorophores with proper channel collection setups.

The following protocol applies to the dissections, immunohistochemistry and imaging of fly brains done post-behavior (Figures 6 and 7), and for the Brp staining (Figures 1D and 2H). These were done principally as previously described[43]; https://www.janelia.org/project-team/flylight/protocols. In brief, brains were dissected in Schneider's insect medium and fixed in 2% paraformaldehyde (diluted in the same medium) at room temperature for 55 mins. Tissues were washed in PBT (0.5% Triton X-100 in phosphate buffered saline) and blocked using 5% normal goat serum before incubation with antibodies. Since flies had to be tracked individually, single dissected tissues were fixed and washed in microwell plates. After washes in the microwell plate, tissues were mounted on poly-L-lysine-coated cover slips before performing immunohistochemistry, post-fixation, and embedding in DPX as described. Tissues expressing GFP and tdTomato were incubated with chicken anti-GFP (1:1000, Fisher) together with rabbit anti-dsRed (1:1000, Clontech), and mouse anti-BRP hybridoma supernatant (1:30, DSHB), followed by Alexa Fluor 488-conjugated goat anti-chicken (Fisher), CyTM3-conjugated goat anti-rabbit (Jackson ImmunoResearch), and CyTM5-conjugated goat anti-mouse (Jackson ImmunoResearch). Some tissues were labeled with mouse anti-ChAT hybridoma supernatant (1:100, DSHB) instead of anti-BRP, while all other antibodies remained the same. Nuclei were stained with DAPI. Image z-stacks were collected using an LSM880 confocal microscope (Zeiss, Germany) fitted with Plan-Apochromat 40X/1.3 and Plan-Apochromat 63X/1.40 oil immersion objectives. All tissues were first imaged at 40X with a voxel size of 0.44 x 0.44 x 0.44 mm3 (1024 x 1024 pixels in xy). Selected tissues were imaged at higher resolution in one of three ways: at 40X with a voxel size of 0.22 x 0.22 x 0.44 mm3 (2048 x 2048 pixels in xy; "40X hi-res"), at 63X with a voxel size of 0.19 x 0.19 x 0.37 mm3 (1024 x 1024 pixels in xy; "63X hi-res-1"), or at 63X with a voxel size of 0.1 x 0.1 x 0.37 mm3 (2048 x 2048 pixels in xy; "63X hi-res-2").

Molecular cloning of mBitbow2.2

DNA fragment of EcoRI-FrtF15-KDRT-FlpN-KDRT-SwaI was synthesized by GeneArt (Thermo Fisher), and cloned in pattB-nSyb-sr(Flp)F15[61] to replace the N-terinal region of flippase, yielding pattB-nSyb-sr(KDonFlp)F15. nSyb-sr(KDonFlp)F15 was then amplified by PCR and integrated into NdeI-linearized mBitbow1.0 through Gibson assembly, yielding mBitbow2.2.

HU ablation

To generate flies with reduced Kenyon cell numbers, we used an existing chemical method to ablate KC neuroblasts.[29,69,70] In *Drosophila*, 4 mushroom body neuroblasts from each hemisphere give rise to ~500 KCs each.[122] Most neuroblasts pause their

Please cite this article in press as: Ahmed et al., Input density tunes Kenyon cell sensory responses in the *Drosophila* mushroom body, Current Biology (2023), https://doi.org/10.1016/j.cub.2023.05.064

divisions during the first 8 hours after larval hatching (ALH), however MB neuroblasts continue to divide. Therefore, by feeding larvae a mitotic poison hydroxyurea (HU) during this time window, Kenyon cell neuroblasts can specifically be ablated.[69] We can achieve a wide range of KC numbers by tweaking the concentration and duration of HU application.[29] This allowed us to generate flies with 0 to 4 KC neuroblasts, and the effect on each hemisphere was independent of the other resulting in a large range of KC numbers. However, as we described previously, the most informative brains, with intermediate numbers of KC neuroblasts remaining, are difficult to obtain—most ablation batches have a preponderance of unaffected or fully ablated mushroom bodies.

The protocol was adapted from Elkahlah et al.[29] and Sweeney et al.[70] We set up large populations of flies in cages two days prior to ablation and placed a 35 or 60 mm grape juice agar plate (Lab Express, Ann Arbor, MI) in the cage with a dollop of goopy yeast. One day prior to the ablation, we replaced the grape juice/yeast plate with a new grape juice/yeast plate. On the morning of the ablation, we removed the plate from the cage and discarded the yeast puck and any hatched larvae on the agar. We then monitored the plate for up to four hours, until many larvae had hatched. Larvae were washed off the plate using a sucrose solution, and eggs were discarded. Larvae were then strained in coffee filters, and submerged in hydroxyurea (Sigma, H8627) in a yeast:AHL mixture, or sham mixture without HU. Ablation condition was 10 mg/mL HU, given for 1 hour. One batch experienced 15 mg/mL HU, given for 1 hour; this was done to gather more data points with a lower KC clone count. Larvae were then strained through coffee filters again, rinsed, and placed in a vial or bottle of B food (for MBON functional imaging and immunohistochemistry) or Janelia food supplemented with 0.2 mM all-trans-retinal (for behavior) until eclosion. We opened a new container of hydroxyurea each month as it degrades in contact with moisture, and we found its potency gradually declined. We achieved a U-shaped distribution of the HU effect, with many samples unaffected and many with all four KC neuroblasts lost. Ablated animals along with the control group (sham) were shipped in temperature-controlled conditions to Janelia Research Campus for behavior. A digital thermometer was kept in each shipment to record the lowest and highest temperature experienced during shipping. Batches that experienced ~15-27 Celsius were used for experiments. Animals were either shipped as larvae or late pupae, and not as adults in order to give enough time window for using the appropriate age of adult flies for behavior experiments.

Identification of relevant MBON driver lines

LexA drivers for MBONs were screened from Janelia FlyLight online collection database and previous split-GAL4 characterization.[43] Among the LexA drivers, R25D01 was selected based on its specific expression in $\gamma2,\alpha'1$ MBON, involvement in odor-associated appetitive memory formation, and ability to drive quantifiable GCaMP6s expression.[44,65] We used R25D01-LexA to drive expression of GCaMP6s in $\gamma2,\alpha'1$ MBON for MBON functional imaging, and to assess connection between KCs and MBONs morphologically.

In vivo functional imaging

Protocol was adapted from Elkahlah et al.[29] and Ruta et al.[123] We prepared 2–5 day old adult flies for *in vivo* two photon calcium imaging on a Bruker Investigator, affixing the fly to packaging tape (Duck EZ Start) with human hair and UV glue (Loctite 3106). The fly was tilted to allow optical access to KC somata, at the dorsal posterior surface of the brain. For MBON axonal imaging, the fly was similarly prepped to allow optical access to the mushroom body lobes for visualizing MBON axons; these flies also carried a Kenyon cell label to serve as an anatomical guide. We waxed the proboscis in an extended position to reduce motion. Imaging was performed in external saline (AHL). For odor delivery, half of a 1200 mL/min airstream, or 600 mL/min, was directed toward the antennae through a Pasteur pipette mounted on a micromanipulator. At a trigger, 10% of the total air stream was re-directed from a 10 mL glass vial containing mineral oil to a vial containing odorants diluted 1:10 in mineral oil, or a second vial of mineral oil (mechanosensory control). Final odor dilution was therefore 1:100. Filter paper 'wicks' were inserted into each vial to allow odor to saturate the vial headspace. Odors were delivered for two seconds, with 30 s in between stimulations. We used a simplified olfactometer capable of delivering five different odorants in which overall airflow was metered by analogue flowmeters (Brooks Instruments) and valve switching controlled by an Arduino. Odor delivery was initially optimized using a mini-PID placed in the half of the air stream not directed at the fly (Aurora Biosciences). Images were collected at ~5 Hertz, and we imaged a single plane for each sample. Odors used were ethyl acetate (EA), isobutyl acetate (IBA), benzaldehyde (BZH), octanol (OCT), and methylcyclohexanol (MCH). Recording neuronal responses to the mineral oil control allows us to monitor sensory components that are a shared across the different odor stimuli, including olfactory responses to volatiles in the oil and mechanosensory responses to slight changes in air flow as vials switch on and off.[124]

Kenyon cell *in vivo* imaging experiments on empty attp2 control and *mud* RNAi cohorts were done with BZH (Figure 1), as were our previous experiments on HU-ablated animals.[29] However, due to a technical issue of odor precipitation with BZH, we switched to OCT in imaging experiments in the fall of 2020. The *Tao* RNAi cohort (Figure 3) were done after this date, with OCT. Due to the difficulty of obtaining stable recordings of Kenyon cell populations *in vivo*, in Figure 3 we compare the *Tao* RNAi animals to the empty attp2 controls imaged earlier using BZH (see legend of Figure 3). To ensure that nothing had changed in our imaging setup or the environment between these dates, we imaged a few empty attp2 controls interspersed with *Tao* RNAi animals, using the OCT setup (not shown); we did not observe any striking difference from the control data shown in Figure 3. Indeed, across our functional imaging experiments with Kenyon cells in variously constituted mushroom bodies for the last four years, we have never observed the prevalent and non-selective odor responses that we observe in *Tao* RNAi Kenyon cells.

Please cite this article in press as: Ahmed et al., Input density tunes Kenyon cell sensory responses in the *Drosophila* mushroom body, Current Biology (2023), https://doi.org/10.1016/j.cub.2023.05.064

Analysis of KC somatic odor responses

We collected data from a total of 14 empty attp2 control animals (14 hemispheres imaged), 13 *mud* RNAi (20 hemispheres imaged), 18 *Tao* RNAi (34 hemispheres imaged), 8 Dscam$^{3.36.25.1}$ animals (17 hemispheres imaged), and 15 yw controls for Dscam (35 hemispheres imaged). For each animal, the two hemispheres were imaged and analyzed separately. Sometimes, only one hemisphere was imaged due to the preparation and a few hemispheres were excluded from analysis because of poor image quality. For some animals, a second plane of cells was imaged from the same hemisphere if the first one looked unstable or did not have enough cells in view, accounting for the instances above in which hemispheres imaged appears greater than two per animal. Mineral oil was delivered twice, and then each of four odors were delivered twice, in sequence. Following mineral oil, odor order varied. Given the convention in the field and due to experiments in locusts showing that the first presentation of certain odors can cause distinct Kenyon cell responses to all subsequent presentations of that same odor, we only analyzed the second presentation of each odor.[106,125]

Following functional imaging, we collected a Z-stack of the mushroom body on the two-photon. We used these images to categorize the extent of KC increase in *mud* RNAi animals, by measuring the maximum cross-sectional calyx area. Only sufficiently expanded hemispheres (maximum cross-sectional calyx area > 1800 μm^2) were included in analysis as ''Kenyon cell-increased'' animals. While sex differences have not been reported in the mushroom body, we tried our best to include an equal mix of males and females in the imaging. However, after the images were filtered for analysis based on the exclusion criteria provided, we ended up with a disproportionate number of males and females. All samples are accounted for here:

Genotype/Condition	Total hemispheres imaged	Damaged/ unresponsive	Poor image quality	Mineral oil frame shaky	Kenyon cells did not look increased	Too much motion	Less than 15 ROIs (cells) stable	Analyzed (# of males and females)
Empty attp2 control (for RNAi)	14	1	2	1	N/A	4	0	6 (5 females, 1 male)
mud RNAi	20	1	1	2	2	7	1	6 (all males)
Tao RNAi	34	3	4	0	N/A	13	2	12 (11 females, 1 male)
yw control (for Dscam)	35	2	6	0	N/A	18	1	8 (4 females, 4 males)
Dscam$^{3.36.25.1}$	17	1	5	0	N/A	3	1	7 (6 females, 1 male)

All samples were motion-corrected using Suite2p.[55] Using FIJI ''Blind Analysis Tools'' package, we blinded ourselves to the motion-corrected datasets. We excluded images if there was too much motion to be able to follow the same cell over time, or the image quality was poor (e.g. warping in the image, cells hard to see). After filtering for these criteria, ROIs were chosen in each of the samples and we measured $\Delta f/f$ (i.e. $(f-f_0)/f_0$), comparing stimulus frames with pre-stimulus frames. ROIs were manually chosen and we were careful about ensuring that the cell remained within its ROI for all frames. For samples where the ROIs were only stable in 3 out of 4 odors, those images were only used to calculate the proportion of cells that were responsive to each odor, and not in calculating the number of odors each cell responded to. Any image where the mineral oil stimulus frames were not stable was not analyzed, and any image with less than 15 ROIs stable was not analyzed. After these gates, there were 6 empty attp2 controls (for *mud* and *Tao* RNA), 6 *mud* RNAi, 12 *Tao* RNAi, 8 controls (for Dscam), and 7 Dscam$^{3.36.25.1}$ images in the analysis. The baseline fluorescence was determined for each odor delivery by taking the average of the frames within the three seconds before the trigger. The stimulus frame was determined by taking the peak response between 0–4 s after stimulus onset, to account for the valve opening and the two second odor delivery. To define 'responsive' cells, we chose to use a cutoff of $\Delta f/f > 0.2$ (20% increase in fluorescence over baseline) across samples. This was to avoid obscuring overall differences in responsiveness across the conditions. In all figures, the proportion of Kenyon cells responding to each stimulus and proportion of Kenyon cells responding to 0, 1 or multiple odors were calculated using this threshold.

For visualization, we used the ''Math'' and ''Image calculator'' tools in FIJI to make a custom colored heatmap of the $\Delta f/f$ responses, where cells with $\Delta f/f$ values < 0.2 were colored black. The background outside the KC somata was cleared for ease of visualization, and the ''$\Delta f/f$ image'' was created by using average value of pixels in baseline frames as f_0 and average of peak frames as f, and applying the calculation $((f-f_0)/f_0)$ to the images. The maximum value for the color scale varies in each figure due to the diverse range of odor responses in the different circuit manipulations tested. The grayscale image displaying the cells was created by creating an average projection of all the frames for that hemisphere.

Control odor responses were in line with what we have previously reported using GCaMP6s and match electrophysiological spiking responses in the previous work by Murthy, but surpass the spiking response rates we observed previously.[29,106,107] Importantly, because GCaMP6s is so sensitive, it is likely to report sub-threshold as well as spiking responses.

Analysis of MBON odor responses

We collected data from a total of 10 empty attp2 (RNAi control) animals (18 hemispheres imaged), 17 *mud* RNAi animals (29 hemispheres imaged), 11 *Tao* RNAi animals (21 hemispheres imaged), 8 sham animals (15 hemispheres imaged), and 9 HU-treated animals (15 hemispheres imaged). Each hemisphere was analyzed separately. Occasionally, only one hemisphere of the animal was imaged due to the MBON/KC signal not being visible in preparation. Guided by vertical lobe of KCs, we used a single focal plane

Please cite this article in press as: Ahmed et al., Input density tunes Kenyon cell sensory responses in the *Drosophila* mushroom body, Current Biology (2023), https://doi.org/10.1016/j.cub.2023.05.064

to image axonal response of γ2,α'1 MBON in each hemisphere. We chose to record axonal responses for the following reasons: (1) axonal imaging is more feasible than dendritic and somatic imaging, as somata of γ2,α'1 MBON are too deep and their GCaMP signal was obscured by fluorescence from the KC lobes, (2) functional KC-MBON connections should allow signal propagation to downstream neurons, which can be seen by axonal activity of MBONs. Similar activity measurements have been used in previous research.[126] Odor delivery was the same as mentioned in the section above except that all odors were delivered in a certain order.

Following functional imaging, we collected a Z-stack of the mushroom body on the two-photon. We used these images to categorize the extent of KC increase or decrease by measuring the maximum cross-sectional calyx area. All samples are accounted for here:

Genotype/Condition	Total hemispheres	Damaged/unresponsive	KCs did not look increased (mud RNAi) or decreased (ablation)	Too much motion	Too low expression	Analyzed
control (attp2)	18	0	N/A	4	3	11 (9 females, 2 males)
mud RNAi	29	0	6	6	8	9 (1 females, 8 males)
Tao RNAi	21	0	N/A	6	3	12 (5 females,7 males)
Sham	15	1	N/A	0	0	14 (7 females, 7 males)
Ablation	15	0	2	2	1	10 (2 females, 8 males)

Only sufficiently expanded *mud* RNAi hemispheres (maximum cross-sectional calyx area > 2200 μm^2; for control(attp2) and *mud* RNAi, each calyx was imaged by two-photon right after Calcium imaging) were included in the analysis of the KC-increased animals. Only sufficiently HU-ablated hemispheres (maximum cross-sectional calyx area < 2100 μm^2; for Sham and Ablation, each calyx was imaged in post hoc dissected brains by two-photon). For RNAi modulation, as LexAop-GCaMP6s in all animals are heterozygous, we excluded images where axonal baseline fluorescence was not distinguishable from the background; these are categorized as ''Too low expression''. In sham and KC-reduced condition, LexAop-GCaMP6s is homozygous and provided robust axonal GCaMP expression. All samples were motion-corrected in batch using Suite2p.[55] ROIs were automatically chosen by applying triangle auto-threshold method in FIJI (v2.3.0) to find pixels with higher intensity than the background in the axonal area, including axon terminals and fibers. For Δf/f, we chose the time window 5 s to 2 s before onset of odor stimulus as baseline, while peak responses were the maximum response between 0 s to 12 s after odor stimulus onset. Corresponding visualization was performed similar to the method described above by averaging 5s to 2s before onset of odor as baseline, and averaging 2s after maximum response as peak. There is no ''0.2 cut-off''.

Y-arena

Single fly behavior experiments were performed in a novel olfactory Y-arena. A detailed description of the apparatus is provided in Rajagopalan et al.[71] Briefly, the Y chamber consists of two layers of white opaque plastic. The bottom is a single continuous circular layer and serves as the floor of the Y that flies navigate. The top is a circular layer with a Y shaped hole serving as the walls of the Y. The length of each arm from center to tip is 5 cm and the width of each arm is 1 cm. These two layers are placed underneath an annulus of black aluminum. A transparent glass disk is located in the center of this annulus and acts as the ceiling of the Y - allowing for video recording of experiments. This transparent disk is rotatable and contains a small hole used to load flies. The black annulus houses three clamps that hold the circular disk in place. All three layers are held together and made airtight with the help of 12 screws that connect the layers. The Y chamber is mounted above an LED board that provides infrared illumination to monitor the fly's movements, and red (617 nm) light for optogenetic activation. Experiments were recorded from above the Y using a single USB3 camera (Flea3, model: FL3-U3-13E4M-C: 1.3 MP, 60 FPS, e2v EV76C560, Mono; Teledyne FLIR, with longpass filter of 800 nm). Each arm of the Y has a corresponding odor delivery system, capable of delivering up to 5 odors. For our experiments, olfactometers injected air/odor streams into each arm at a flow rate of 100 ml/min. The center of the Y contains an exhaust port connected to a vacuum, which was set at 300 ml/min using a flow meter (Dwyer, Series VF Visi-Float acrylic flowmeter) - matching total input flow in our experiments. We wrote custom MATLAB code (MATLAB 2018b, Mathworks) to control the Y-arena and run experiments.

Behavioral Protocol

Odorant information

The following odorants were used to form cue-reward relationships in the Y-arena task:

1. 3-Octanol (OCT), diluted in paraffin oil at a 1:500 concentration and then air-diluted to a fourth of this concentration.
2. 4-Methyl-cyclo-hexanol (MCH), diluted in paraffin oil at a 1:500 concentration and then air-diluted to a fourth of this concentration.

Y-arena behavioral task structure and design

Flies were starved between 36-60 hrs before being aspirated into the Y-arena for experiments. Flies were inserted randomly into one of the three arms. This arm was injected with a clean airstream and the two odors were randomly assigned to the other two arms. For

Please cite this article in press as: Ahmed et al., Input density tunes Kenyon cell sensory responses in the *Drosophila* mushroom body, Current Biology (2023), https://doi.org/10.1016/j.cub.2023.05.064

a given fly, one of the odors was paired with reward 100% of the time. Once a fly reached the choice zone of either odor arm, a choice was considered to have been made. If the rewarded odor was chosen, the fly was rewarded with a 500 ms flash of red LED (617 nm, 1.9mW/cm^2) to activate the appropriate reward-related neurons. The arena was then reset with the arm chosen by the fly injected with clean air and odors randomly assigned to the other two arms. This was repeated for many trials with flies making either 40 or 60 naïve choices where neither option was rewarding and 40 or 60 training choices where one option was consistently rewarded.

For each behavior batch, at least one control fly was also run the same day to account for any batch effects. The exception to this is the batch of *Tao* RNAi flies. Due to technical reasons, we were unable to get behavior results from control flies on the same day. Therefore, we used the controls from the *mud* RNAi behavior batches to compare their behavior to, since the control genotype is the same for both the RNAi conditions.

Circular arena behavioral task structure and design

Groups of approximately 15-20 females, aged 4-10 day post-eclosion were anesthetized on a cold plate and collected two days prior to experiments. They were transferred to starvation vials containing nutrient-free agarose. Starved females were trained and tested at 25°C at 50% relative humidity in a dark circular arena described in Aso and Rubin.[64] The arena consisted of a circular chamber surrounded by four odor delivery ports that divide the chamber into quadrants. The input flow rate through each port was 100 mL/min, which was actively vented out a central exhaust at 400 mL/min. Odors were pentyl acetate (PA), butyl acetate (BA) (Sigma-Aldrich product numbers 109584 and 287725, respectively). These odors were diluted by an odor delivery system which utilizes air dilution of saturated odorant vapor, and delivered odors at a 1:16 dilution of saturated vapor.

Flies were aspirated into the arena via a small port, and allowed 60s to acclimatize before training commenced. Training consisted of exposing the flies to either PA or BA while providing optogenetic stimulation via a square array of red LEDs (617 nm peak emission, Red-Orange LUXEON Rebel LED, 122 lm at 700mA) which shone through an acrylic diffuser to illuminate flies from below. LED activation consisted of 30 pulses of 1s duration with a 1s inter-flash interval, commencing 5s after switching on the odor valves and terminating 5s after valve shut-off. The other odor was then provided for 60s without LED activation. Three training repeats, separated by 60 seconds, were used.

Following training, testing was carried out with PA and BA. In the test configuration, the two different odor choices are presented in opposing quadrants for 60s. Videos of fly behavior were captured at 30 frames per second using MATLAB (Mathworks, USA) and BIAS (http://archive.iorodeo.com/content/basic-image-acquisition-software-bias.html) and analyzed using custom-written code in MATLAB.

QUANTIFICATION AND STATISTICAL ANALYSIS

Image analysis

Analysis considerations

We analyzed males for immunohistochemistry in our manipulations. For functional imaging experiments, we used mixed-sex populations, and did not observe any correlation with sex (not shown). The Y-arena and circular arena behavior used females due to the size of the arena not being optimal for males. Therefore, the flies dissected post-behavior and used for calyx area quantification in those animals and Brp staining (Figures 1D, 2H, and 6F) were also females. Sex differences in the fly are well-documented, including in our own previous work, and anatomic and physiologic sex differences have not been observed in the mushroom body.[8,127] Any brains that appeared damaged from dissections, or those with the mushroom body region obscured due to insufficient tracheal removal, were not included in the analysis.

Researchers performing quantification could not generally be blinded to experimental condition due to the overt changes in neuron numbers and brain structures induced by our manipulations. However, analysis was performed blind to the goals of the experiment when possible, and quantitation of features on the anterior and posterior sides of the brain were recorded independent of one another and merged after all quantifications were completed. Moreover, many of our analyses make use of variation within an experimental condition or genotype, providing an additional bulwark against observational bias.

Calyx area

To measure the size of the mushroom body calyx, we used genetically-encoded fluorescence driven in Kenyon cells by OK107-Gal4. In cases where the fluorescent marker was not added, we used markers such as ChAT to visualize the structure. We then identified its largest extent in Z (i.e. along the A-P axis), outlined it in FIJI (as in white outlines in Figure 2H) and calculated the cross-sectional area using the 'Measure' command. We have previously shown the calyx area to positively correlate with KC number and hence, serve as a readout for KC number in the hydroxyurea-treated, KC-reduced and *mud* RNAi-driven, KC-increased conditions.[29]

Kenyon cell numbers

To count Kenyon cells, we again used genetically-encoded fluorescence driven by OK107-Gal4. We counted labeled somata in every third slice in the stack (every third micron along the A-P axis), with reference to DAPI to distinguish individual cells from one another. We initially determined that somata in slice 0 could also be seen in slices −2, −1, +1, and +2 but not in slice −3 or +3. To avoid double-counting, we therefore counted every third micron. For Figure 4, Kenyon cells were counted using a cellular segmentation tool called Cellpose.[116] The confocal stack for each hemisphere was split into single planes every third micron, and those slices were cropped to where the KC somata are present and given as input image into Cellpose. The count from each slice was then summed up to get the total count. The software used the Kenyon cell fluorescence, nuclear signal (DAPI) in the Kenyon cells, and an automatically calibrated cell diameter to identify individual cells. We verified that the counts obtained matched manual counts.

Please cite this article in press as: Ahmed et al., Input density tunes Kenyon cell sensory responses in the *Drosophila* mushroom body, Current Biology (2023), https://doi.org/10.1016/j.cub.2023.05.064

Kenyon cell and projection neuron neuroblast state

For quantifying Kenyon cell neuroblast state in Figure 6, as we have done previously,[29] we used 58F02 to fluorescently label late-born Kenyon cells and counted clumps of labeled somata surrounding the calyx as well as groups of labeled neurites leaving the calyx and entering the pedunculus. These estimates usually matched; in the few cases where they did not, we used the number of axon clumps, as somata are closer to the surface of the brain and more susceptible to mechanical disruption during dissection. This resulted in numbers between 0-4 for each hemisphere. Any additional labeling of neurons by 58F02 was easy to discriminate from KCs as those neurons did not enter the calyx or pedunculus.

For scoring presence of the PN neuroblast (PN INB/BAlc) in sham-treated and hydroxyurea-treated animals, we included Mz19 driving a fluorescent reporter in PNs from this lineage.[128,129] In the absence of INB/BAlc, 12 glomeruli lose their typical PN partners; 40 glomeruli are innervated by the anterodorsal PN neuroblast, which is not affected by HU ablation.[130,131] Mz19 labels PNs that innervate DA1 and VA1d glomeruli on the anterior side, and DC3 on the posterior side of the antennal lobe; DA1 is innervated by INB/BAlc PNs.[128] We quantified the presence or absence of the most distinctly labeled glomerulus – DA1, as a way to score the PN INB/BAlc getting ablated. In some cases, we observed mislocalization of DA1. For simplification, we scored this in the "absence" category.

Projection neuron bouton numbers

To count aggregate boutons, we used ChAT signal as previously described in Elkahlah et al.[29] We counted as separate structures ChAT signals that were compact and appeared distinct from one another and that were 2+ micrometers in diameter (except in Figure 2, *Tao* RNAi images where boutons appeared smaller than wildtype). When KC fluorescence was available, two boutons would be counted separately if ChAT signals were separated by KC signal. We found that boutons in slice 0 often appeared in slices −1 and +1 as well, but never in slices −2 or +2. To avoid overcounting, we began at the most superficial slice in the stack where boutons were visible, and counted every other slice, i.e. every second micron. For ChAT-positive counts in Figure 4, we combined data from two batches of experiments done on different dates – one of them carried a KC-driven fluorescent marker, the other batch did not.

Kenyon cell claw counts

To count Kenyon cell claws, we used sparse labeling of Kenyon cells driven by mBitbow2.2. We traced the dendritic projections by scrolling through the z stack, counting any claw-like dendritic structures that appeared and stopping when we reached the pedunculus. To ensure we counted all the cells labeled, we matched the puncta-like signal in the pedunculus to the number of KC soma visible. When ChAT or nc82 signal was available, we used that to define the calyx extent. We generally found the mAmetrine Bitbow signal (shown in Figure 2C) to be the cleanest and brightest for counting the claws. We then counted the number of KC soma labeled in the same color in which the claws were counted to obtain a "claws per KC" measurement by dividing claws of that color by the KC soma labeled in that color. Any image with more than 6 cells labeled was not counted as it was considered too dense to get an accurate claw count. An exception to this were the Dscam$^{3.36.25.1}$ animals (Figure 4) where the drastic claw number decrease allowed us to count claws for up to 10 Kenyon cells.

Bruchpilot density

We measured Bruchpilot intensity in the calyx as a readout of synaptic density. First, we identified the Z plane with the largest extent of the calyx in the A-P axis, and then took three measurements of the average fluorescence signal in the Brp channel in a defined ROI region measuring ~40 μm^2. The three measurements were taken randomly in different locations in the calyx to account for any variability in intensity. For normalization, the calyx Brp signal was divided by Brp signal measured in an unmanipulated brain region, the protocerebral bridge. We chose this brain region as it was the closest to the calyx and was in the field of view in all calyx images taken. These quantifications were done in the "63X hi-res-1" and "63X hi-res-2" sets of images (defined in the "Immunostainings" section above).

Correlation matrix of odor responses

To assess the linear relation between each pairwise odor comparison across the cells in the control and *Tao* RNAi animals, we plotted a Pearson correlation matrix using the "corrplot" package in R (v3.5.1). The range of the Pearson correlation is –1 to +1, with positive values indicating a positive correlation and negative values indicating a negative correlation.

Behavior analysis

Y-arena

Analysis of data resulting from the Y-arena was performed using MATLAB 2020b (Mathworks). In a given experiment, the *(x,y)* coordinates of the fly and metadata from the experiment to determine arm-odor relationships were analyzed to determine which odor the fly chose on a given trial. This allowed us to make a list of choices made by the fly as a function of trial number. This list was used to calculate the fly's average preferences for the rewarded odor over the unrewarded odor (in the naïve block, this was defined based on which odor was rewarding in the training block). Time spent in the air arms was not recorded as a choice.

The proportion correct choice metric was calculated for both naïve and training blocks and used in Figures 6 and 7. This was defined as the number of choices to the rewarded option divided by the total number of choices. Only the second half of trials in each block were used. The first half of trials were excluded from this calculation as flies take around 15-20 trials to reach a plateau learnt performance in the training block and we did not want this metric to be diluted by trials in which learning was incomplete. To plot individual learning curves in Figure 7, the cumulative number of choices towards the rewarded and unrewarded options were calculated as a function of trial number and then plotted against each other. Since the control genotype for *mud* RNAi, KC-increased and *Tao* RNAi, KC claw-increased animals was the same, we plotted the behavioral data from these three genotypes together.

Please cite this article in press as: Ahmed et al., Input density tunes Kenyon cell sensory responses in the *Drosophila* mushroom body, Current Biology (2023), https://doi.org/10.1016/j.cub.2023.05.064

Circular arena

Videos recorded during the test phase were analyzed using custom-written MATLAB code. The centroid of each fly was identified and the number of centroids in each quadrant computed for every frame of the experiment. For discrimination experiments, a Performance Index (PI) was calculated as the number of flies in the quadrants containing the paired odor minus the number in the quadrants with the unpaired odor, divided by the total number of flies.[83] This value was calculated for every frame of the movie, and the change in average PI values over the final 30 s of the test period compared to the average PI in the 30 seconds prior to the odor onset was used to compute a single ΔPI for one set of flies.

Statistical considerations

Brains were prepared for imaging in batches of 5–10. In initial batches, we assessed the variability of the manipulation, for example if we were trying to change Kenyon cell number, we looked at how variable the size of the Kenyon cell population was following the manipulation. We used this variability to determine how many batches to analyze so as to obtain enough informative samples. To avoid introducing statistical bias, we did not analyze the functional consequence of the manipulation until after completing all batches; for example, if the manipulation was intended to alter Kenyon cell claw numbers, we did not quantify odor responses until after completing all samples. Similarly, we did not measure the effect on other cell types (such as assessing projection neuron bouton phenotypes) until after completion of all samples. Genotypes or conditions being compared with one another were always prepared for staining together and imaged interspersed with one another to equalize batch effects except in occasional cases that have been highlighted in methods above. Since our developmental manipulations seemed to affect the mushroom body in each hemisphere independently and variably, we treated each hemisphere as an independent sample in our staining and functional imaging. In the case of hydroxyurea-treated animals, if one hemisphere was affected severely, the other one is likely affected to a similar extent but not necessarily equally, e.g. we observed KC clone counts of "[1,0]" or "[3,2]" but never "[4,0]".

We excluded from analysis samples with overt physical damage to the cells or structures being measured. In figures and analyses, we treated outliers the same way as other data points. For *in vivo* functional imaging experiments, full criteria for inclusion and exclusion of each sample are discussed above under "Analysis of KC somatic odor responses" and "Analysis of MBON odor responses".

Statistical tests applied are mentioned in each figure legend along with the p-value significance. Asterisks indicate p values associated with these tests: *: $p<0.05$; **: $p<0.01$; ***: $p<0.001$; ****: $p<0.0001$; ns: non-significant. To communicate our findings in the simplest and most complete way, we have displayed each data point for each sample to allow readers to assess effect size and significance directly. When sample size could be determined from the figures, we did not explicitly state it in the figure legends. Statistical analyses were performed in GraphPad Prism, Excel, or R.

Current Biology, Volume *33*

Supplemental Information

Input density tunes Kenyon cell sensory responses in the *Drosophila* mushroom body

Maria Ahmed, Adithya E. Rajagopalan, Yijie Pan, Ye Li, Donnell L. Williams, Erik A. Pedersen, Manav Thakral, Angelica Previero, Kari C. Close, Christina P. Christoforou, Dawen Cai, Glenn C. Turner, and E. Josephine Clowney

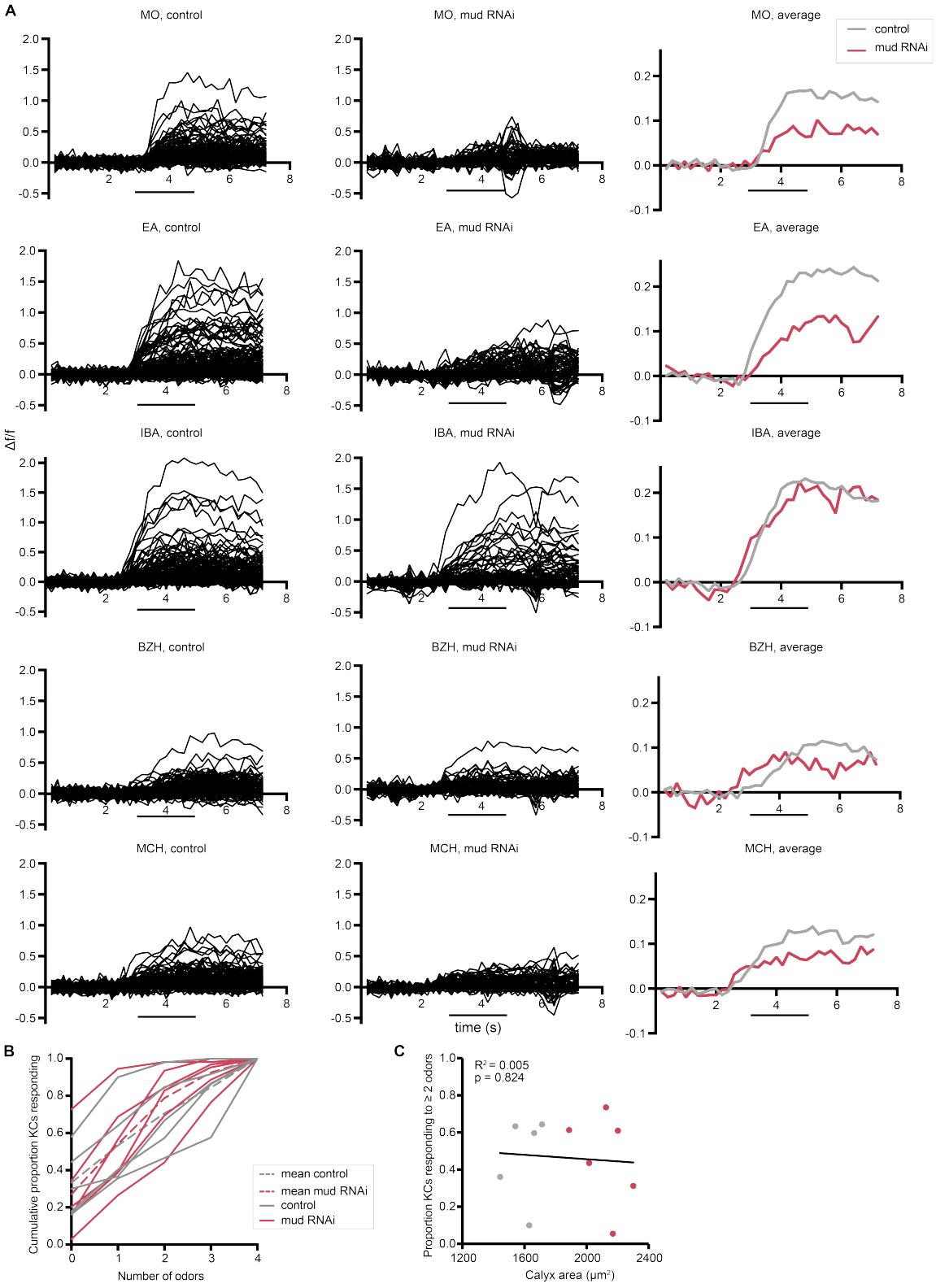
A
MO, control
MO, mud RNAi
MO, average
control
mud RNAi
EA, control
EA, mud RNAi
EA, average
IBA, control
IBA, mud RNAi
IBA, average
BZH, control
BZH, mud RNAi
BZH, average
MCH, control
MCH, mud RNAi
MCH, average
Δf/f
time (s)
B
Cumulative proportion KCs responding
Number of odors
mean control
mean mud RNAi
control
mud RNAi
C
R² = 0.005
p = 0.824
Proportion KCs responding to ≥ 2 odors
Calyx area (μm²)

Figure S1. Cellular odor responses in supernumary populations of Kenyon cells, related to Figure 1.

(A) Odor responses over time for Kenyon cells shown in Figure 1G. x axes: seconds, y axes: Δf/f. Black bars: odor delivery. Each black line is one cell, with graphs at right showing responses averaged across all cells of the sample. Each cell was normalized to average fluorescence in the 3s period before stimulus onset. An example of a motion artifact can be seen in 'MO, mud RNAi' trace around 5s. n = 124 cells (control), 62 cells (*mud* RNAi). (B) Cumulative proportion of Kenyon cells responding from 0 up to 4 odors. Each line represents an individual control hemisphere (gray) or increased-KC *mud* RNAi hemisphere (red), with the mean of all control or *mud* RNAi samples shown with a dotted line. (C) Relation of proportion of KCs responding to 2 or more odors, and maximum cross-sectional calyx area of control (gray) and KC-increased *mud* RNAi (red) hemispheres. Here and throughout, linear regressions are performed across all data points shown in the figure, i.e., for the distribution of the two sample types taken together across the variation in calyx size.

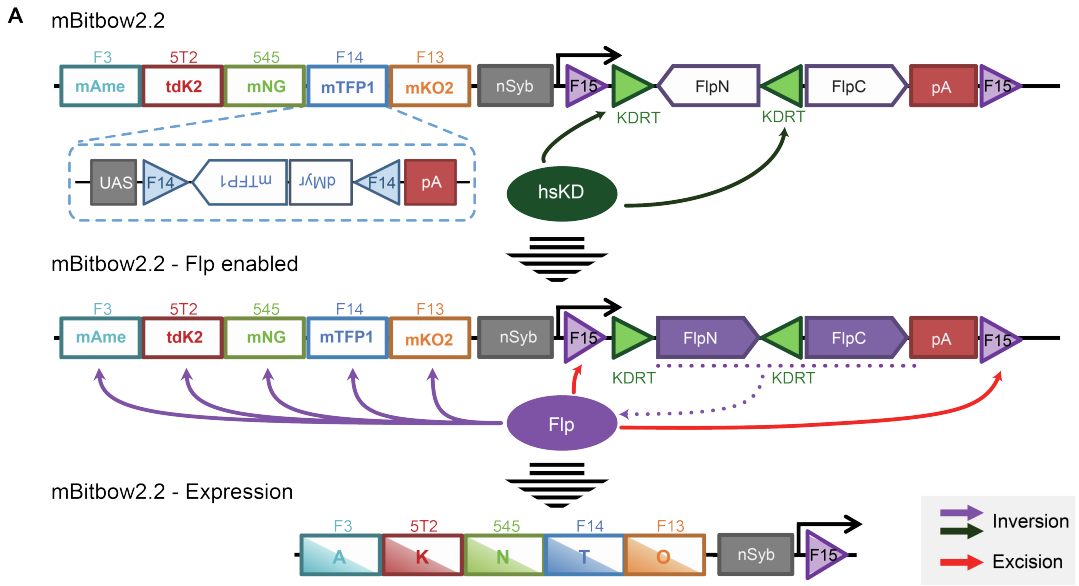

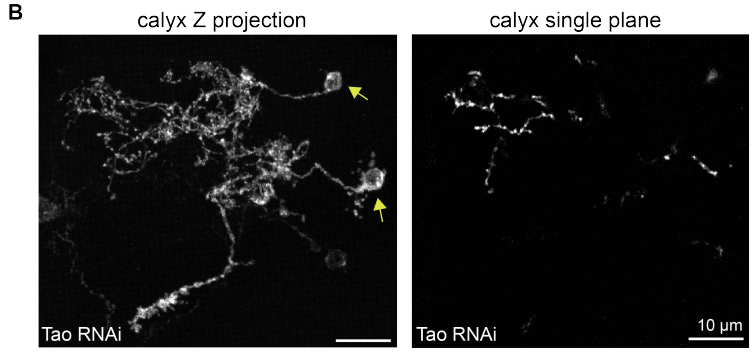

Figure S2. mBitbow2.2 schematic and dendritic morphology in *Tao*-knockdown Kenyon cells, related to Figure 2.

(A) Detailed schematic of mBitbow2.2 design; a simplified version is shown in Figure 2A. In the presence of KD, the N-terminal portion of flippase will be inverted to the correct orientation, hence enabling the expression of flippase under nSyb control in mature neurons. Similar to the mBitbow2.1 design, the flippase will initiate a Bitbow combination. Flippase can also excise itself, preventing sustained recombinations. (B) Images of sparsely labeled KCs in a KC>*Tao* RNAi calyx showing highly branched but non-clawed dendritic projections that we observe in some samples: maximum z projection (left), single confocal slice (right). In the example shown, arrows mark 2 KCs labeled by mBitbow2.2 mAmetrine. Faint third soma is labeled by an additional mBitbow2.2 color.

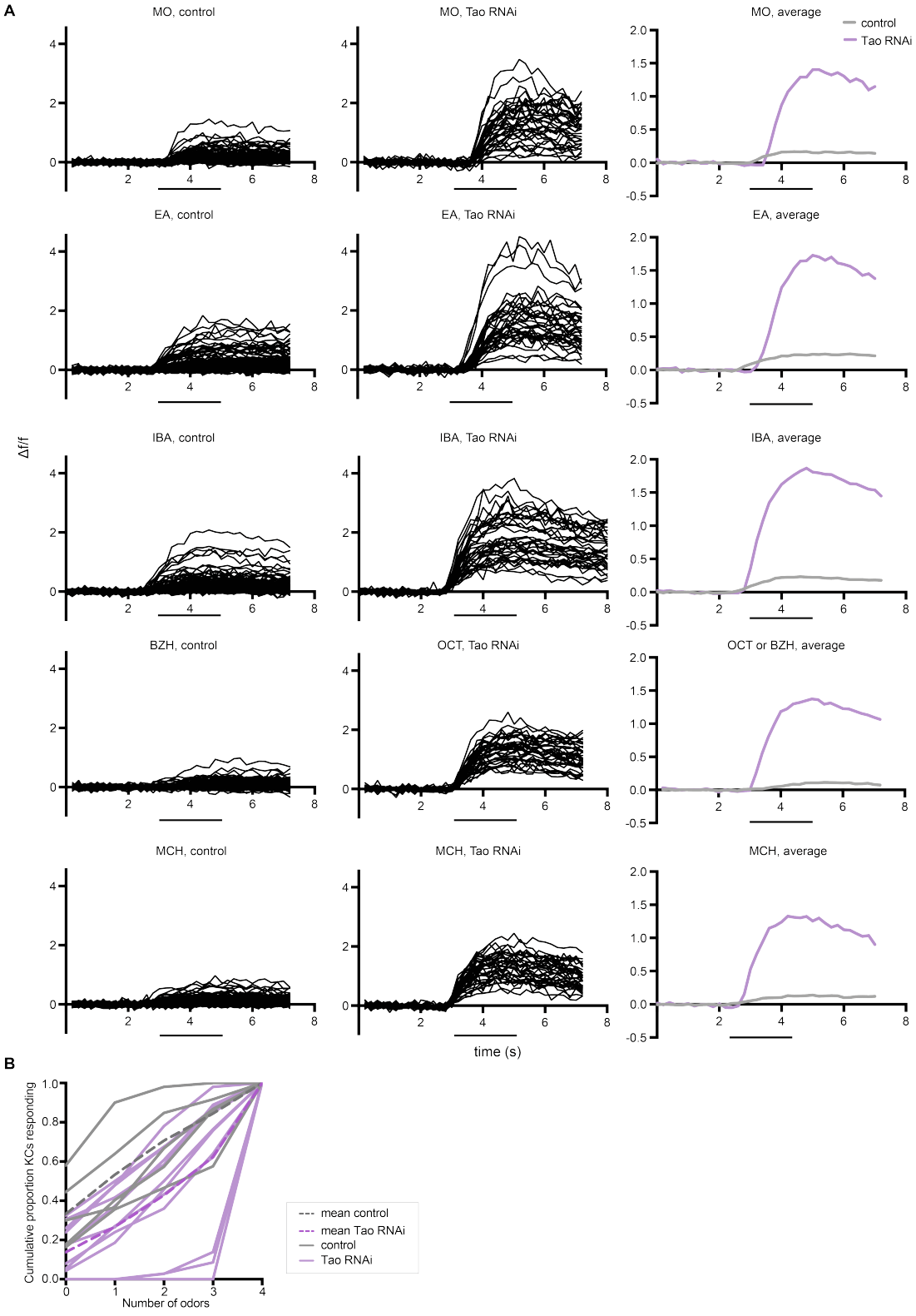

Figure S3. Cellular odor responses in animals with excess Kenyon cell claws, related to Figure 3.

(A) x axes show seconds, y axes show Δf/f. Black bars indicate odor delivery. Each black line is one cell, with graphs at right showing responses averaged across all cells of the sample. Each cell was normalized to average fluorescence in the 3 s period before stimulus onset. MO: Mineral oil (mechanosensory control), EA: Ethyl Acetate, IBA: Isobutyl Acetate, BZH: benzaldehyde, OCT: Octanol, MCH: Methylcyclohexanol. Control sample is the same sample shown in Figure S1; we have replotted the data to allow quantitative comparison with the robust responses of excess-claw KCs. n = 124 cells (control), 36 cells (*Tao* RNAi). (B) Cumulative proportion of Kenyon cells responding from 0 up to 4 odors. Each line represents an individual control hemisphere (gray) or *Tao* RNAi hemisphere (purple), with the mean of all control or *Tao* RNAi samples shown with a dotted line.

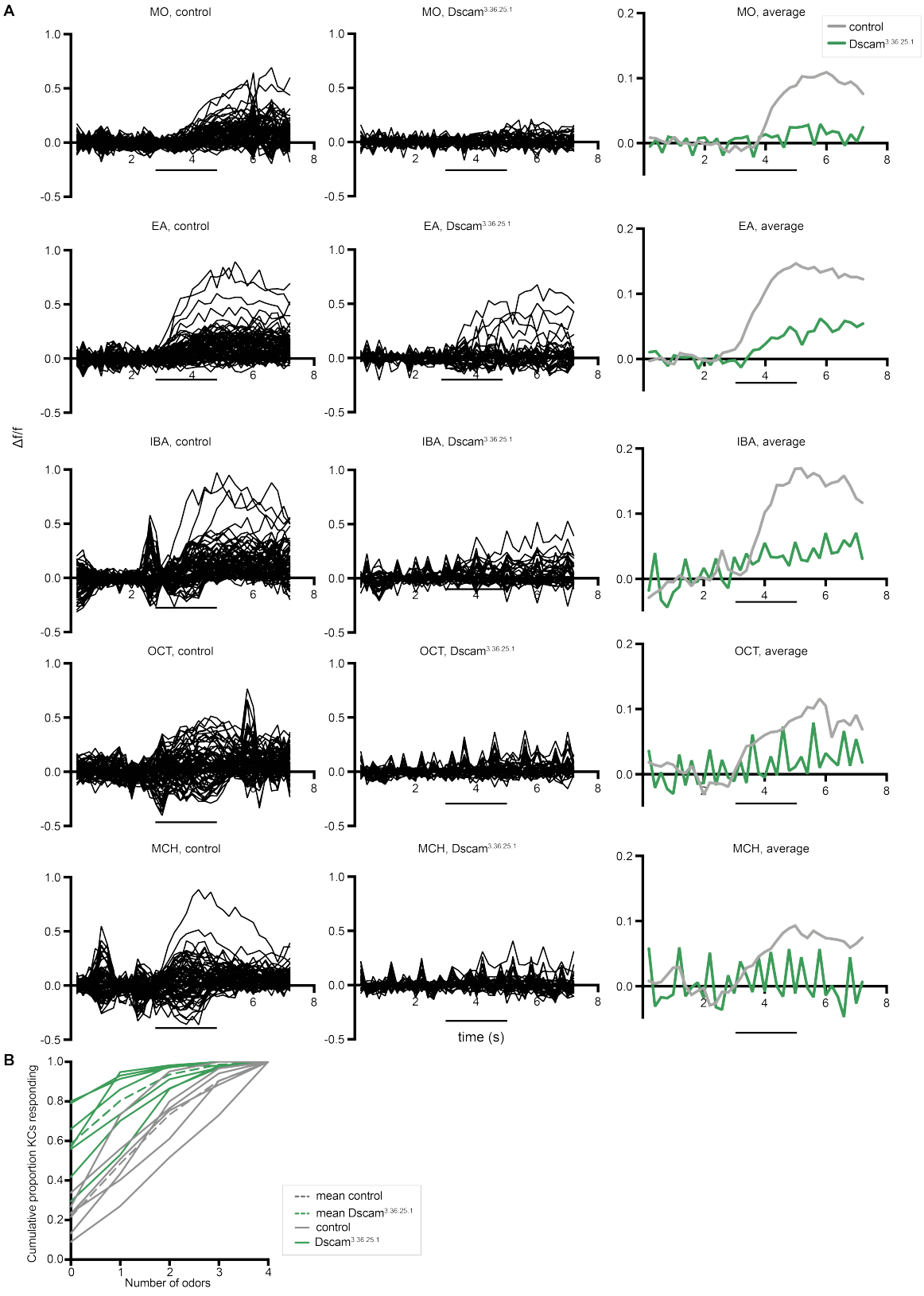
A
MO, control
MO, Dscam3.36.25.1
MO, average
control
Dscam3.36.25.1
EA, control
EA, Dscam3.36.25.1
EA, average
IBA, control
IBA, Dscam3.36.25.1
IBA, average
OCT, control
OCT, Dscam3.36.25.1
OCT, average
MCH, control
MCH, Dscam3.36.25.1
MCH, average
Δf/f
time (s)
B
Cumulative proportion KCs responding
Number of odors
mean control
mean Dscam3.36.25.1
control
Dscam3.36.25.1

Figure S4. Cellular odor responses in animals with diminished Kenyon cell claws, related to Figure 5.

(A) x axes show seconds, y axes show Δf/f. Black bars indicate odor delivery. Each black line is one cell, with graphs at right showing responses averaged across all cells of the sample. Each cell was normalized to average fluorescence in the 3 s period before stimulus onset. MO: Mineral oil (mechanosensory control), EA: Ethyl Acetate, IBA: Isobutyl Acetate, OCT: Octanol, MCH: Methylcyclohexanol. n = 72 cells (control), 35 cells ($Dscam^{3.36.25.1}$). (B) Cumulative proportion of Kenyon cells responding from 0 up to 4 odors. Each line represents an individual control hemisphere (gray) or $Dscam^{3.36.25.1}$ hemisphere (green), with the mean of all control or $Dscam^{3.36.25.1}$ samples shown with a dotted line.

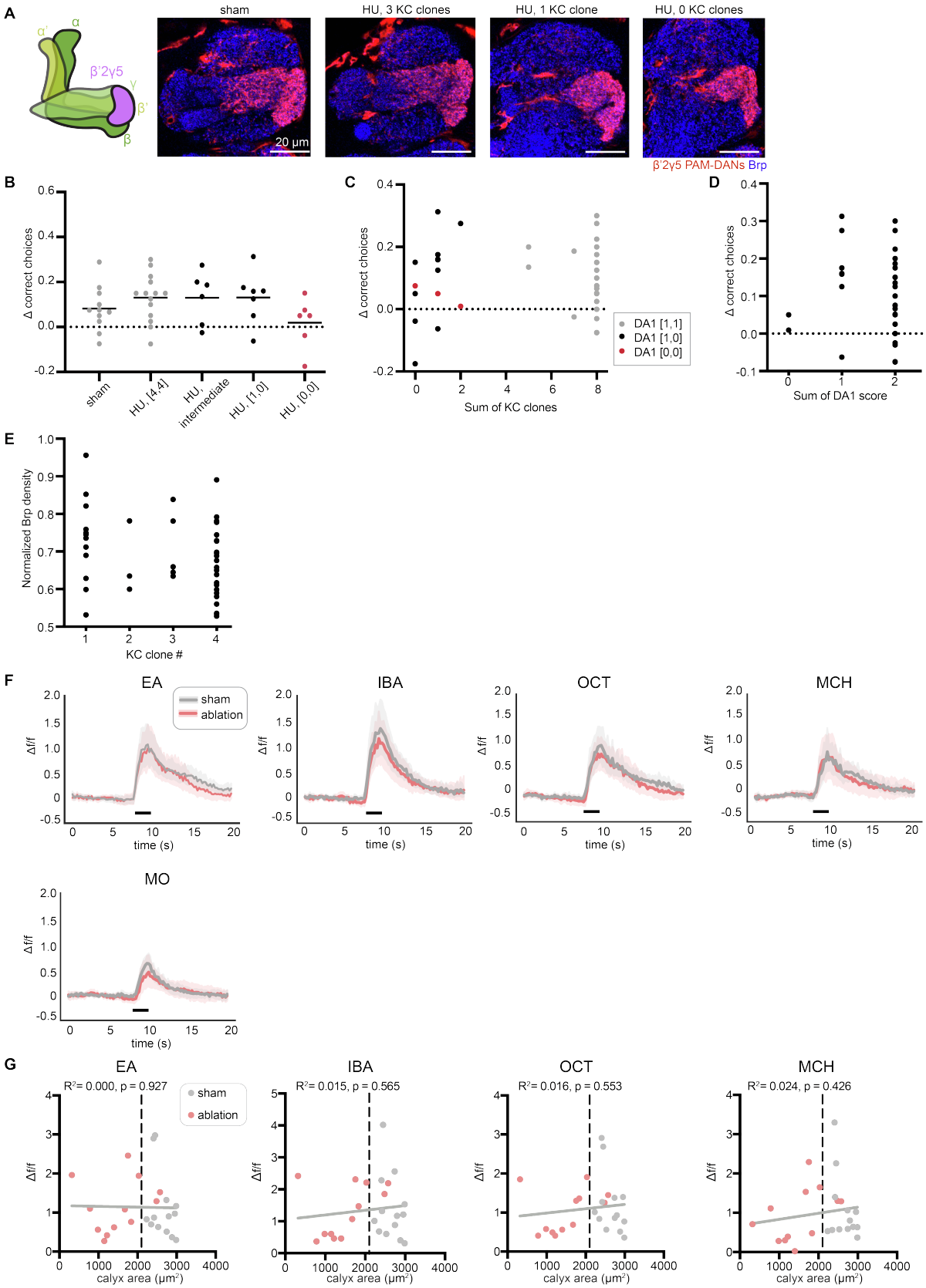
A
sham
HU, 3 KC clones
HU, 1 KC clone
HU, 0 KC clones
α
α'
β'2γ5
γ
β'
β
20 µm
β'2γ5 PAM-DANs Brp
B
Δ correct choices
sham
HU, [4,4]
HU, intermediate
HU, [1,0]
HU, [0,0]
C
Δ correct choices
Sum of KC clones
DA1 [1,1]
DA1 [1,0]
DA1 [0,0]
D
Δ correct choices
Sum of DA1 score
E
Normalized Brp density
KC clone #
F
EA
IBA
OCT
MCH
MO
sham
ablation
Δf/f
time (s)
G
EA
IBA
OCT
MCH
R²= 0.000, p = 0.927
R²= 0.015, p = 0.565
R²= 0.016, p = 0.553
R²= 0.024, p = 0.426
sham
ablation
Δf/f
calyx area (µm²)

Figure S5. Additional functional, behavioral, and anatomic data in mushroom bodies with diminished populations of Kenyon cells, related to Figure 6.
(A) Left: Schematic of the mushroom body lobe anatomy with KCs in green and β'2γ5 PAM-DANs in magenta. Axons of β'2γ5 DANs in the lobe compartment are shown. Right: Single confocal slices of the MB lobe (identified by location and Brp staining shown in blue). Mz19 driver labels β'2γ5 DANs (red). Representative images shown of sham-treated and HU-treated hemispheres with 3, 1, or 0 KC clones. (B) Δ correct choices of sham-treated and HU-treated animals shown in Figure 6D. Black bars indicate the medians. In B-D, each data point is an individual fly. (C) Relation of Δ correct choices, sum of KC clone number from both hemispheres and lNB/BAlc ablation status. DA1 present in both hemispheres is indicated as "DA1 [1,1]", presence in one hemisphere is indicated as "DA1 [1,0]", and absent in both hemispheres is indicated as "DA1 [0,0]" . (D) Relation of Δ correct choices to sum of DA1 score (presence/absence). The data shown excludes fully KC ablated animals. Jitter added in (C-E) to display all the data points. (E) Relation of normalized Brp density in the mushroom body calyx to Kenyon cell clone number in sham-treated and HU-treated animals, excluding fully ablated animals as there is no calyx present. (F) Average odor responses over time for γ2,α'1 MBONs in Figure 6I. x axes show seconds, y axes show Δf/f. Black bars indicate odor delivery. Shadows are 95% confidence intervals for corresponding averaged traces. Each cell was normalized to average fluorescence in the 5 s to 2 s period before stimulus onset. MO: Mineral oil (mechanosensory control), EA: Ethyl Acetate, IBA: Isobutyl Acetate, OCT: Octanol, MCH: Methylcyclohexanol. n= 12 hemispheres (sham), 10 hemispheres (ablation). Only HU-partially ablated hemispheres smaller than every control (maximum cross-sectional calyx area < 2100 μm^2) are included. This cutoff is labeled as black vertical dashed line in (G). (G) Relationship between γ2,α'1 MBON peak odor responses and maximum cross-sectional calyx area. Gray line is linear regression for all samples. n= 12 hemispheres (sham), 12 hemispheres (ablation). 2 HU-treated animals with maximum cross-sectional calyx area > 2100 μm^2 are also shown.

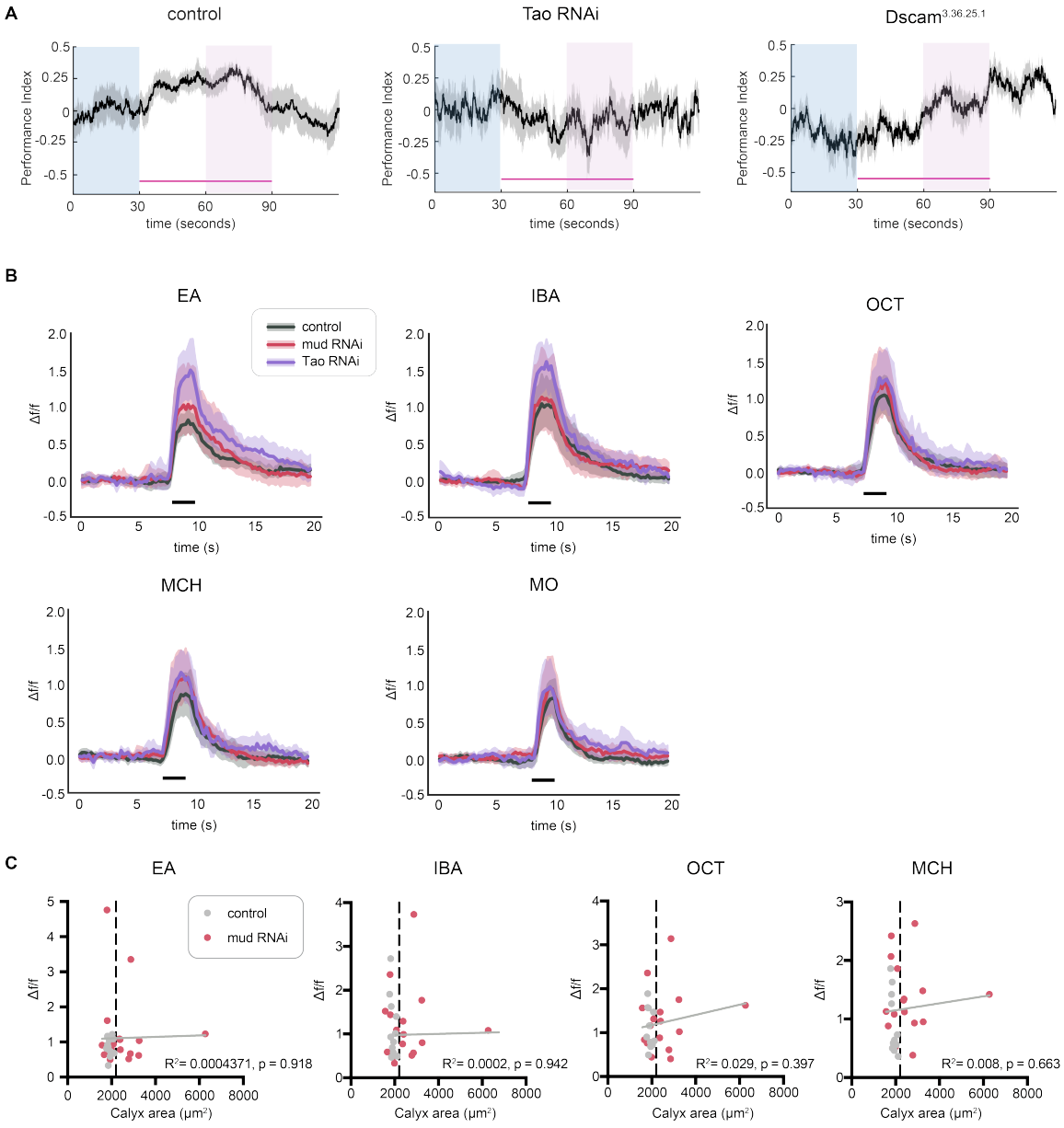

Figure S6. Additional functional and behavioral data in mushroom bodies of animals with excess Kenyon cells or altered Kenyon cell dendrites, related to Figure 7.
(A) Mean and standard error of group performance indices over time in the circular arena "hard discrimination" assay. Positions of all animals were monitored for the 30 seconds prior to odor onset (blue), at t=30s. Odor was presented for one minute (red bar, t=30-90s). Performance index at each time point is calculated as ((animals in quadrants assigned to paired odor)-(animals in quadrants assigned to unpaired odor))/total animals. In Figure 7E we subtract the animals' time-averaged PI before odor onset (blue shading) from the time-averaged PI during odor test (t=60-90s, pink shading). n=5-6 groups per genotype of 15-20 animals each. (B) Average odor responses over time for γ2,α'1 MBONs shown in Figure 7G. x axes show seconds, y axes show Δf/f. Black bars indicate odor delivery. Shadows are 95% confidence intervals for corresponding average trace. Each cell was normalized to average fluorescence in

the 5 s to 2 s period before stimulus onset. MO: Mineral oil (mechanosensory control), EA: Ethyl Acetate, IBA: Isobutyl Acetate, OCT: Octanol, MCH: Methylcyclohexanol. n= 10 hemispheres (control), 9 hemispheres (*mud* RNAi), 12 (*Tao* RNAi). For *mud* RNAi, only Kenyon cell-increased hemispheres (maximum cross-sectional calyx area > 2200 μm^2) are included. This threshold is labeled as black vertical dashed line in (C). (C) Relationship between γ2,α'1 MBON peak odor responses and maximum cross-sectional calyx area. Gray line is linear regression for all samples. n= 10 hemispheres (control), 15 hemispheres (*mud* RNAi); six hemispheres from *mud* RNAi calyces with calyx cross-sectional area overlapping controls (< 2200 μm^2) are included among these 15.

Parameter	MB Name	Variable Name	Number in natural MB	Number engineered here
Number of inputs	Olfactory projection neuron types	N	52	40-52
Number of expansion layer neurons	Kenyon cells per hemisphere	M	2000	500-4000
Expansion ratio (M/N)	Kenyon cell number/odor channels	E	38	10-77
Number of inputs to each expansion layer neuron	Claw number	K	5	1-12
Spiking threshold	Number of input channels active for KC to spike	n/a	For most cells, at least 2, though some cells have been observed to spike with one input active	*We suspect it has not changed
Strength of feedback inhibition	APL activity	Σ	Unknown	Unknown
Total connections between sensory and expansion layer	Total number of Kenyon cell claws	S	10,000	2,000-24,000

Table S1. Quantitative variables of mushroom body calyx wiring and function, related to Figure 1.
We use the framework developed by Litwin-Kumar et al [1].

Condition	Result	N	M	E	K	KC spike threshold	Σ	S
Wild type	KCs respond to 0-1 odors	52	2000	38	5-6	~2 claws	unknown	10,000
5HU ablation	Fewer KCs, but each responds to the same number of odors	40-52	500-2000	10-50	5-6	~2 claws (inferred)	Proportional to KCs active (inferred)	2,500-10,000
Mud knockdown	More KCs, but each responds to the same number of odors	52	2000-4000	38-77	6	~2 claws (inferred)	Proportional to KCs active (inferred)	10,000-24,000
Tao knockdown	Each KC responds to more odors	52	1700	32	12	~2 claws (inferred, as described in legend)	Proportional to KCs active (inferred)	~20,400
Dscam1[TM1] overexpression	Each KC responds to fewer odors	52	1800	35	1	1-2 claws (inferred, as described in legend)	Proportional to KCs active (inferred)	1800

Table S2. Summary of the effects of our developmental manipulations on mushroom body calyx connectivity variables, related to Figures 1-7.

To estimate Kenyon cell spike threshold when claw number varies, we used the following reasoning: In our previous work, we found that 5-80% of PNs were activated by different odors, with a median of 23% [2]. This is consistent with assessment of glomerular responses in the antennal lobe [3]. To model the relationship between claw number and spike threshold, we make three simplifications: That bouton responsiveness does not influence claw connectivity, weights of connections between boutons and claws are uniform, and activity of each bouton is independent of each other. This allows us to model the process of Kenyon cell receiving inputs from PNs as a Boolean process, such that each PN connected with a Kenyon cell can provide an active input with a probability of 0.23. Then, the number of active inputs (X) a Kenyon cell receives follows a binomial distribution: $X \sim Binomial(p, n)$, in which p is the probability of a PN being active (p=0.23) and n is the claw number of a given Kenyon cell. We can then calculate the probability of a Kenyon cell receiving k ($k \in [0, n]$) active inputs with: $\Pr(X = k) = \binom{n}{k} p^k (1-p)^{n-k} = \binom{n}{k} 0.23^k 0.77^{n-k}$. If a Kenyon cell receives inputs greater than or equal to its firing threshold (th), this Kenyon cell will be activated. The probability of a KC being activated could be calculated as: $\Pr(X \geq th) = \sum_{i=th}^{n} \Pr(X = i) = \sum_{i=th}^{n} \binom{n}{i} 0.23^i 0.77^{n-i}$. With this model, we estimate that for wild type animals, 41% of Kenyon cells with six claws would receive at least

two inputs from among the 23% of boutons that are active in response to a median odor, and that 13% of six-clawed Kenyon cells would have at least three active inputs. A spiking threshold of 2-3 claws is therefore consistent with our experimental observation here that 20-40% of Kenyon cells respond to each odor. Dscam1[TM1]-overexpressing Kenyon cells had 0-2 claws (median of 1). If the spiking threshold was reduced in these animals, such that only one active claw was required for the Kenyon cell to fire, we would expect ~23% of Kenyon cells to respond to a median odor, because 23% of boutons would be active. However, we found that odor responses were more dampened than this, with only ~10% of Kenyon cell responding per odor. This result suggests that the number of active claws needed to spike the Kenyon cell remained the same in this condition. *Tao*-knockdown Kenyon cells had ~10-14 claws. If the "active claws needed" threshold rises in these animals, such that ~5 or more active claws were required for the Kenyon cell to fire, we would expect only ~10% of cells to respond to a median odor (i.e. only 10% of Kenyon cells would have five or more claws innervating the 23% of active boutons). Again, this is inconsistent with what we see. For a Kenyon cell with 12 claws, 53% of cells would have at least three active claws in response to a median odor, and 79% would have at least two active claws. This threshold, the same as for a wild type six-clawed Kenyon cell, is more consistent with our experimental observation that 80% of expanded-claw Kenyon cells in the *Tao* knockdown condition are activated by each odor.

Supplemental References

S1. Litwin-Kumar A, Harris KD, Axel R, Sompolinsky H, Abbott LF. Optimal Degrees of Synaptic Connectivity. Neuron. 2017 Mar 8;93(5):1153-1164.e7.

S2. Gruntman E, Turner GC. Integration of the olfactory code across dendritic claws of single mushroom body neurons. Nat Neurosci. 2013 Dec;16(12):1821–9.

S3. Knaden M, Strutz A, Ahsan J, Sachse S, Hansson BS. Spatial Representation of Odorant Valence in an Insect Brain. Cell Reports. 2012 Apr 19;1(4):392–9.